5-2012

Photocatalytic Reactor using TiO2 Thin Film on Quartz Tubes

Ram Mahipal Kouda
University of Arkansas, Fayetteville

PHOTOCATALYTIC REACTOR USING TiO_2 THIN FILM ON QUARTZ TUBES

PHOTOCATALYTIC REACTOR USING TiO_2 THIN FILM ON QUARTZ TUBES

A dissertation submitted in partial fulfillment
of the requirements for the degree of
Doctor of Philosophy in Engineering

By

Ram Mahipal Kouda
J. N. Technological University
Bachelor of Technology in Chemical Engineering, 2002
University of Arkansas
Master of Science in Engineering, 2006

May 2012
University of Arkansas

ABSTRACT

Photocatalysis process, as an environmental application is an advanced oxidation process with tremendous potential in the near future. Previously many researchers, have conducted photocatalysis in different reactor configuration using TiO_2 slurry and thin film, using a UV light source, the constraints for these reactors are the need for the removal of TiO_2 particles at the outlet stream in a slurry reactor and poor environment for the efficient use of TiO_2 film using UV light, as the UV light penetration depth in water is about an inch[42].

Taking all this into consideration, we propose a design for reactor with efficient contact of the aqueous phase to the TiO_2 film so that UV light doesn't need to penetrate through water, the TiO_2 particles need not be removed from the outlet stream of water. The wok involves the deposition of TiO_2 on quartz tubes with TiO_2 and TiO_2-Fe doped film by sol-gel and ESA (electrostatic self assembly) method and testing the performance of the coated film in proposed photocatalytic reactor in degradation of congo red, KI and Nitro phenol.

This dissertation is approved for recommendation

to the Graduate Council.

Dissertation Director:

_____

Prof. Greg Thoma

Dissertation Committee:

_____

Prof. Ed Clausen

_____

Prof. Richard K Ulrich

_____

Prof. Greg Salamo

_____

Dr. Andrew Wang (*ex officio*)

DISSERTATION DUPLICATION RELEASE

I hereby authorize the University of Arkansas Libraries to duplicate this dissertation when needed for research and/or scholarship.

Agreed _____
Ram Mahipal Kouda

Refused _ _____
Ram Mahipal Kouda

ACKNOWLEDGEMENTS

I would like to thank Professor Greg Thoma, my advisor, for his many suggestions, patience and constant support and encouragement during the dissertation work. I sincerely appreciate chemical engineering department for generous financial support of my graduate work at University of Arkansas as well as the valuable input I received from the dissertation committee members. I also would like to thank the staff and members of chemical engineering department in their support for my graduate work.

I am grateful to University of Arkansas for giving me this great educational opportunity. I thank my parents and siblings for their and support, especially my wife who really supported and encouraged me last three years in completing the dissertation.

Ram Mahipal Kouda April 19, 2012

DEDICATION

I would like to dedicate my dissertation to my advisor Professor Greg Thoma for his support in the research work and helping me with patience in completing the dissertation, and also helped me in growing as a person.

TABLE OF CONTENTS

TABLE OF FIGURES

LIST OF TABLES

1 INTRODUCTION

1.1 Introduction

Water is a daily necessity in every industry and domestic life. The industrial effluent is often contaminated with organic and inorganic materials. These effluents need to be treated before being released into the lakes/rivers or being reused. Wastewater treatment is becoming ever more critical due to diminishing water resources, increasing wastewater disposal costs, and stricter discharge regulations that have lowered permissible contaminant levels.

Currently, most water treatment methods such as separation processes can remove most of the contaminants, but they remove the hazardous compounds without decomposing them into non-hazardous compounds. The hazardous compounds need to be treated further before discharging them to biological processes that can decompose them.

In the past 10 years, there has been considerable research and commercial interest in the use of advanced oxidation processes (AOP) for the treatment of organic contaminants in liquid and gas phases[1-10]. Advanced oxidation processes are essentially reactions that utilize oxidants to destroy contaminants in liquid and gas phases[1] such as ozonation, hydrogen peroxide and hydrogen with UV light treatment. The advanced oxidation process (AOP) has been successfully used to decompose many hazardous chemical compounds to acceptable levels, without producing additional hazardous by-products or sludge which requires further handling[22]. The term advanced oxidation processes refers specifically to processes in which oxidation of organic contaminants occurs primarily through reactions with hydroxyl radicals. AOPs usually refer to a specific subset of processes that involve O_3, H_2O_2, and/or UV light:

- Ozone/ultraviolet light (O_3/UV)
- Hydrogen peroxide/ozone (H_2O_2/O_3)
- Hydrogen peroxide/ozone/ultraviolet (H_2O_2/O_3/UV) processes

The most widely applied advanced oxidation processes (AOP) have been based on peroxide/ultraviolet light (H_2O_2/UV)[1].The processes have shown considerable potential in the treatment of recalcitrant[6,9] as well as organic pollutants as diverse as humic substances and textile dye waste[5,7,8].

Among the several available advanced oxidation processes, photocatalysis has been more efficient in the generation of OH* radicals in water without generation of any byproducts, and no direct reaction of the catalyst[1,2] has been observed. Sseveral semi-conducting oxides have been investigated as potential photocatalysts. The ideal material for the photocatalytic application must be photoactive, photo stable, biologically or chemically inert and inexpensive[1,3,8,10]. There are semi-conducting materials such as TiO_2, SnO_2, ZnO_2[14], CdS, and WO_3 which are currently used as photocatalysts. TiO_2 among these photo catalysts is very attractive because the price is relatively cheap and it is chemically stable[18].

Advantages of Advanced Oxidation Processes

- Rapid reaction rates[1,22]
- Small foot print(equipment size).
- Potential to reduce toxicity and possibly complete mineralization of organics treated[1,22].

- Does not concentrate waste such as in membranes process, which need further treatment.
- Does not produce materials that require further treatment such as "spent carbon" from activated carbon absorption[1,22].
- Does not create sludge as with physical chemical process or biological processes (wasted biological sludge)[1,22].
- Non selective pathway allows for the treatment of multiple organics at once

Disadvantages of Advanced Oxidation Processes

- Capital Intensive
- Complex chemistry must be tailored to specific application
- For some applications quenching of excess peroxide is required

The selection of a specific advanced oxidation process is application dependent based on the type of compounds to be removed, treatment objectives, concentrations, site considerations and budget, etc.

For example, for higher COD removal rates, UV/Ozone/Peroxide/Catalyst systems can be more effective as illustrated below[22].

Table 1-1. COD removal percentage (%) using various AOP process.

Process	H_2O_2/O_3/Catalyst	O_3/UV/Catalysts	H_2O_2/O_3/UV/Catalyst
COD Removal %	30%	49%	59%

Advanced oxidation processes are designed to both efficiently produce and use hydroxyl ions for oxidation. They have a wide range of applications mainly for oxidation of refractory compounds, TOC and COD reduction [1, 33]:

- gas effluent treatment
- water reclaim / reuse / recycling
- drinking water supplies
- industrial & municipal wastewater
- process water, ultra-pure water
- electronic & pharmaceutical industries
- cooling water systems
- fish hatcheries and farm

AOP acts on organic compounds in water by converting one compound into another, and thereby reducing the toxicity and breaking down of the organic compound to CO_2 and inorganic salts[1,10]. In some cases, discharge permits simply require conversion from a compound of interest to another compound that is not covered by the permit[22]. For example, some permits require taking phenol to a fraction of a ppm. In other cases, permitting authorities require the

toxicity of the compound/wastewater to be reduced prior to discharge. In some cases, mineralization is needed as measured by a reduction of TOC.

1.2 Photocatalysis Reaction Mechanism

The basic mechanism of the photocatalysis involves using the light energy by means of photocatalyst to degrade (oxidize) the organic compounds. So, the photocatalyst TiO_2 is not being consumed during the process.

When a photon is absorbed by TiO_2 particle, the electron in the valence band of the TiO_2 particle moves to the conduction band and hole in the valence band absorbs the electron from a hydroxyl radical.

$$TiO_2 + h\nu \rightarrow h^+ + e^-$$

$$h^+ + OH^- \rightarrow OH^*$$

$$e^- + O_2 \rightarrow O_2^-$$

$$\text{Organic Compounds} + OH^* \rightarrow CO_2 + H_2O + \text{etc.}$$

In the photocatalysis[13-20] process the hole-electron pair is formed when a photon of energy equivalent to the band–gap of the semi conductor strikes the semiconductor TiO_2. The hole receives an electron from OH^- radical forming OH* and, in oxygenated environment, an O_2 molecule absorbs the electron in the valence band forming O_2^- , and thereby TiO_2 changes back

to its original state to absorb another photon. The OH* radical is used in oxidation process of organic molecules and O_2^- is used in the reduction process.

The factors that are significant are discussed in later chapters includes the reactor configuration, TiO2 film coating/ deposition, experimental design and results, and computational fluid dynamic model of the reactor.

1.3 Advanced Oxidation Process and Photocatalysis

An advanced oxidation process involves oxidizing species of higher potential compared to the normal oxidation process. The capability of the oxidizing species depends on the oxidation potential of the oxidizing species.

Advanced oxidation processes generally involve generation and use of powerful oxidizing species, primarily the hydroxyl radical (OH*)[1-10]; in some advanced oxidation processes, singlet oxygen or O (1D) has also been identified as the dominant oxidizing species. Table 1-2 shows that OH* has one of the highest[1] oxidation potential which is perhaps why OH* based oxidation processes have gained much attention of many advanced oxidation technology/process developers for implementation. In addition to that as shown in Table 1-3, most environmental contaminants react much faster[1] with OH* compared with O_3. OH* can be generated by both photochemical processes (ultraviolet [UV] radiation or in combination with O_3, H_2O_2, or a photo sensitizer) and non-photochemical processes (electron beam irradiation O_3 in combination with H_2O_2, or Fenton's reagent).

Table 1-2. Oxidation potential of several oxidants[1,2] in water

Oxidant	Oxidation Potential (eV)[2]
OH*	2.8
O (1D)	2.42
O_3	2.07
H_2O_2	1.77
Perthyroxy radical	1.7
Permanganate Ion	1.67
Chlorine dioxide	1.5
Chlorine	1.36
O_2	1.23

Table 1-3. Rate constants[1] for O_3 and OH* reactions with organic compounds in water.

	Rate Constant ($M^{-1}S^{-1}$)	
Compound Type	**O_3**	OH*
Acetylenes	50	10^8 to 10^9
Alcohols	10^{-2} to 1	10^8 to 10^9
Aldehydes	10	10^9
Alkanes	10^{-2}	10^6 to 10^9
Aromatics	1 to 10^2	10^8 to 10^{10}
Carboxylic acids	10^{-3} to 10^{-2}	10^7 to 10^9
Chlorinated alkenes	10^{-1} to 10^3	10^9 to 10^{11}
Ketones	1	10^9 to 10^{10}
Nitrogen-containing organics	10 to 10^2	10^8 to 10^{10}
Olefins	1 to 450 *10^3	10^9 to 10^{11}
Phenols	10^3	10^9 to 10^{11}
Sulfur-containing organics	10 to 1.6 *10^3	10^9 to 10^{11}

AOP technologies can be broadly divided into the following groups:

1) Vacuum ultraviolet (VUV) photolysis

2) Ultraviolet (UV)/Oxidation processes

3) The Photo-Fenton

4) Sensitized AOP processes.

1.3.1 VUV Photolysis

Photolysis[1,2] of water by using UV radiation of a wavelength shorter than 190 nanometers yields hydroxyl radical OH* (oxidizing agent) and hydrogen radicals $H^{\cdot}$ (reducing agent). Contaminants in water and in a relatively high-humidity air stream can be degraded through oxidation by OH* and reduction by $H^{\cdot}$.

1.3.2 UV/Oxidation Processes

This processes generally involves generation of OH* through UV photolysis[1,2] of conventional oxidants hydrogen peroxide (H_2O_2) and ozone. Both UV/H_2O_2 and UV/O_3 processes are commercially available and have been successfully implemented[1,2].

1.3.3 Photo - Fenton Processes

In this process generation of OH* is achieved by decomposition of H_2O_2 using ferrous ion/ferric iron (Fe (II))/ (Fe (III))[1,2] under the acidic conditions. The rate of removal of organic pollutants and the extent of mineralization using the Fe (II)/H_2O_2 reagents are improved considerably by irradiation with near UV radiation and visible light.

1.3.4 Sensitized AOP processes

Sensitized AOP processes, are broadly categorized as dye sensitized and semiconductor sensitized processes. In a dye-sensitized AOP process, visible light is absorbed by a sensitized dye[1,2, 10-15] and it excites the dye molecules to a higher energy state. The excited dye molecule then transfers some of its excess energy to other molecules present in the waste stream, which results in a chemical reaction. When dissolved oxygen in water accepts energy from the excited dye molecule, the dissolved oxygen is converted into singlet oxygen (O), a powerful oxidant.

In a semiconductor[1,2,10-15] sensitized AOP process, metal semiconductors are used to destroy/degrade the environmental contaminants by means of light-induced redox reactions. These reactions involve generation of hole-electron pair by the transfer of electron from valence band to the conduction band by absorbing UV irradiation in semiconductor materials such as titanium dioxide (TiO_2). In this process, the formation and availability of OH* can be maximized by the addition of oxidants such as H_2O_2 and O_3.

In order for photocatalysis to be used commercially, design of the reactor plays a significant role for maximum utilization of UV light by photocatalyst particles. The reactor design also should be able to provide interface for the contact of the photocatalyst and the contaminant.

It is better for the photocatalyst to be immobilized to avoid the complicated separation of ultrafine photocatalyst particles from the treated water. Since the reaction takes place only on the surface of the photocatalyst illuminated by UV light, the effective sites in a photocatalytic reactor are those places where photocatalyst, UV light and reactants exist at the same time. By

using the immobilized photocatalyst a uniform distribution of the UV light can be made on the photocatalyst surface by proper design of the light source to illuminate uniform intensity across the photocatalytic surface. The constraint of limited UV light penetration depth must be taken into consideration in the reactor design, as UV light cannot penetrate more than 2-3cm in water.

1.4 Photocatalysis

A photocatalyst[10-25] is substance whose function is activated by the absorption of a photon (light energy). It appears in the rate expression describing a reaction without appearing in the stoichiometric equation of the reaction.

Organic Pollutant + O_2 $\xrightarrow{\text{(light + photocatalyst)}}$ $CO_2 + H_2O + \ldots$

One can induce organic redox reactions photochemically with either organic or inorganic catalysts.

$$TiO_2 \xrightarrow{h\nu} e^- + h^+$$ (Photogenertion of electron and hole pairs)

$$h^+ + H_2O \rightarrow OH^\bullet + H^+$$ (Formation of radicals)

$$e^- + O_2 \rightarrow O_2^-$$

The UV light of wavelength less than 385 nm, which corresponds to a band gap (band gap is the energy required to excite the electron from the valence band to the conduction band) of 3.2 eV is used in the excitation of TiO_2 molecule in photocatalysis process.

A wide variety of chemical compounds (organic and inorganic compounds) are being successfully[10-15] treated using photocatalysis as listed by the EPA[1]. The list of compounds includes priority pollutants, air toxics as compiled by the EPA.

1.4.1 Significance of TiO_2

The oxide of choice is TiO_2 because it is inexpensive, non-toxic, and does not undergo photocorrosion[15]. From the band gap perspective, absorption of a near UV photon (wavelength, 385 nm) is regarded as exciting an electron from the valence band to the conduction band as shown in the Figure 1-2[15]. TiO_2 is the most commonly used among all the photocatalysts; Considerable research has been done in use of TiO_2 photocatalyst in degradation of organic compounds[1].

1.4.1.1 Structure

Titanium dioxide is used as photocatalyst in two crystallographic structures[15]: rutile and anatase (Figure 1-3). In both structures, each titanium ion is at the center of an oxygen octahedron. In the rutile form, the oxygen ions form a slightly distorted hexagonal compact lattice.

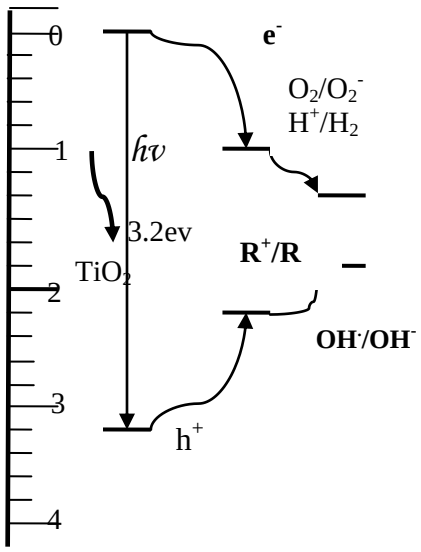

Figure 1-1. Band gap of TiO_2[15,18,19] (R=reductant)

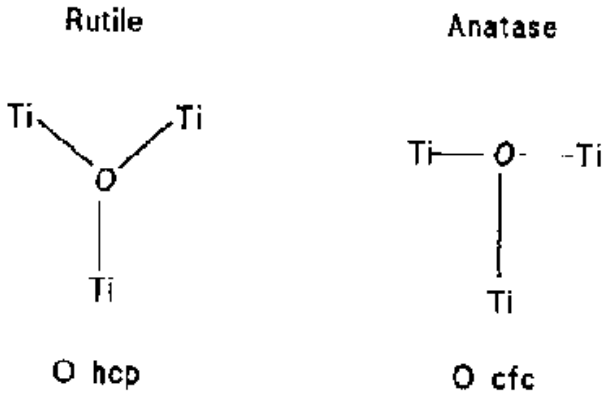

Figure 1-2. Anatase and Rutile[15,18,19] TiO_2 Structure[10]

In the anatase form, the oxygen atoms form a CFC (face centered cubic) lattice. In both structures, each oxygen has three coplanar neighbor titanium cations. But in rutile, the three Ti-O-Ti angles are roughly equal to 120°. In anatase, on the other hand, one of the Ti-O-Ti angles is about 180º while the two others are close to 90º. Because of the Hall mobility difference, the movement of electrons in the anatase structure is easy compared to rutile. This makes the anatase form more favorable for photocatalysis, as the electron from the conduction band in anatase phase reaches the valence band (surface of the TiO_2 particle) more easily when compared to rutile phase. The anatase TiO_2 was observed to be more effective[15] when compared to rutile TiO_2 and there was difference in the reaction rates from anatase TiO_2 and rutile TiO_2 in degradation of organic contaminants[15].

Anatase form is preferred[15,18] when compared to the rutile form in the photocatalysis process. It has been observed[26] during the synthesis of the TiO_2 particles, the anatase particles are formed when the particles are calcined at temperatures ranging from the 500-900 ºC.

Table 1-4. Selected physical properties[15,18,19] of rutile and anatase TiO_2

	Rutile	Anatase
Band gap energy	3.03 eV	3.2 eV
Hall mobility	0.1 $cm^2/(Vs)$	4 $cm^2/(Vs)$

1.4.2 Oxidation-Reduction Reactions

At this point, I would like to go into slightly greater detail concerning the photocatalytic reactions occurring on the surface of titanium dioxide.

The reaction starts with the absorption of light by the titanium dioxide, which results in two types of carriers: electrons (e^-) and holes (h^+) are generated due to the transfer of an electron from the valence band to the conduction band. In most materials that are electrically conductive, i.e, metals, the bands overlap so they are never separated. On semiconductors such as titanium dioxide, however, they survive for longer periods of time[15,18,19]. The ratio of the recombination rate (between electrons and holes) to the rate of production of electron–hole pairs is a good indicator of the maximum efficiency of a photocatalytic reaction.

On the surface of the catalyst, there is a single layer of tightly adhering (adsorbed) [10-15] water molecules. When these adsorbed water molecules interact with holes, hydroxyl radicals are formed. The hydroxyl radicals can then react with organic compounds, initially producing free radicals. When molecular oxygen O_2 is present in the water, because it also has unpaired electrons, it often reacts[1-15] with some other contaminants as a oxidizing agent. In a short time, organic compounds are completely degraded, *i.e,* converted into carbon dioxide and water.

The electron produced in the electron-hole pair is used in a reduction process *i.e,* add electrons to oxygen dissolved in the water or in the air. Because oxygen is easier to reduce than water, it will tend to be reduced producing the superoxide radical anion (O_2^-). The superoxide anion attaches itself to the peroxyl organic radicals. Superoxide (electron rich) greatly increases the reduction process, in the form of a combustion process.

Organic compounds are easier to oxidize than water. Therefore, when the concentration of the organic compound is high, the photo-generated holes can react directly with these compounds rather than the predominant process of first reacting with water to produce hydroxyl radicals. Anytime you eliminate one of the intermediate steps like this, you can increase the overall efficiency.

The hole and electron pair formed on the surface of the catalyst can recombine which reduces the effectiveness of the catalyst. The rate determining step of photocatalysis process is the transfer of electrons to molecular oxygen. The reaction rate can be increased by decreasing the recombination rate of hole-electron pair.

1.4.3 Sequence of events in Photocatalysis

The sequence of events[15,18,19] in a photocatalysis process are described below

1. Photons of incident light are absorbed by the semiconductor.

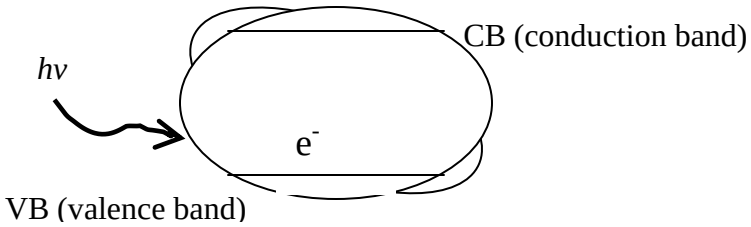

2. Electrons are promoted from the valence band to conduction band thereby creating an electron hole pair.

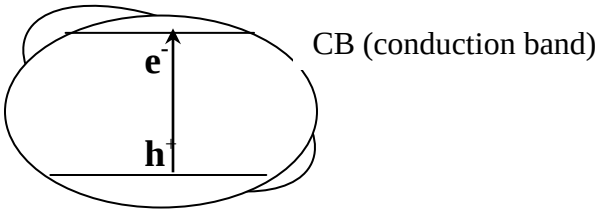

3. Mobile electron & hole each participate in a reaction, and catalyst is "regenerated". The surface electron e^- is involved in reduction process and the h^+ is involved in the oxidation process.

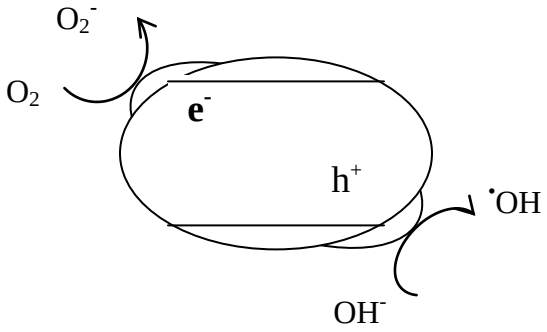

As mentioned earlier, the form of TiO_2 particles, whether it is an anatase or rutile form, plays a significant role in the photocatalytic behavior/performance of the TiO_2 particles. The form of TiO_2 particles is based on the synthesis mechanism used in the synthesis of TiO_2 particles as discussed below.

1.4.4 TiO_2 particle size

During the synthesis of TiO_2, rate of hydrolysis controls[20,23] the size of the TiO_2 particle formed, and the size of the particle has an influence[20,23] on the photocatalysis because the smaller size particle has greater specific surface area[20,21,23]. However, if the TiO_2 particle size is too small[20,21,22], light scattering effects can reduce light absorption efficiency.

The limiting factors in the photocatalysis process using TiO_2 particles is the high recombination rate of hole-electron pair and the narrow range of band gap energies for the excitation of electron. To overcome these limiting factors, doping of TiO_2 particles/film with metal dopants is common.

1.4.5 Significance of Doping

A mechanism of increasing the overall efficiency of the photo catalytic process is by increasing the transfer of electrons to oxygen molecules. This can be accomplished by depositing very small particles (*e.g*, on the order of several nanometers in diameter) of a metal such as palladium or iron on the titanium dioxide particles to act as electrochemical catalysts or "electro-catalysts." This process is known as doping[24-28] of the TiO_2 surface. Usually metallic compounds are used for the purpose of doping to enhance[24-28] the photocatalysis process, where the metallic atoms on the surface of the TiO_2 attract the electron and prevent recombination[24-28] of electron-hole pair.

It has been observed that there was significant increase in the reaction rate of the photocatalytic process based on the dopant. The dopant attracts the electron[24-28] in electron-hole pair in the conduction band, decreasing the recombination rate of the electron-hole pair and increasing the life time of the hydroxyl radicals allowing more opportunity to oxidize the organic contaminant and the reduction reaction of the electron.

The other significant behavior noticed because of doping is the shift in band gap[24,25] of the wavelength of the photon required for the excitation of the electron in TiO_2 particles, for a wide

range of the wave length of ultra violet to visible region. Although not fully successful yet, considerable research[24-28] is going in the photocatalysis process using visible light by the application of dopants.

1.4.6 Photocatalysis using Photocatalyst Thin Film

Most of the recent research work[28-42] in the field of photocatalysis has been using the thin film photocatalysts. The thin film properties such as thickness, porosity and UV light transmission play significant role in the photocatalysis process. Thin film coating using various methods such as sputtering[43], chemical vapor desposition[44], Sol-Gel[45] and ESA[46] methods have been used in the creation of photocatalytic films.

1.4.6.1 Photocatalysis Using slurry and Thin Film

Several reactor configurations have been evaluated using TiO_2 particles in a slurry[47-49]. The reactors were successfully used in the degradation of many contaminants, but had several limitations such as UV light penetration depth (UV light can penetrate no more than 2-3cm)[15,18,28,30,31] post treatment of water to remove the TiO_2 particles in the slurry.

Many of the drawbacks in the photocatalytic process using slurry can be overcome by deposition of the film on quart surface which eliminates the limitations caused by slurry particles, which are shown below:

Significance of immobilized TiO_2 thinfilm on quartz tubes:

- The TiO_2 photocatalyst deposited as thin film on quartz tubes overcomes the difficulty in recycling the photo catalyst or separation of the photocatalyst from the treated water.
- The light penetration depth in water is too small. This can be overcome by using TiO_2 immobilized film with an environment for the contact of the UV light and TiO_2 particles.
- TiO_2 immobilized on quartz/glass provides more feasible environment for photocatalytic activity than TiO_2 on stainless steel or glass because of the high UV light transmission of quartz.

Because of the constraints of using TiO_2 slurry as photocatalyst and advantages of using the thin film photocatalyst, the thin film gives the opportunity for efficient usage of UV light and doesn't require any post treatment process.

1.5 Summary

Most of the existing water treatment processes that degrade the hazardous compounds to non-hazardous compounds are too slow or expensive. The degradation of the hazardous compounds using biological process is quite slow when compared to AOP. The AOPs are currently the strongest oxidizing process which can degrade the hazardous compounds into non-hazardous compounds.

Most of the AOP process use strong oxidant chemicals which must be handled safely, where as photocatalysis process does not use any chemicals of safety concern. The photocatalyst uses UV light as the energy source for the reaction. It was also observed that the photocatalysis process

performance was better when compared to direct UV treatment of contaminant by photolysis process.

Based on the limitations described in this chapter in reactor design and usage of photocatalysis, the photocatalysis process needs to be implemented by coming up with a mechanism to enhance the film behavior and reactor design for effective and most efficient usage of TiO_2 film and light source. I will explain my work in the following chapters for solving the problems for photocatalyst film deposition and reactor design.

1.6 References

1. EPA (1998), Handbook on Advanced Photochemical Oxidation Processes, *EPA/625/R-98/004*.

2. Parsons, S. A. (Ed.) (2004), Advanced Oxidation Processes for Water and Waste Water Treatment, IWA Publishing, London.

3. Bolton, J. R. (2001), Figures of Merit for the Technical Development and Application of Advanced Oxidation Technologies, *Pure Appl. Chem, 73*, 627.

4. Murray, C. A. and S. A. Parsons (2003), Comparison of AOPs for the Removal of NOM: Performance and Economic Assessment, 3rd Conference on Oxidation Technologies for Water and Waste water Treatment, Goslar, Germany, 18-22 may 2003.

5. Oppenländer, T. (2002), Photochemical Purification of Water and Air: Advanced Oxidation Processes (AOPs): Principles, Reaction Mechanisms, Reactor Concepts, 1st ed, 368 pp, Wiley-Vch.

6. Enric, B, M. Eva, S. Roser, S. Laura, P. José, D. Xavier, and C. Juan (1998), Aniline mineralization by AOP's: anodic oxidation, photocatalysis, electro-Fenton and photoelectro-Fenton processes, *Applied Catalysis B: Environmental, 16*, 31-42.

7. Gramith, J. T. (1995), Oxidation Processes: Advanced Oxidation Processes. Advances in Taste and Odor Treatment and Control, AWWARF/LDE,Denver, Colarado.

8. Haag, W. R. (1992), Photooxidation of Organic Compounds in Water and Air Using Low-Wavelength Pulsed Xenon Lamps, ACS Symposium on Aquatic and Surface Photochemistry, San Francisco.

9. Von, G. U. and Y. Oliveras (1998), Advanced Oxidation of Bromide-Containing Waters: Bromate Formation Mechanisms, *Environmental Science & Technology, 32*, 63-70.

10. Alvares A.B.C, D, C. and S. A. Parsons (2001), Partial oxidation of hydrolysed and unhydrolysed textile azo dyes by ozone and the effect on biodegradability, *Transactions of the Institution of Chemical Engineers (Part B), 79*, 103-109.

11. Alvares, A. B. C, C. Diaper, and S. A. Parsons (2001), Partial oxidation by ozone to remove recalcitrance from waste waters - a review, *Environmental Technology, 22*, 409-427.

12. Spartan water treatmnet, Advanced Oxidation Process, *http://www.* spartanwatertreatment. com/advanced-oxidation-processes. html, 2011.

13. Joon, C. L, S. K. Moon, and W. K. Byung (2002), Removal of paraquat dissolved in a photo reactor with TiO_2 immobilized on the glass-tubes of UV lamps, *Water research, 36*, 1776-1782.

14. Paola, A. B, A. E. Carina, E. F. Rosana, A. G. Eduardo, T. G. Raquel, and I. L. Marta (2001), Kinetics and Mechanism of EDTA Photocatalytic degradation with TiO_2, *Water Science and Technology, 44*, 179-185.

15. Schiavello, M. (1997), *Heterogeneous Photocatalysis*, 208 pp, John Wiley & Sons Canada, Ltd.

16. Ignjatovic, N, Z. Brankovic, M. Dramicanin, J. M. Nedeljkovic, and D. P. Uskokovic (1998), Preparation of TiO_2 and Zno Thin Films by Dip-Coating method, *Material Science Forum, 282-283*, 147-152.

17. Lim, T. H, S. M. Jeong, S. D. Kim, and J. Gyenis (2000), Degradation characteristics of NO by photocatalysis with TiO_2 and CuO/TiO_2, *React. Kinet. Catal. Lett, 71*, 223-229.

18. Akira, F, H. Kazuhito, and W. Toshiya (Eds.) (1999), *TiO_2 Photocatalysis: Fundamentals and Applications*, 1st ed, Bkc, Inc, Tokyo.

19. Schiavello, M. (Ed.) (1988), *Photocatalysis and Environment Trends and Applications*, 1st ed, 732 pp, Springer.

20. Lee, E. A, S. W. Lee, C. H. Choi, H. S. Kjim, and B. Hockey (2003), Effect of TiO_2 powder size on the reactivity of Photocatalyst, *Materials Science forum, 439*, 288-296.

21. Chen, D, F. Li, and K. R. Ajay (2000), Effect of Mass Transfer and Catalyst Layer Thickness on Photocatalytic Reaction, *AICHE Journal, 46*, 1034-1045.

22. Jia-guo, Y, Z. Xiu-jian, Z. Gao-ke, H. Jian-jun, and Z. Qing-nan , Grain size and photocatalytic Activity of nanometer TiO_2 thin Films Prepared by the Sol-Gel Method".Ed, Vol .16 No.2, *Journal of Wuhan University of Technology-Mater. Sci, 16*.

23. Kim, S. J. (2001), Photocatalytic Effects of Rutile Phase TiO_2 Ultrafine Powder with high Specific Surface Area Obtained by a Homogenous precipitation Process at Low Temperatures, *Journal of Sol-Gel Science and technology, 22,* 63-74.

24. Akihiko, H. (2001), Highly Photocatalytic activity of F-Doped TiO_2 Film on Glass, *Journal of Sol-Gel Science and technology, 22*, 47-52.

25. Xiaobo, C, L. Yongbing, D. Smita, Q. Xiaofeng, K. C. B. Robert, Z. Chengfang, and B. James (2005), Doped Semiconductor Nano materials, *Journal of Nano science and Nanotechnology, 5*, 1408-1420.

26. Shah, S. I, W. Li, C. P. Huang, O. Jung, and C. Ni (2002), Study of Nd^{3+}, Pd^{2+}, Pt^{4+}, and Fe^{3+} , dopant effect on photoreactivity of TiO_2 nanoparticles **,** *PNAS, 99*, 6482-6486.

27. Kim, S. and W. Choi (2002), Dual Photocatalytic Pathways of Trichloroacetate Degradation on TiO2:Effects of Nanosized Platinum Deposits on Kinetics and Mechanism, *J. Phy. Chem B, 106*, 13317.

28. Dvoranova, D, V. Brezova, M. Mazur, and M. A. Malati , Investigations of metal-doped titanium dioxide photocatalyst, *Applied Catalysis B: Environmental, 37*, 91-105.

29. Joon, C. L, S. K. Moon, and W. K. Byung (2002), Removal of paraquat dissolved in a photo reactor with TiO_2 immobilized on the glass-tubes of UV lamps, *Water research, 36*, 1776-1782.

30. Chen, A, G. Lu, Y. Tao, Z. Dai, and H. Gu (2001), Novel photocatalyst Immobilized on springs and Packed Photo reactor, *Mater. Phys. Mech, 4*, 121-124.

31. Masuda , Y, T. Sugiyama, W. S. Seo, and K. Koumoto (2003), Deposition Mechanism of anatase TiO_2 on self –assembled Monolayer's from an aqueous solution, *Chem Mater, 15*, 2469-2476.

32. Shirkhanzadeh, M. (1995), Fabrication and characterization of Alkoxy Derived Nano phase TiO_2 Coatings, *nano structured Materials, 5*, 33-40.

33. Yasumori, A, H. Shinoda, Y. Kameshima, S. Hayashi, and K. Okada (2001), Photocatalytic and photo electrochemical properties of TiO_2 –based multiple layer thin film prepared by sol-gel and reactive sputtering methods, *J. Mater. Chem, 11*, 12533.

34. Mansor, A. H. and A. R. Ismail (2003), Preparation of titanium dioxide(TiO_2) thin films by sol gel dip coating methods, *Malaysian Journal of chemistry, 5*, 086-091.

35. Nobuaki, N. and T. Koti (2001), Preparation of TiO_2 thin Film Photocatalysts by Dip Coating Using a Highly Viscous Solvent, *Journal of Sol-gel Science and Technology, 22*, 23-31.

36. Miah, M. Y, i. Hiroaki, and H. Hiroshi (2002), Preparation of porous Titania film by Modified Sol-Gel Method and its application to Photocatalyst. 25, 65-74, *Journal of Sol-gel Science and Technology*, 65-74.

37. Michael, G. (2001), Sol-Gel processed TiO_2 Films for Photovoltaic Applications, *Journal of Sol-gel Science and Technology, 22*, 7-13.

38. Walid, A. D. and H. X. John (2004), Low temperature Sol-Gel processed photocatalytic Titania Coating, *Journal of Sol-Gel Science and Technology, 29*, 25-29.

39. Masanari, T, M. Keisuke, and T. Hiroshi (1989), Pt-TiO_2 thin film on glass substrates as efficient photocatalysts, *Journal of Material Science, 24*, 243-246.

40. Fukayama, S. (1995),Highly Transparent and Photoactive TiO_2.sub.2. Thin Film Coated on Glass Substrate, *Electrochemical Society, 187TH*, 1102-1103.

41. Byrne, J. A, A. Davidson, P. S. M. Dunlop, and B. R. Eggins (2002), Water treatment using nano-crystalline TiO_2 electrodes, *Journal of photochemistry and photobiology. A, Chemistry, 148*, 365-374.

42. Butterfield, I. M, P. A. Christensen, A. Hamnett, K. E. Shaw, G. M. Walker, and S. A. Walker (1997), Applied studies on immobilized titanium dioxide films as catalysts for the photo-electrochemical detoxification of water, *Journal of Applied Electrochemistry, 27*, 385-395.

43. Karunagaran, B, R. T. Rajendra kumar, C. Viswanathan, D. Mangalaraj, S. K. Narayandass, and G. Mohan Rao (2003), Optical constants of DC magnetron sputtered

titanium dioxide thin films measured by spectroscopic ellipsometry, *Cryst. Res. Technol, 38*, 773-778.

44. Hugh, O. P. (Ed.) , Handbook of Chemical Vapor Deposition: Principles Technology and Applications, 2nd ed, Noyes Publications.

45. Yasumori, A, H. Shinoda, Y. Kameshima, S. Hayashi, and K. Okada (2001), Photocatalytic and photo electrochemical properties of TiO_2 –based multiple layer thin film prepared by sol-gel and reactive sputtering methods, *J. Mater. Chem, 11*, 12533.

46. Spillman Jr, W. B, T. Zeng, and R. O. Claus (2002), Modeling the Electro-static self-assembly process using stochastic cellular automata, *Smart mater Structure, II*, 623-630.

47. Kim, S. and W. Choi (2002), Kinetics and Mechanisms of Photocatalytic Degradation of (CH3)nNH4-n +(0<n<4) in TiO_2 suspension: the role of •OH radicals. . 2002, 36, 2019-2025, *Environ. Sci. Technol, 36*, 2019-2025.

48. Nguyen, V. N. H, A. Rose, and B. Donai (2003), Effect of formate and methanol on photo reduction/removal of toxic cadmium ions using TiO_2 semiconductor as photocatalyst, *Chemical Engineering Sciences, 58*, 4429-4439.

49. Wilcoxon, J. P. (1999), Photo-oxidation of organic Chemicals Using semiconductor Nano clusters, Rocky Mountain conference on Analytical Chemistry, Denver, CO, August 11 1999.

2. REVIEW OF PHOTOCATALYTIC REACTOR DESIGN

2.1 Importance of Photocatalytic Reactor Design

Photocatalytic reactor design and configuration plays a significant role in the effectiveness of photocatalytic reactors. The essential factors influencing the reactor performance is the environment for the contact of light, TiO_2 and the contaminant.

A well-designed photocatalytic reactor should have effective high rate of mass transfer of contaminant during the photocatalysis process, where the contaminant degrades on the surface of the TiO_2 photocatalyst. Once the contaminant molecule is degraded at TiO_2 surface, another contaminant molecule needs to be transported from the bulk of the liquid to the surface of the TiO_2 particle. The reactor requires proper mixing inside the reactor for the movement of the contaminant.

The light source should be designed to focus most of the light being utilized directly on to the TiO_2 surface, rather than being transmitted through the water. The UV light transmission of the substrate material on which the TiO_2 film is to be coated plays a significant role in light propagation along the substrate material or any other medium light needs to propagate to reach the film surface.

Previously many researchers[1-14] have examined photocatalysis in different reactor configurations using TiO_2 slurry and thin film with different UV light sources. As discussed in chapter 1, the constraints for these reactors are the need for the removal of TiO_2 particles at the outlet stream, poor environment for efficient use of TiO_2 film and UV light as the UV light penetration depth in

water is about an inch[42]. The reactor configuration should be designed where the UV light source and TiO_2 film need to be separated by a distance of no more than an inch in water.

2.2 Reactor Configurations

A number of photocatalytic reactors have been proposed, but none has been successfully implemented on a large scale[1-18]. The reactors can be categorized based on the manner in which the catalyst is used (slurry or thin film), and on the arrangement of the light source and the reactor vessel, some of the reactor configurations are explained below. Even though there were several reactor configurations being researched, we will be discussing some of the designs which were effective in degradation of organic compounds but had several shortcomings; the individual reactor configuration, results and shortcomings are explained in table 2-2.

2.2.1 Distributive Type Reactor

Distributive reactors[15] are reactors in which the light from the source is transmitted by optical means such as reflectors and light transmitting medium such as optical fibers/quartz rods. The light is transmitted through the reactor by reflection and refraction inside the rod and external surface of the rod was coated with the photocatalyst. The drawback of the system was the light intensity drops across the reactor by reflection and refraction and large scale reactors can't be designed due to this.

This reactor design is limited to small scales by the low values of the key design parameters. The only way to apply these systems to large-scale applications is by using multiple units.

2.2.2 Glass Tubular Photo Chemical Reactor

Glass tube photochemical reactor performance, shown in Figure 2-1, was analyzed with and without a TiO_2 film[9]. The dimensions of the glass tubular photochemical reactor were 330 mm high, with inner diameter of 55 mm and volume capacity of 0.6 L. The TiO_2 film was coated on an aluminum sheet of height 300 mm, 180 mm wide and 0.18 mm thick which was attached to the interior surface of the reactor.

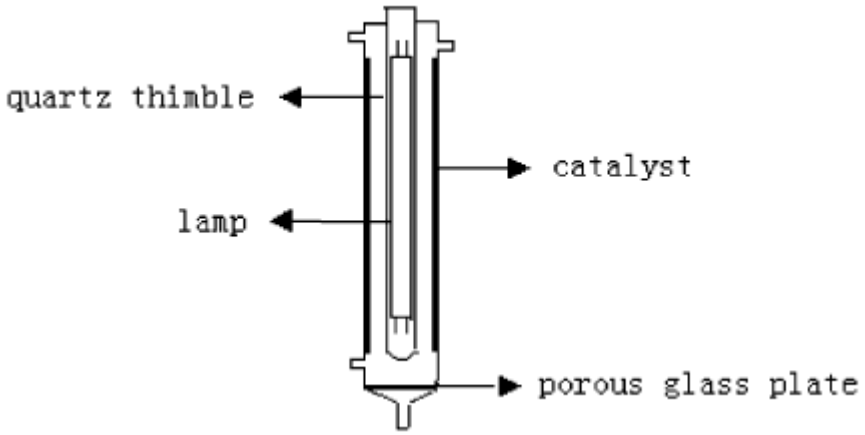

Figure 2-1: Tubular Photochemical Reactor[9](with copyright permission 2.5.1)

The aluminum sheet was used with and without TiO_2 catalysis to measure the reaction rate with and without the film by photolysis process. The experiment was also performed using different wavelengths to evaluate the best wavelength for the photocatalyst performance[9]. Two types of low-pressure mercury lamps were used to provide UV or VUV illumination, where UV lamp emitted at 254 nm (8 W), and a VUV lamp emitted at both 254 nm and 185 nm (8 W). The UV lamp was placed in the center of the cylindrical photo reactor enclosed in a quartz tube of external diameter 25 mm. The distance to the photocatalyst surface of the reactor wall and the light source quartz tube external surface was 15 mm.

Degradation of p-chloro benzoic acid was performed to evaluate the reaction kinetics based on the initial concentration of p-CBA. The presence of titanium dioxide increased the decomposition of p-CBA and TOC reduction, and the TiO_2/VUV combination was the most efficient process among all the process as shown in table 2-1.

Table 2-1: First Order Reaction rate constants at different initial concentration using different experimental setup and conditions[9](copyright permission 2.5.1).

UV		TiO_2/UV		VUV		TiO_2/VUV	
Con. (μg/L)	K (min^{-1})	Con. (μg/L)	K (min^{-1})	Con. (μg/L)	K (min^{-1})	Con. (μg/L)	K (min^{-1})
449	0.0220	454	0.0361	432	0.2197	431	0.2381
1108	0.0266			1145	0.1619		
1709	0.0221			1691	0.1232		
2196	0.0250	2109	0.0333	2135	0.0843	2089	0.1001

Even though the results (table 2-1) showed the photocatalytic degradation, there wasn't considerable improvement compared to UV oxidation of contaminant[9]. Among the factors affecting the photocatalyst performance is the distance between the photocatalytic surface and the UV light source, in the experiment setup the light needs to travel through the water to illuminate the photocatalyst surface for photocatalyst process to occur.

2.2.3 Multiple Tubular Reactor

The reactor modeled was based on a bench scale using hollow tubes[18]. The reactor is a cylindrical vessel of diameter 0.056 m with 54 hollow quartz tubes of diameter 0.006 m inserted inside. Both the ends of the tubes are held by Teflon plates with perforated holes to pass the quartz tubes through it.

The reactor configuration imitates a shell and tube heat exchanger, where the water solution with contaminant flows in the shell side and the light from light source is transmitted along the hollow tubes (tubular side). The external surface of tubes was coated with the photocatalyst exposed to the shell side. The tubes were arranged at a triangular pitch of 0.7 cm.

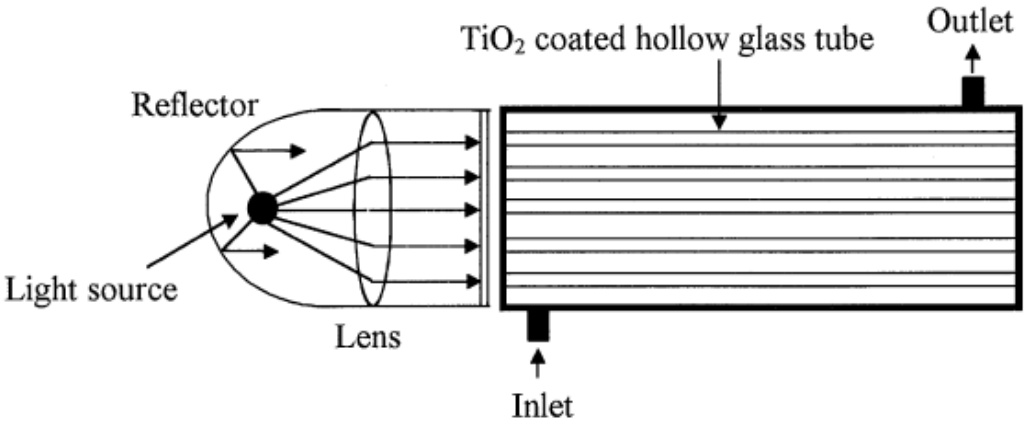

Figure 2-2: Multiple Tubular Reactor [18(Copyright permission 2.5.2)].

The reactor performance is dependent on the penetration of UV light from one end of the reactor through a lens across the reactor length inside the hollow tubes by reflection and refraction, the light penetration is dependent on the parameters intensity of light, angle of incident on the centre of tube, tube diameter and thickness of the hollow tubes.

The experiment was performed changing the reactor parameters in a semi-batch process with flow from a reservoir using a gear pump to the reactor and back to the reservoir in degradation of SBB dye. Along the flow line to the reservoir a cuvette spectrophotometer was used for continuous online measurement of the solution concentration. The experimental results showed 90% of pollutant was degraded in 100 min.

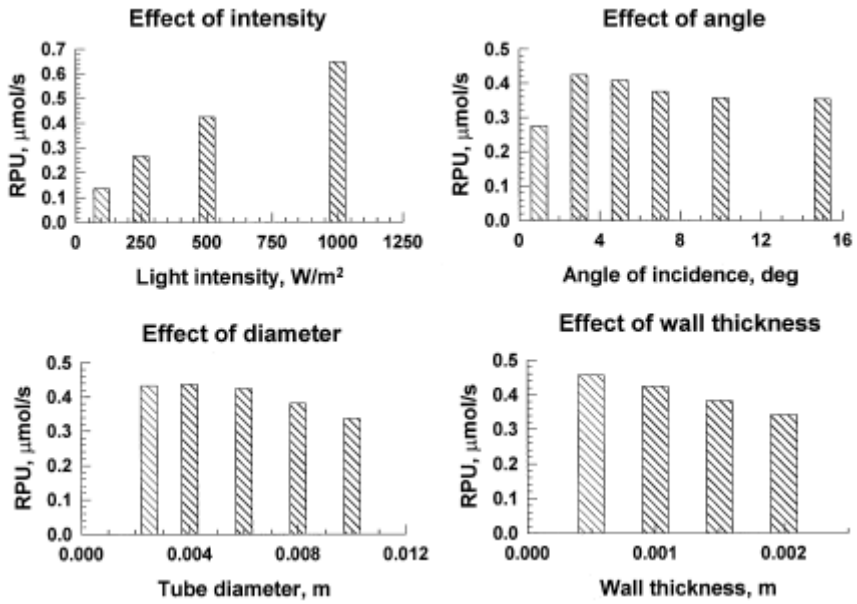

Figure 2-3: Effect of individual parameters Intensity of light, angle of incident, tube wall thickness and diameter of the tube on the reactor performance [18(Copyright permission 2.5.2)].

The major drawbacks/constraints of this reactor design were insufficient mixing inside the reactor, for the mass transfer of contaminant from bulk liquid to TiO_2 surface and back to the bulk liquid after reaction. The light intensity is non-uniformly distributed across the length of the reactor and thereby the photocatalyst surface is not used affectively, and the light travels a very short distance by reflection and refraction across the length of reactor.

2.2.5 Tubular Lamp Reactor

Tubular lamp reactor[19] consists of a stainless steel flat top plate with 21 holes, which was welded to another plate perpendicularly in the middle. 21 U-shaped lamps were placed around the second vertical plate and with both ends extended through the holes of the top plate for electrical connections. The exterior surfaces of the tubes were coated with the TiO_2 film.

The reactor was tested using SBB dye solution with an initial concentration of 0.5 mol/m3, 90% of the dye solution got degraded in 1hr. It was also observed the increase in flow rate increased the reaction rate and after sometime it resulted in bubbles inside the reactor.

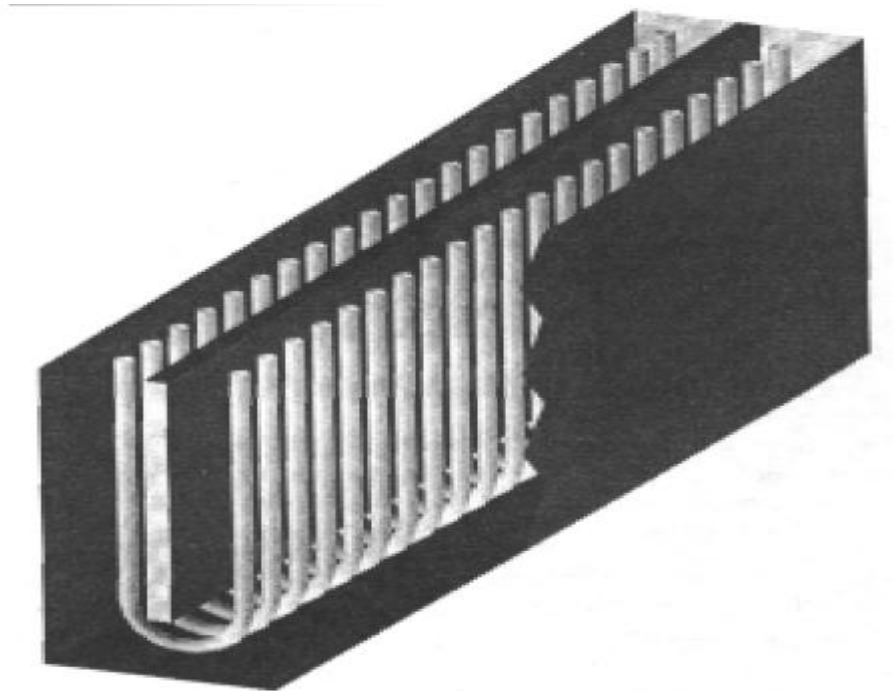

Figure 2-4: Tubular Lamp Reactor [19] **(Copyright permission 2.5.3)**

Even though the reactor provided the direct contact light to photocatalyst without transmitting through the liquid, the shortcomings of the reactor are it doesn't provide enough mixing and there is potential possibility of short circuit of flow in the reactor which will result in flow of pollutant through reactor without contacting the photocatalyst surface. The other drawback is the coating of the TiO_2 on the UV lamps which will impact the ability to reuse the lamps by recoating them with TiO_2 film after few runs.

2.2.6 Taylor Vortex Reactor

The experiments were conducted using concentric hollow tubes with annular space for the flow of the liquid[20]. Taylor vortices are formed when the annular gap *d* the space between the inner cylinder and the outer cylinder was small when compared to the inner cylinder radius.

Sczechowski observed that, when the photocatalyst particles were used as slurry in the reactor[21], the reaction occurred periodically when the fluid was in contact with the light illuminated inner cylinder surface. The light source was inside the rotating inner cylinder.

Taking into consideration the constraints of using a slurry reactor, the TiO_2 film was immobilized on the outer surface of the inner cylinder. This eliminates the constraints such as the separation of the TiO_2 particles and proper mixing was achieved by the centrifugal motion by the rotation of the inner cylinders. The reactor was tested in the degradation of Phenol and SBB dye at low concentration of 100ppm and was able to degrade 60% of initial concentration in 240 seconds, both the compounds showed the same final concentration suggesting the overall reaction is primarily controlled by mass transfer and not by intrinsic kinetics as SBB dye degradation rate is 400 times lower than phenol[21].

Even though the reactor provided the required mixing the reactor volume to surface area is quite small due to smaller annular space between cylinders, a small volume of the liquid can be filled in annular space which doesn't help in large scale treatment of water. The reactor can be used only on lab scale for treating very small amount of water.

2.2.7 Membrane TiO_2 Reactor

Membrane application in photocatalytic reactor was used in basically two ways[22]:

In photocatalytic TiO_2 slurry reactor, the membrane systems are used to separate the TiO_2 particles from the photocatalytic reactor outlet stream. The TiO_2 particles separated from the outlet stream of the reactor using membrane can be reused if the TiO_2 particles can be separated from other contaminants.

In the second process, the Alumina template membrane was coated with a TiO_2 film. The system acts as particulate separation membrane process, and also acts as an organic degradation process by TiO_2 photocatalytic degradation of the organic contaminant when illuminated with UV light.

The membrane system was tested in the degradation of 1000ml of 100 mg/L of Direct Black 168, The experimental results showed 80% degradation of Direct black 168 on the permeate side of the membrane after 420 min.

The shortcomings/drawbacks of both membrane processes are: in the first process where the membrane used for TiO_2 particle removal is quite expensive for large scale application. In the second process of Photocatalytic TiO_2 film membrane it provides the dual advantages of particulate separation and the photocatalytic activity in degradation of organic compounds, but the distance of 10 cm between the UV lamps and membrane doesn't help as most of the light will be absorbed by the water and pollutants in water before reaching the membrane surface.

Table 2.2: Individual reactor configurations, results and shortcomings

Reactor	Reactor Configuration	Results	Scale up of Reactor	Shortcomings/Disadvantages
Distributive type reactor	Multiple hollow lamps or quartz/glass rods coated with TiO2 Film.	Phenols, Dyes were succesfully treated.	Laboratory scale, not possible for large scale.	Light penetration through optical fibre, hollow tube is a constraint
Taylor Vortex Reactor	concentric hollow tubes with liquid passing between the tubes, the rotation of inner cyclinder for mixing (vortex).	Phenols, SBB Dyes were succesfully treated.	Not feasible for large scale reactor due to small reactor volume per film surface area.	The reactor has to be used in lab scale and due to small annular space between the tubes small volume of liquid to be treated per batch.
Tubular Lamp Reactor	Multiple U shaped inside the reactor coated with TiO2 particles.	SBB dye was succesfully degraded	Lab Scale, potential for large scale.	Not enough mixing inside the reactor for efficient mass transfer of contaminant and expensive for custom designed lamps
Multiple Tube Reactor	Multiple tubes with TiO2 film coated on quartz surface, the light penetrates through reflection and refraction.	Was able to degrade the SBB dye.	Lab Scale, potential for large scale.	The light pentrates short distance across the length of the reactor by relfection and refraction. Non-uniform distribution of light intensity across the film surface. Potential for short circuit of flow inside the reactor, not enough mixing inside the reactor.
Membrane	Membranes are used in two methods: in first methods in Slurry reactor for TiO2 Particles separation after photocatalysis process. In second methods the membrane surface is coated with TiO2 film by sol-gel method, which is being illuminated with UV light.	In second method Was able to degrade the Direct Black 168	Lab Scale.	It's a expensive setup to use the slurry reactor and usage of membrane for the separation of TiO2 particles. In the second method the distance of 10cm between UV lamp source and the TiO2 film on membrane doesn't allow the efficient usage of light as its being observed by water and contaminants before reaching the TiO2 film
Glass tubular Photochemical Reactor	The inner surface of reactor coated with TiO2 film, the UV lamps are inserted in the middle of reactor.	p-chloro benzoic acid was degraded using the process.	Lab Scale	UV light pentration through water to reach the photocatalyst surface and not enough mixing

2.3 Proposed Multiple Tube Reactor

Based on the fact that adequate reactor design has been the drawback for successful application of photocatalysis process. Even though a number of different reactors have been proposed most of them have design constraints, in direct contact of UV light to TiO_2 surface without traveling through water, the removal of TiO_2 particles in slurry, and not providing enough mixing inside the reactor resulting in potential short circuit of flow inside the reactor.

I propose a reactor using thin film of TiO_2 coated on quartz tubes. The light source UV lamps are inside the quartz tubes. The light is transmitted through the quartz material on to the TiO_2 film coated on the external surface of quartz tubes. The light doesn't need to penetrate light through the water to reach the TiO_2 film surface. The TiO_2 particles being coated on the quartz surface overcomes the problem of removal of TiO_2 particles as in slurry reactors.

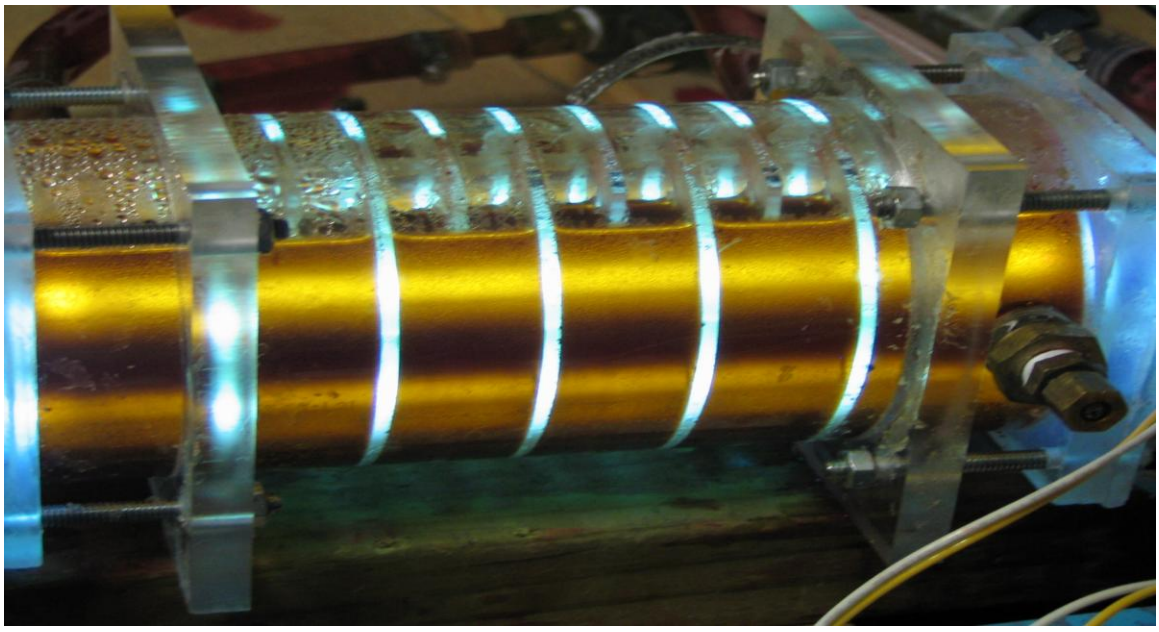

Figure 2-5: Proposed Photocatalytic Reactor.

The reactor is similar to the shell and tube heat exchanger with quartz tubes coated with TiO_2 film on the external surface. The shell side contains the water to be treated. Baffles are arranged on the shell side of the reactor with opening in opposite direction for alternate baffles, acting as flow interrupter for mixing in the reactor.

The reactor has influent and effluent ports at the opposite ends of the reactor. The water is fed in a recirculating batch reactor to feed the reactor and back to tank using a pump. The reactor will be tested in degradation of Congo red, nitro phenol and potassium iodide (KI). The influence of reactor parameters baffles, lamps and flow rate of the water on the reactor performance by performing the design of experiments.

The flow field inside the reactor was analyzed by performing 3D CFD model of the reactor for potential dead zones for mixing and for any potential short circuit of flow, the results to be discussed in chapter 5.

2.4 Summary

Some observations on the reactor design configurations are given below:

1. In slurry reactor it was observed that the surface area of contact of TiO_2 surface to the organic contaminant was good, but the effective area of TiO_2 particle that was illuminated by the UV light was not good, and also the TiO_2 particles need to be separated from the outlet stream[17].

2. In multiple tubular reactors, UV light was made to pass through quartz hollow tubes[18] which were coated with TiO_2 film. The light travels along the quartz tube by reflection

and refraction along the tube, where some of the light transmits through of the quartz tubes. The drawback is light energy wasn't utilized efficiently and non-uniform distribution of lights across the reactor.

3. The reactor with TiO_2 film coated UV lamps was observed to have an increase in performance when compared to a slurry reactor[19,20], the ratio of area which was being illuminated to the reactor volume was high. The drawbacks of the reactor were short circuit of flow and insufficient mixing.

2.4.1 Slurry vs. Film Reactor

Previously, many researchers have done research using slurry of TiO_2 particles[22-26]. The drawbacks of it compared to thin film are listed below.

- The exponential decrease of the light availability due to the scattering of UV light by particles and the UV light is being absorbed by the water[25].
- The photocatalyst particles need to be removed from the outlet stream[17].

Advantages of using immobilized thin TiO_2 film on quartz tube:

- The TiO_2 particles need not be removed from the outlet stream of treated waste water in the reactor as it is immobilized.
- The UV light doesn't need to penetrate through the water if the reactor is designed where the light reaches the film surface before reaching the water. It helps in efficient use of the UV light.

Taking all this into consideration, we propose the design for reactor where I can create an environment for the TiO_2 film-UV light for effective photocatalysis. The advantages of this reactor configuration are the UV light does not need to penetrate through water and the TiO_2 particles need not be removed from the outlet stream of water.

2.5 Appendix

2.5.1 License Details for Figure 2-1

ELSEVIER LICENSE
TERMS AND CONDITIONS

Apr 22, 2012

This is a License Agreement between ram mahipal kouda ("You") and Elsevier ("Elsevier") provided by Copyright Clearance Center ("CCC"). The license consists of your order details, the terms and conditions provided by Elsevier, and the payment terms and conditions.

All payments must be made in full to CCC. For payment instructions, please see information listed at the bottom of this form.

Supplier	Elsevier Limited The Boulevard,Langford Lane Kidlington,Oxford,OX5 1GB,UK
Registered Company Number	1982084
Customer name	ram mahipal kouda
Customer address	411 palm dr glendale, CA 91202
License number	2831540815306
License date	Jan 17, 2012
Licensed content publisher	Elsevier
Licensed content publication	Water Research
Licensed content title	Photocatalysis of*p*-chlorobenzoic acid in aqueous solution under irradiation of 254nm and 185nm UV light
Licensed content author	Wenya Han,Pengyi Zhang,Wanpeng Zhu,Jingjing Yin,Laisheng Li
Licensed content date	November 2004
Licensed content volume number	38
Licensed content issue number	19
Number of pages	7
Start Page	4197
End Page	4203
Type of Use	reuse in a thesis/dissertation
Portion	figures/tables/illustrations
Number of figures/tables /illustrations	1
Format	both print and electronic
Are you the author of this Elsevier article?	No
Will you be translating?	No
Order reference number	None
Title of your thesis/dissertation	Photocatalytic Reactor using Thin TiO2 film on Quartz tubes
Expected completion date	Apr 2012
Estimated size (number of pages)	150
Elsevier VAT number	GB 494 6272 12
Permissions price	0.00 USD
VAT/Local Sales Tax	0.0 USD / 0.0 GBP
Total	**0.00 USD**
Terms and Conditions	

INTRODUCTION

1. The publisher for this copyrighted material is Elsevier. By clicking "accept" in connection with completing this licensing transaction, you agree that the following terms and conditions apply to this transaction (along with the Billing and Payment terms and conditions established by Copyright Clearance Center, Inc. ("CCC"), at the time that you opened your Rightslink account and that are available at any time at http://myaccount.copyright.com).

GENERAL TERMS

2. Elsevier hereby grants you permission to reproduce the aforementioned material subject to the terms and conditions indicated.
3. Acknowledgement: If any part of the material to be used (for example, figures) has appeared in our publication with credit or acknowledgement to another source, permission must also be sought from that source. If such permission is not obtained then that material may not be included in your publication/copies. Suitable acknowledgement to the source must be made, either as a footnote or in a reference list at the end of your publication, as follows:
"Reprinted from Publication title, Vol /edition number, Author(s), Title of article / title of chapter, Pages No., Copyright (Year), with permission from Elsevier [OR APPLICABLE SOCIETY COPYRIGHT OWNER]." Also Lancet special credit - "Reprinted from The Lancet, Vol. number, Author(s), Title of article, Pages No., Copyright (Year), with permission from Elsevier."
4. Reproduction of this material is confined to the purpose and/or media for which permission is hereby given.
5. Altering/Modifying Material: Not Permitted. However figures and illustrations may be altered/adapted minimally to serve your work. Any other abbreviations, additions, deletions and/or any other alterations shall be made only with prior written authorization of Elsevier Ltd. (Please contact Elsevier at permissions@elsevier.com)

2.5.2 License details for Figure 2-2

ELSEVIER LICENSE
TERMS AND CONDITIONS

Apr 22, 2012

This is a License Agreement between ram mahipal kouda ("You") and Elsevier ("Elsevier") provided by Copyright Clearance Center ("CCC"). The license consists of your order details, the terms and conditions provided by Elsevier, and the payment terms and conditions.

All payments must be made in full to CCC. For payment instructions, please see information listed at the bottom of this form.

Supplier	Elsevier Limited The Boulevard,Langford Lane Kidlington,Oxford,OX5 1GB,UK
Registered Company Number	1982084
Customer name	ram mahipal kouda
Customer address	411 palm dr glendale, CA 91202
License number	2832630114195
License date	Jan 19, 2012
Licensed content publisher	Elsevier
Licensed content publication	Chemical Engineering Science
Licensed content title	Design, modelling and experimentation of a new large-scale photocatalytic reactor for water treatment
Licensed content author	Ajay K. Ray
Licensed content date	July 1999
Licensed content volume number	54
Licensed content issue number	15–16
Number of pages	13
Start Page	3113
End Page	3125
Type of Use	reuse in a thesis/dissertation
Intended publisher of new work	other
Portion	figures/tables/illustrations
Number of figures/tables /illustrations	4
Format	both print and electronic
Are you the author of this Elsevier article?	No
Will you be translating?	No
Order reference number	None
Title of your thesis/dissertation	Photocatalytic Reactor using Thin TiO2 film on Quartz tubes
Expected completion date	Apr 2012
Estimated size (number of pages)	150
Elsevier VAT number	GB 494 6272 12
Permissions price	0.00 USD
VAT/Local Sales Tax	0.0 USD / 0.0 GBP
Total	**0.00 USD**
Terms and Conditions	

INTRODUCTION

1. The publisher for this copyrighted material is Elsevier. By clicking "accept" in connection with completing this licensing transaction, you agree that the following terms and conditions apply to this transaction (along with the Billing and Payment terms and conditions established by Copyright Clearance Center, Inc. ("CCC"), at the time that you opened your Rightslink account and that are available at any time at http://myaccount.copyright.com).

GENERAL TERMS

2. Elsevier hereby grants you permission to reproduce the aforementioned material subject to the terms and conditions indicated.
3. Acknowledgement: If any part of the material to be used (for example, figures) has appeared in our publication with credit or acknowledgement to another source, permission must also be sought from that source. If such permission is not obtained then that material may not be included in your publication/copies. Suitable acknowledgement to the source must be made, either as a footnote or in a reference list at the end of your publication, as follows:
"Reprinted from Publication title, Vol /edition number, Author(s), Title of article / title of chapter, Pages No., Copyright (Year), with permission from Elsevier [OR APPLICABLE SOCIETY COPYRIGHT OWNER]." Also Lancet special credit - "Reprinted from The Lancet, Vol. number, Author(s), Title of article, Pages No., Copyright (Year), with permission from Elsevier."
4. Reproduction of this material is confined to the purpose and/or media for which permission is hereby given.
5. Altering/Modifying Material: Not Permitted. However figures and illustrations may be altered/adapted minimally to serve your work. Any other abbreviations, additions, deletions and/or any other alterations shall be made only with prior written authorization of Elsevier Ltd. (Please contact Elsevier at permissions@elsevier.com)

2.5.3 License details for Figure 2-4

ELSEVIER LICENSE
TERMS AND CONDITIONS

Apr 22, 2012

This is a License Agreement between ram mahipal kouda ("You") and Elsevier ("Elsevier") provided by Copyright Clearance Center ("CCC"). The license consists of your order details, the terms and conditions provided by Elsevier, and the payment terms and conditions.

All payments must be made in full to CCC. For payment instructions, please see information listed at the bottom of this form.

Supplier	Elsevier Limited The Boulevard,Langford Lane Kidlington,Oxford,OX5 1GB,UK
Registered Company Number	1982084
Customer name	ram mahipal kouda
Customer address	411 palm dr glendale, CA 91202
License number	2831541186094
License date	Jan 17, 2012
Licensed content publisher	Elsevier
Licensed content publication	Catalysis Today
Licensed content title	A new photocatalytic reactor for destruction of toxic water pollutants by advanced oxidation process
Licensed content author	Ajay K. Ray
Licensed content date	30 September 1998
Licensed content volume number	44
Licensed content issue number	1–4
Number of pages	12
Start Page	357
End Page	368
Type of Use	reuse in a thesis/dissertation
Intended publisher of new work	other
Portion	figures/tables/illustrations
Number of figures/tables /illustrations	4
Format	both print and electronic
Are you the author of this Elsevier article?	No
Will you be translating?	No
Order reference number	None
Title of your thesis/dissertation	Photocatalytic Reactor using Thin TiO2 film on Quartz tubes
Expected completion date	Apr 2012
Estimated size (number of pages)	150
Elsevier VAT number	GB 494 6272 12
Permissions price	0.00 USD
VAT/Local Sales Tax	0.0 USD / 0.0 GBP
Total	**0.00 USD**
Terms and Conditions	

INTRODUCTION

1. The publisher for this copyrighted material is Elsevier. By clicking "accept" in connection with completing this licensing transaction, you agree that the following terms and conditions apply to this transaction (along with the Billing and Payment terms and conditions established by Copyright Clearance Center, Inc. ("CCC"), at the time that you opened your Rightslink account and that are available at any time at http://myaccount.copyright.com).

GENERAL TERMS

2. Elsevier hereby grants you permission to reproduce the aforementioned material subject to the terms and conditions indicated.
3. Acknowledgement: If any part of the material to be used (for example, figures) has appeared in our publication with credit or acknowledgement to another source, permission must also be sought from that source. If such permission is not obtained then that material may not be included in your publication/copies. Suitable acknowledgement to the source must be made, either as a footnote or in a reference list at the end of your publication, as follows:
"Reprinted from Publication title, Vol /edition number, Author(s), Title of article / title of chapter, Pages No., Copyright (Year), with permission from Elsevier [OR APPLICABLE SOCIETY COPYRIGHT OWNER]." Also Lancet special credit - "Reprinted from The Lancet, Vol. number, Author(s), Title of article, Pages No., Copyright (Year), with permission from Elsevier."
4. Reproduction of this material is confined to the purpose and/or media for which permission is hereby given.
5. Altering/Modifying Material: Not Permitted. However figures and illustrations may be altered/adapted minimally to serve your work. Any other abbreviations, additions, deletions and/or any other alterations shall be made only with prior written authorization of Elsevier Ltd. (Please contact Elsevier at permissions@elsevier.com)

2.6 References

1. Schiavello, M. (Ed.) (1988), *Photocatalysis and Environment Trends and Applications*, 1st ed, 732 pp, Springer.

2. Herrmann, J. M, C. Guillard, J. Disdier, C. Lehaut, S. Malato, and J. Blanco (2002), New Industrialist titania photocataysts for the solar detoxification of water containing various pollutants, *Applied Catalysis B: Environmental, 35*, 281-294.

3. Dionysiou, D. D, A. A. Burbano, and M. T. Suidan (2002), Effect of oxygen in a thin-film rotating disk photocatalytic reactor, *Environ Sci Technol, 36*, 3834-3843.

4. Nakashima, T, Y. Ohko, D. A. Tryk, and A. Fujishima (2002), Decomposition of endocrine-disrupting chemicals in water by use of TiO_2 photocatalysis immobilized on Poly-tetrafluoroethylene mesh sheet, *Journal of Photochemistry and Photobiology A:Chemistry, 151*, 207-212.

5. Parra, S, S. Malato, and C. Pulgarin (2002), New integrated photocatalytic-biological flow system using supported TiO2 and fixed bacteria for the mineralization of isoproturon, *Appl. Cat B:Environ, 36*, 131-144.

6. Choi, W. K, J.Y, H. Park, and J. S. Chung (2001), Investigation on TiO2 coated optical fibers for gas –phase photocatalytic oxidation of acetone, *Appl. Cat. B:Environ, 31*, 209-220.

7. Molinari, R, C. Grande, E. Drioli, L. Palmisano, and M. Schiavello (2001), Photocatalytic membrane reactors for degradation of organic pollutants in water, *Catalysis Today, 67*, 273-279.

8. Yatmaz, H. C, C. Wallis, and C. R. howarth (2001), The spinning disc reactor-studies on a novel TiO_2 photocatalytic reactor, *Chemosphere, 42*, 397-403.

9. Mandelbaum, P. A, A. E. Regazzoni, M. A. Blesa, and S. A. Bilmes (1999), Photo-Electro-Oxidation of Alcohols on Titanium Dioxide Thin Film Electrodes, *J. Phys. Chem. B, 103*, 5505-5511.

10. Stafford, U, K. A. Gray, and P. V. Kamat (1997), Photocatalytic degradation of 4-chlorophenol: a mechanistically-based model, *,Res. Chem. Intermed, 23*, 355-388.

11. Butterfield, I. M, P. A. Christensen, T. P. Curtis, and J. Gunlazuardi (1997), Water disinfection using an immobilized titanium dioxide film in a photochemical reactor with electric field enhancement, *Water research, 31*, 675-677.

12. Fernandez, A, G. Lassaletta, J. M. Jimenez, A. Justo, E. A. R. Gonzalez, J. M. Herrmann, H. Tahiri, and I. Y. Ait (1995), Preparation and characterization of TiO2 photocatalysis

supported on various rigid supports(glass, quartz and stainless steel). Comparative studies of Photocatalytic activity in water purification, *Appl. Catal. B:Environmental, 7*, 49-63.

13. Hofstadler, K, R. Bauer, S. Novalic, and G. Heisler (1994), New Reactor Design for Photocatalytic Wastewater Treatment with TiO_2 on Fused Silica Fibers: Photomineralization of 4-Chlorophenol, *Environ. Science. technology*, *28*, 670-674.

14. Pareek, V. K, M. P. Brungs, and A. A. Adesina (2001), Continuous Process for Photodegradation of Industrial Bayer Liquor, *Industrial and Engineering Chemistry Research, 40*, 5120-5125.

15. Ajay, K. R, A. C. Antonie, and M. Beenackers (1998), Novel Photocatalytic Reactor for Water Purification, *AIChE Journal, 44*, 477-483.

16. Wenya, H, Z. Pengyi, Z. Wanpeng, Y. Jingjing, and L. Laisheng (2004), Photocatalysis of p-chlorobenzoic acid in aqueous solution under irradiation of 254nm and 185nm UV light, *Water Research, 38*, 4197-4203.

17. Dingwang, C, L. Fengmei, and K. R. Ajay (2000), Effect of Mass Transfer and Catalyst Layer Thickness on Photocatalytic Reaction, *AICHE Journal, 46*, 1034-1045.

18. Ajay, K. R. (1999), Design, modelling and experimentation of a new large-scale photocatalytic reactor for water treatment, *Chemical Engineering Science, 54*, 3113-3125.

19. Ajay, K. R. (1998), A new photocatalytic reactor for destruction of toxic water pollutants by advanced oxidation process, *Catalysis Today*, *44*, 357-368.

20. Tapan, K. S, F. K. Mohammad , and K. R. Ajay (2001), A Taylor Vortex Photocatalytic Reactor for Water Purification, *Ind. Eng. Chem. Res, 40*, 5268-5281.

21. Sczechowski, J. G, C. A. Koval, and R. D. A. Noble (1995), Taylor Vortex Reactor for Heterogeneous Photocatalysis, *Chem. Eng. Sci, 50*, 3163.

22. Diaper, C. D, P. Jarvis, and S. A. Parsons (2002), Combined membrane photocatalysis process for dye waste treatment: adsorption and degradation studies. Advanced Oxidation Processes for Water and Wastewater Treatment, Cranfield, UK, 3 APRIL.

23. Maira, A. J, J. M. Coronado, V. Augugliaro, K. L. Yeung, J. C. Conesa, and J. Soria (2001), Fourier Transform Infrared study of the performance of Nanostructured TiO_2 Particle for the Photocatalytic Oxidation of Gaseous Toluene, *Journal of Catalysis, 202*, 413-420.

24. Nguyen, V. N. H, R. Amal, and B. Donia (2003), Effect of Formate and methanol on photoreduction/removal of toxic cadmium ions using TiO_2 semiconductor as photocatalyst, *Chemical Engineering Science, 58*, 4429-4439.

25. Chenthamarakshan, C. R. and k. Rajeshwar (2000), Photocatalytic reduction of divalent zinc and cadmium ions in aqueous TiO_2 suspensions: An interfacial induced adsorption-reduction pathway mediated by formate ions, *Electrochemistry Communications, 2*, 527-530.

26. Hisahiro, E, H. Masafumi, F. Shigeru, and I. Takashi (2003), Generation of Active Sites for CO Photooxidation on TiO_2 by Platinum Deposition, *J. Physicsal. Chemistry B, 107*, 9290-9297.

27. Tunesi, S. and M. Anderson (1991), Influence of chemisorptions on the photodecomposition of salicyclic acid and related compounds using suspended TiO2 ceramic membranes, *J. Physical. Chemistry*, *95*, 3399-3405.

3 REVIEW OF TiO_2 FILM MAKING PROCESS

3. Review of TiO_2 Film Making Processes

The photocatalyst synthesis mechanism and the deposition method have a significant role in the characteristics of the photocatalyst. In this chapter I will be reviewing the significance of the various properties of the photocatalyst and their influence on photocatalyst performance. Observations based on the review of different processes for the synthesis of TiO_2 particles, different mechanisms for photocatalyst film deposition and, drawbacks and advantages of individual film coating method are presented.

3.1 TiO_2 Film Coating

The TiO_2 film surface characteristics and morphology have a significant role in a successful photocatalysis process. The thin film coating mechanism has a significant influence on the resulting characteristics of the film such as the porosity of the film, thickness of the film, uniformity of the film on the substrate surface, and the adhesiveness of the film to the substrate surface.

The porosity and thickness of the film governs UV light penetration[1, 2], thereby influencing the photocatalytic activity. The adhesiveness[1, 2] of the film plays a significant role in the absorption of photons by the photocatalyst on the substrate surface and the resulting photocatalytic activity.

The porosity of the film influences the passage of organic contaminants and water in and out of the TiO_2 film. Based on the film coating mechanism and process conditions, anatase or rutile forms of the TiO_2 film can be formed and it has been observed that the anatase film has better[1, 2]

photocatalytic activity when compared to rutile, the individual form properties were mentioned in chapter 1.

The most common coating mechanisms for TiO_2 film are described below:

3.1.1 Sputter deposition

Sputter deposition is one of the PVD (physical vapor deposition) methods to deposit thin films. In the sputtering process, atoms are ejected from a solid target material due to bombardment of the target by energetic particles. During deposition of thin film using the sputtering process, the first step is to create gaseous plasma and then accelerate the ions from the plasma to the source material. The source material is eroded due to the energy transfer ejecting neutral particles as either individual atoms or a cluster of atoms or molecules. As the neutral particles are ejected they travel in a straight line and get deposited on any material in their path. If the substrate surface is placed in the path of traveling particles, they form as a thin film on the substrate. Based on the required film, a reactive gas (such as O_2) is introduced for chemical reaction to form the resulting product as a thin film on the substrate.

In TiO_2 film deposition using the sputtering process, the cathode surface (titanium substrate) is bombarded with the oxygen atoms in a stable environment of argon. The titanium particles generated from the cathode surface react with O_2 atoms and form a TiO_2 film on the substrate (anode) [3,5] to be coated. The composition of the film is controlled[3,4,5] by varying the relative pressures of the inert and reactive gases. As results of the chemical reaction between the target material and the reactive gas, the product formed is deposited on the substrate to be coated

The TiO_2 film formed using the sputtering process is usually a non-porous film, which is not effective for photocatalysis as it blocks the light penetration through the film surface.

3.1.2 Chemical Vapor Deposition(CVD)

In chemical vapor deposition, the material to be coated is formed by a chemical reaction/decomposition of its precursor with gases[6,7,8]. CVD relies on a carrier gas which acts as a transporting medium for the precursor of the material to be deposited on the substrate surface, where the precursor molecules react with the other gases to form the film on the substrate. Other byproducts formed in the process are removed from the surface by gas flow through the chamber[6,7,8]. The CVD process is one of the widely used processes using a precursor of material to be coated on the substrate [6,7,8].

The coating of TiO_2 film using the CVD process is not feasible on all the substrate surfaces and shapes due to the equipment used for the film coating; in addition, the film formed by CVD process is normally non-porous. For the successful application of TiO_2 film to be used in proposed reactor(as mentioned in chapter 2), the film formed needs to be porous and needs to coated on quartz tubes.

3.1.3 Sol-gel film coating

Sol-gel coatings result from dipping a substrate into a chemical solution. The solution is a mixture of suspended precursor particles known as a sol-gel[9-21].

Although the films are normally deposited at room temperature, a high temperature heat treatment of the film is required to create a dense film and drying of the film, along with drying the evaporation of the solvent in the film which was used in the sol-gel process. Sintering temperatures are typically in excess of 400 $^{\circ}$C[9-21]. The final thickness formed using the sol-gel method is typically in the range of 50 nm to 1 mm as described in Figure 3-1.

The sol-gel solution chemical composition is determined by the material to be deposited, because this process involves a hydrolysis. The solution is commonly based on a metal alkoxide M(OR)x precursor where the R representing an alkoxy group[9-21]. In the sol-gel process, the metal alkoxide is dissolved in a solvent with or without water and the solution is destabilized by hydrolysis, resulting in the formation of a gel solution of metal alkoxide particles in the solvent[9-21]. Catalysts are used to modify the rate of reaction (hydrolysis) which controls the age of the solution before it turns in to a total gel solution and hence it is used to control the properties of resulting film[9-21].

The advantages of this process include high purity, the film can be deposited on different substrates of different shapes, and the films can be coated in a simple laboratory setup without requirement of any sophisticated equipment [9-21]. The primary disadvantage is narrow range of materials that can be deposited with this technique. A number of applications have been demonstrated for this process[9-21].

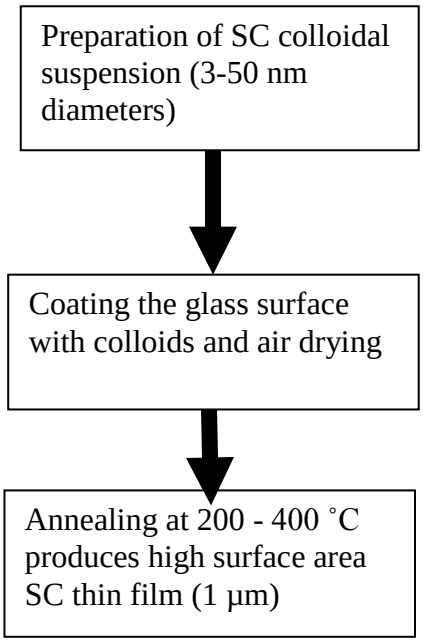

Figure 3-1. The sol-gel film coating procedure.

It has been reported that many metal alkoxides can be easily formulated in the thin film form on various substrates by using sol–gel with dip coating techniques[9-21]. Titania films prepared by this method can be of high purity and the process is relatively cheap. The latter advantage results from the availability of high-purity chemical precursor materials in conjunction with the simplicity of sol–gel preparation at room temperature[9-21].

The film formed using the sol-gel method is porous and the film thickness can be controlled by the dipping rate of the substrate in the solution and the solution viscosity. Variations in the composition of the solution will result in the variation of the performance of the photocatalyst. Based on the process involved the TiO_2 film can be deposited on any substrate and shape in a lab environment.

For the proposed multiple tube photocatalytic reactor(mentioned in chapter 2), which requires a porous TiO_2 film to be deposited on the quartz tubes, the sol-gel can be used in a laboratory setup with a dip-coater to coat the TiO_2 film on quartz tubes.

3.1.4 Electro-static self assembly process (ESA)

The basic concept of the thin film coating using the ESA process is building up of multilayer thin films of opposite charges as shown in Figure 3.2, where cationic and anionic polymeric materials are shown to be deposited[23]. Initially the substrate surface is rinsed thoroughly in acid medium followed by base medium, and then it is cleaned rigorously in deionized water to remove any particles so the outermost substrate (glass or metal) surface layer has a net negative charge[22-25].

The substrate is then dipped into a solution containing water-soluble "cation" polymer molecules that have net positively charged functional groups fixed to the polymer backbone[23]. The net negative charge on the substrate is thus masked from other positive groups along the polymer chain so the surface forms a net positive charge distribution on the outermost surface. Since the total polymer layer is neutral, negative charges with relatively loose binding to the polymer network pair up with positive ions. Subsequent poly-anion and poly-cation monolayer's are added to produce a multilayer structure.

The basic process involved in ESA film deposition is a charged substrate dipped in a solution containing molecules that can bond to the surface. A layer (or multilayer) of the cation/anion charges from the solution are bonded to the surface layer by layer[22-25], after every layer deposition the substrate is rinsed in water. Physical forces of the neutral rinsing solution (water)

strip away all the particles bonded by physisorption (physically bonded), but not the molecules more strongly bound by chemisorption (chemically bonded) to the surface, leaving the surface partially covered with the charged solution molecules[22-25]. If the chemistry is done properly, an uniform coating will be formed after the substrate has been dipped in alternate charged solutions (and then rinsed)[22-25]. It involves laborious and time-consuming deposition steps for practical device applications.

In this instance of coating TiO_2 film, alternatively dip the substrate *i.e* quartz rod into PSS (polysodium styrene sulfonate) and PDDA (polydiallyl di-ammonium acetic acid) as shown in Figure 3-2 and then follow by dipping the solution in TiO_2/PSS solution.

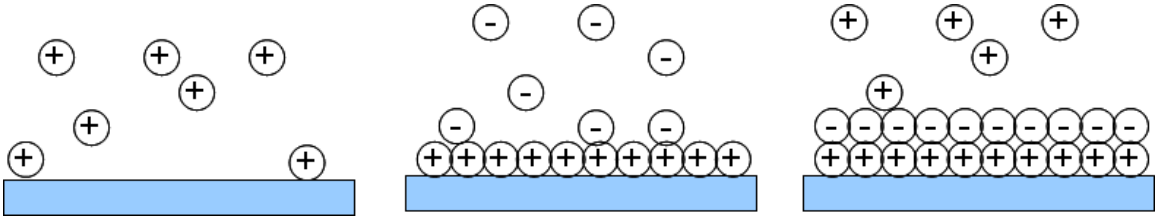

Figure 3-2. ESA process for formation of multilayer thin films[23].

In between every dip in a solution, the substrate is cleaned by shaking vigorously in de-ionized water to remove excess material from the surface. Only the compound that is chemisorbed[23] onto the substrate remains.

In ESA method, the film thickness can be controlled based on two factors, the particle size which is controlled during the synthesis of TiO_2 particles by controlled hydrolysis and the number of dips in the solution, where coat multiple layer of the TiO_2 particle.

The ESA method can be effectively applied in the photocatalytic process. The thickness of the TiO_2 can be effectively controlled by controlling the TiO_2 particle size and number of dips during coating process, the film generated can be porous and it can be replicated if the variation in the synthesis of TiO_2 particles and film coating are controlled.

The ESA method can be successfully used in coating porous TiO_2 film on quartz tubes in a laboratory setup, as required for the proposed multiple tube reactor.

3.2 Charge Carrier Separation

Charge carrier separation the separation of electron-hole pair formed during the photocatalysis process, the separated electron-hole pair is used in oxidation-reduction process of compounds to be treated in water. To enhance the performance of the photocatalyst, we have to accelerate the formation of the electron-hole pair and also decrease the recombination of electron-hole pair. The charge carrier separation of the electron-hole pair can happen by absorbing the photon of sufficient intensity to provide energy for both the electron and hole pair formed in the photocatalytic process to move in the opposite direction to each other. The minimum amount of force required for this process is the columbic force of attraction between them. So any intensity of greater the columbic force of attraction between hole-electron pair will prevent recombination [26-28].

The overall concept of the electric field application was to decrease the recombination rate of the electron-hole pair, but the application of electric field is limited in the water treatment process as the surface of the TiO_2 surface is exposed to the water.

One successful method to decrease the recombination rate is using of metal dopant the TiO_2 film, which attract the electron and thereby reduce the electron-hole pair recombination rate.

3.3 Iron doping of the TiO_2 Film

One of the significant factors in the photocatalyst performance is the recombination rate of the hole-electron pair in activated TiO_2. The smaller the recombination rate, the better the photocatalyst performance in terms of efficiency and rate of degradation. This has been a subject of immense interest in photocatalytic surface research.

Considerable improvement has been observed by several researchers[29-38] in the photocatalyst behavior by doping of the TiO_2 film using transition metals[29-34]. In doping the TiO_2 film, one of the most commonly used methods in the sol-gel process is using the iron precursor, mostly iron nitrate solution during the TiO_2 solution preparation. The introduction of iron[29-34] particles affects the TiO_2 film surface in two ways as mentioned below.

The primary phenomenon observed is the formation of conductive particles on the surface on the TiO_2 film, which reduces[29-34] the electron-hole recombination rate by attracting the electron generated by photocatalysis process as shown in Figure 3-3.

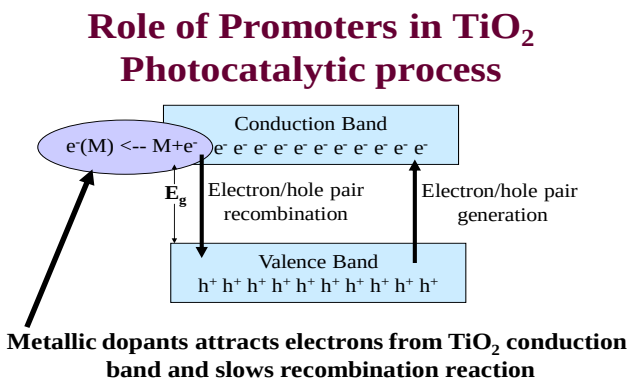

Figure 3-3. Role of metallic promoters in photocatalytic process[29-34].

Transition metals such as Fe(III) have been successfully[29-34] used in the photocatalytic process, where the TiO_2 film surface is immersed in an Fe(III) solution. The surface transition metal (Fe(III)) dopant particle reduces[31] the recombination rate as shown in reaction mechanism in Figure 3-4.

$TiO_2 \xrightarrow{h\nu} e^- + h^+$ → Photo-generation electron/hole pairs

$h^+ + H_2O \rightarrow OH\bullet + H^+$
$e^- + O_2 \rightarrow O_2^-\bullet$
$O_2^-\bullet + H^+ \rightarrow HO_2\bullet$
→ Formation of radicals (*Ox*- radical)

$TOC + Ox \rightarrow TOC$ *(partially oxidized species)* $+ CO_2 + H_2O$ → Radical oxidation of organic compound.

$h^+ + e^- \rightarrow TiO_2 + energy$ → Recombination of electron/hole pair

$M + e\text{-} \rightarrow M(e\text{-})$ → Metal attracts free electron slows recombination and promotes radical formation

Figure 3-4. Role of metallic promoters in photocatalytic process[29-37].

The other phenomenon observed is change in crystal lattice structure of the TiO_2 molecule by the introduction of iron (doped) particle. The change in crystal structure shifts the band gap energy level of the photocatalyst towards the visible light wavelengths. With increase in dosage of Fe 3+

dopant, it was observed[38] to have resulted in decrease of the TiO_2 band gap as shown in below figure 3-5.

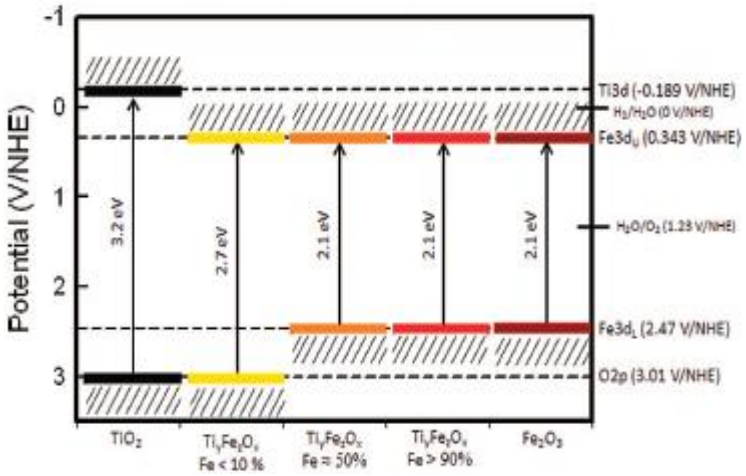

Figure 3-5: Band gap of Iron doped TiO_2 film at different Fe^{3+} concentration[38](Copyright Permission 3.5.1)

3.4 Conclusion

Based on the literature review of the film coating processes sputtering, CVD, Sol-gel and ESA. The sputtering and CVD process are used for coating non-porous films. Based on the process equipment used for the film deposition in CVD and sputtering the dimension and type of the substrate is a constraint.

The sol-gel and ESA methods normally produce porous films and are not sensitive to the type or shape of substrate. The process doesn't involve any sophisticated equipment and can be coated in a laboratory setup.

3-5 Appendix

3.5.1 License Details for Figure 3-5

Home | Account Info | Help

Copyright Clearance Center RightsLink®

ACS Publications High quality. High impact.

Title:	Predicting the Band Structure of Mixed Transition Metal Oxides: Theory and Experiment
Author:	Elijah Thimsen et al.
Publication:	The Journal of Physical Chemistry C
Publisher:	American Chemical Society
Date:	Feb 1, 2009
Copyright © 2009, American Chemical Society	

Logged in as:
ram mahipal kouda
Account #:
3000488295
LOGOUT

PERMISSION/LICENSE IS GRANTED FOR YOUR ORDER AT NO CHARGE

This type of permission/license, instead of the standard Terms & Conditions, is sent to you because no fee is being charged for your order. Please note the following:

- Permission is granted for your request in both print and electronic formats.
- If figures and/or tables were requested, they may be adapted or used in part.
- Please print this page for your records and send a copy of it to your publisher/graduate school.
- Appropriate credit for the requested material should be given as follows: "Reprinted (adapted) with permission from (COMPLETE REFERENCE CITATION). Copyright (YEAR) American Chemical Society." Insert appropriate information in place of the capitalized words.
- One-time permission is granted only for the use specified in your request. No additional uses are granted (such as derivative works or other editions). For any other uses, please submit a new request.

3.6 References

1. Akira, F, H. Kazuhito, and W. Toshiya (Eds.) (1999), *TiO_2 Photocatalysis: Fundamentals and Applications*, 1st ed, Bkc,Inc, Tokyo.

2. Schiavello, M. (1997), *Heterogeneous Photocatalysis*, 208 pp, John Wiley & Sons Canada, Ltd.

3. Perry, F, A. Billard, and C. Frantz (1997), An optical emission spectroscopy study of a reactive magnetron sputtering Ar-O2 discharge modulated at low frequency, *Surface and Coating Technology, 94-95*, 681-685.

4. Karunagaran, B, R. T. Rajendra kumar, C. Viswanathan, D. Mangalaraj, S. K. Narayandass, and G. Mohan Rao (2003), Optical constants of DC magnetron sputtered titanium dioxide thin films measured by spectroscopic ellipsometry, *Cryst. Res. Technol, 38*, 773-778.

5. Atsuo , Y, S. Hiroyuki, K. Yoshikazu, H. Shigeo, and O. Kiyoshi (2001), Photocatalytic and photoelectrochemical properties of TiO_2 –based multiple layer thin film prepared by sol-gel and reactive sputtering methods, *J. Mater. Chem, 11*, 12533.

6. Hugh, O. P. (Ed.) yr?, *Handbook of Chemical Vapor Deposition: Priciples Technology and Applications*, 2nd ed, Noyes Publications.

7. Mills, A, N. Elliot, I. P. Parkin, S. A. O'Neil, and R. J. Clark (2002), Novel TiO_2 CVD films for semiconductor photocatalysis, *Journal of Photochemistry and Photobiology A;Chemistry, 151*, 171-179.

8. Ding, Z, X. Hu, P. L. Yue, G. Q. Lu, and P. F. Greenfield (2001), Synthesis of anatase supported on porous solids by chemical vapor deposition, *Catalysis Today, 68*, 173-182.

9. Jefrey, C. B. and W. S. George (1990), *Sol-Gel Science: The Physics and Chemistry of Sol-Gel Processing*, 1st ed, 912 pp, Academic Press.

10. Sol-gelForum (2011), WWW.Sol-gelforum.com. , *2008*.

11. Mansor , A. H. and A. R. Ismail (2003), Preparation of titanium dioxide(TiO_2) thin films by sol-gel dip coating methods, *Malaysian Journal of chemistry, 5*, 086-091.

12. YU, J. G. Z, Z. Xiu-jian, H. Gao-ke, and Z. Jian-jun , Grain size and photocatalytic Activity of nanometer TiO_2 thin Films Prepared by the Sol-Gel Method, *Journal of Wuhan University of Technology-Mater. Sci. Ed, 16*.

13. Nobuaki, N. and T. Koti (2001), Preparation of TiO_2 thin Film Photocatalysts by Dip Coating Using a Highly Viscous Solvent, *Journal of Sol-gel Sciences and technology, 22*, 23-31.

14. Miah , M. Y, I. Hiroaki, and H. Hiroshi (2002), Preparation of porous Titania film by Modified Sol-Gel Method and its application to Photocatalyst, *Journal of Sol-gel and technology, 25*, 65-74.

15. Michael, G. (2001), Sol-Gel processed TiO_2 Films for Photovoltaic Applications, *Journal of Sol-gel Science and technology, 22*, 7-13.

16. Akihiko, H. (2001), Highly Photocatalytic activity of F-Doped TiO_2 Film on Glass, *Journal of Sol-Gel Science and technology, 22*, 47-52.

17. Sun-Jae, K. (2001), Photocatalytic Effects of Rutile Phase TiO_2 Ultrafine Powder with high Specific Surface Area Obtained by a Homogenous precipitation Process at Low Temperatures, *Journal of Sol-Gel Science and technology, 22*, 63-74.

18. Yoshimi , T. and S. Motohiro (2001), Effects of Heat treatement on photocatalytic property of Sol-Gel derived Polycrystalline TiO_2, *Journal of Sol-Gel Science and Technology, 22*, 83-89.

19. Walid, A. D. and H. X. John (2004), Low temperature Sol-Gel processed photocatalytic Titania Coating, *Journal of Sol-gel Science and Technology, 29*, 25-29.

20. Eugene, H. and Z. Alfred (1997), *Optics*, 3rd ed, 694 pp, Addison Wesley Publishing Company.

21. Hassan, A. K, N. B. Chaure, K. R. Ajay, a. v. Nabok, and s. Habesch (2003), Structural and electrical studies on sol-gel derived spun TiO_2 thin films, *J. Physics. D:applied Physics, 36*, 1120-1125.

22. Spillman Jr, W. B, T. Zeng, and R. O. Claus (2002), Modeling the Electro-static self-assembly process using stochastic cellular automata, *Smart mater Structure, II*, 623-630.

23. Liu, Y, A. Rosidian, K. Lenahan, W. You-Xiong, Z. Tingying, and R. O. Claus (1999), Characterization of electrostatically self-assembled nanocomposite thin films, *Smart mater Structure, 8*, 100-105.

24. Masuda, Y, D. Wang, T. Yonezawa, and K. Koumoto (2002), Site-Selective Deposition of TiO_2 Thin Films Using Self-Assembled Monolayers and Their Dielectric properties, *Key engineering Materials, 228-229*, 125-130.

25. Masuda , Y, T. Sugiyama, W. S. Seo, and K. Koumoto (2003), Deposition Mechanism of anatase TiO_2 on self –assembled Monolayers from an aqueous solution". Chem Mater,2003,15,2469-2476, *Chem Mater, 15*, 2469-2476.

26. Schiavello, M. (Ed.) (1988), *Photocatalysis and Environment Trends and Applications*, 1st ed, 732 pp, Springer.

27. Akira, F, H. Kazuhito, and W. Toshiya (Eds.) (1999), *TiO_2 Photocatalysis : Fundamentals and Applications*, 1st ed, Bkc,Inc, Tokyo.

28. Choi, W, A. Termin, and R. Hoffmann (1994), The role of metal-ion dopants in quantum sized TiO_2: C W, Correlation between photo reactivity and charge-carrier recombination dynamic, *Journal of Physical Chemistry, 98*, 13651-13669.

29. Ohno, T, F. Tanigawa, K. fijuhara, S. Izumi, and M. Matsumara (1998), Photocatalytic oxidation of water on TiO_2 coated WO_3 particles by visible light using Iron(III) ions as electron acceptor, *Journal of Photochemistry and Photobiology A: Chemistry, 118*, 41-44.

30. Doong, R. A, R. A. Maithreepala, and S. M. Chang (2000), Heterogeneous and homogeneous photocatalytic degradation of chloro phenols in aqueous titanium dioxide and ferrous ion , *Water Science and Technology, 42*, 253-260.

31. Akihiko, H. (2001), Highly Photocatalytic activity of F-Doped TiO_2 Film on Glass, *Journal of Sol-Gel Science and technology, 22*, 47-52.

32. Shah, S. I, W. Li, C. -. Huang, O. Jung, and C. Ni (2002), Study of Nd^{3+}, Pd^{2+}, Pt^{4+}, and Fe^{3+} , dopant effect on photo reactivity of TiO_2 nano particles , *PNAS, 99*, 6482-6486.

33. Navio, J. A, J. J. Testa, P. Djedjeian, J. R. Padron, D. Rodriguez, and M. I. Litter (1999), Iron doped titania powders prepared by a sol-gel method. Part II: Photocatalytic properties, *Applied Catalysis A: general, 178*, 191-203.

34. Pacheco, F, R. Palomino, G. Martinez, A. Mendoza-Galvan, R. Rodriguez Talavera, and V. M. Castano (1998), Optical characterization of titania thin films produced by the sol-gel method and doped with CO^{2+} at different concentrations, *Applied optics, 37*, 1867-1872.

35. Chungchen, C, X. Li, W. Ma, J. Zhao, h. Hidaka, and N. Serpone (2002), Effect of transition metal ions on the TiO_2 assisted photo degradation of dyes under visible irradiation: a probe for the interfacial electron transfer process and reaction mechanism, *J. Phys. Chem. B, 106*, 318-324.

36. Gesenhues, U. (2001), Al-doped TiO_2 pigments: influence of doping on the photocatalytic degradation of alkyd resins, *Journal of Photochemistry and Photobiology A: Chemistry, 139*, 243-251.

37. Matsuo, S, N. Sakaguchi, E. Obuchi, K. Nakano, R. Perera, T. Watanabe, T. Matsuo, and H. Wakita (2001), x-ray absorption spectral analyses by theoretical calculations for TiO_2 and Ni-doped TiO_2 thin films on glass plates, *Analytical Sciences, 17*, 149-153.

38. Elijah Thimsen, Subhashis Biswas, Cynthia S. Lo, and Pratim Biswas, Predicting the Band Structure of Mixed Transition Metal Oxides: Theory and Experiment, *J. Phys. Chem. C,* 2009*, 113,* 2014–2021.

4 MATERIALS AND METHODS

OF TiO_2 FILM MAKING AND RESULTS

4.1 TiO_2 Film Making

As mentioned in Chapter 3 the film properties porosity, thickness, uniformity of the film on the substrate surface, and the adhesion of the film to the substrate surface play significant roles in photocatalysis process and the reactor performance.

Taking into consideration the limitations of CVD and sputtering processes, in deposition of porous thin film on a glass/quartz tube substrate as mentioned in chapter 3. The sol-gel and ESA methods are favorable processes for thin film deposition on different substrates of varied dimension.

Experiments were performed using sol-gel and ESA TiO_2 films with different reactor configurations. The reactor configuration and the experimental results of the reactor performance are reported in Chapter 5.

The TiO_2 films made using the sol-gel and ESA methods with and without Fe doping were analyzed using Photonics Model 420 UV–Visible spectrophotometer for the absorbance peak and spectrum of the film formed.

4.2 Dip Coater

The dip coater (Figure 4-1) was constructed for the purpose of TiO_2 film depositions using the sol-gel and ESA methods. The purpose of the dip coater was to enhance the reproducibility of thickness of the TiO_2 film on the substrate using TiO_2 solution.

For reproducibility of the film in a solution *i.e.* the reproducibility of the film thickness, each time the dip coater was used to dip the substrate in the same solution. The motor speed must be kept constant to control the substrate dipping rate.

The dip coater was marked at various speeds of the motor for different rates of immersion. The reproducibility of the film using dip coater depends on the factors immersion rate of the substrate in the solution, and the solution age (Assuming the chemical characteristics of the solution remains same during each dip of the substrate in the TiO_2 solution).

Figure 4-1. Dip coater with a magnetic stirrer place on it and a motor located on the left side to move the dip-coater.

The substrate was dipped vertically by mounting it to the dip coater, the thickness of the film increases from the top portion (mounted to dip coater) to the bottom portion. The thickness increase was due to the increase in residence time from top to bottom portion of substrate as gravity drives the solution on the substrate surface to drip towards the bottom portion.

4.3 TiO_2 film by ESA Method:

4.3.1 TiO_2 Nano particle Solution

TiO_2 nano particles were prepared by controlled hydrolysis of Titanium (IV) tetraisopropoxide[1] in water under controlled pH conditions. A 100ml solution consisting of 5 ml of liquid $Ti[OCH(CH_3)_2]_4$ (Aldrich, 97% purity) dissolved in 95 ml of isopropyl alcohol, was added drop wise at a rate of approximately 1 ml/min to 900 ml of deionized water (5^o C) at a acidity of around pH=2 (measured by pH meter) controlled by addition of HNO_3. After continuous stirring for 12 hr or longer, the solution became transparent as TiO_2 nano particles were formed. The rate of addition of titanium isopropoxide solution is controlled[1] as the size of the nano particles depends on it. The colloidal solution was continuously stirred for a few days after the initial reaction to ensure stable and more uniform size distribution[1] of TiO_2 particles.

4.3.2 Coating procedure

A glass microscope slide was cleaned in ethanol solution and followed by nitric acid solution. Later, the microscope slide was dipped in a PDDA (poly diallyl diammonium acetic acid)[1,2] solution and PSS (poly sodium styrene sulfonate) [1,2] solution alternatively for an equal number of times. The glass slide was then dipped in PSS solution and TiO_2 solution for an equal number of times (5, 10, 15 times). After every dip in one of the solution, the microscope slide was dipped in water and shaken vigorously for 1 minute to detach any of the loosely attached particles by physisorption . The slide was then calcined in an oven at 450°C for an hour.

From the graph (Figure 4-2), it can be concluded that the increase in thickness of the film layer formed for each dip of the glass strip in solution is uniform, as the absorbance increased linearly with respect to the number of layers of coating using the same solution.

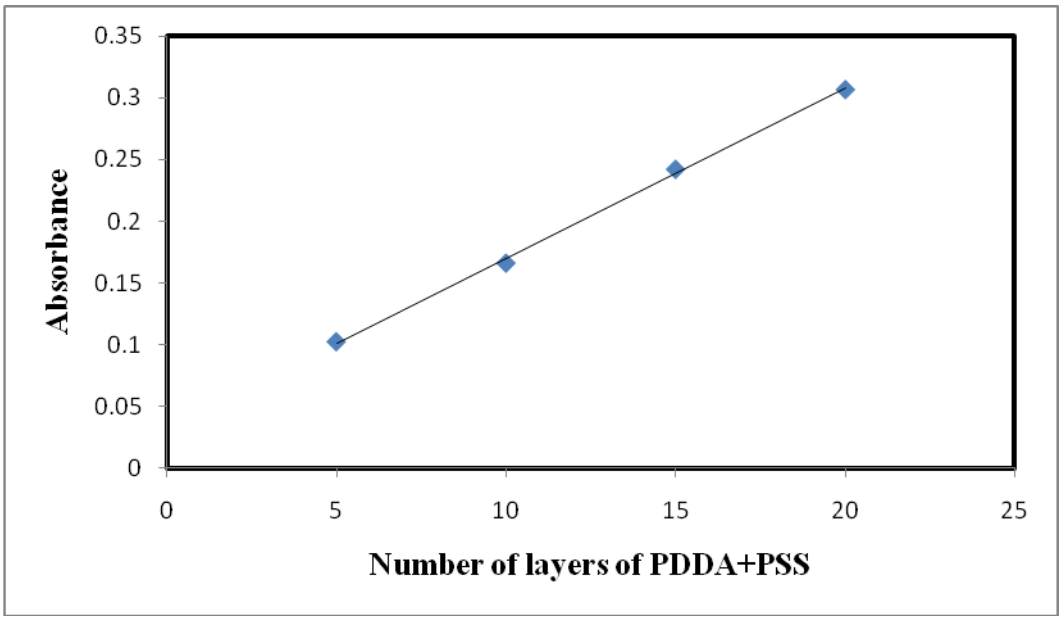

Figure 4-2. Absorption vs. number of layers of the film (PDDA+PSS) by ESA method. (Wave length: 483 nm).

4.4 Sol-Gel TiO_2 Solutions

The TiO_2 solution for the sol-gel method[3,4] was prepared using the following procedures[4].

4.4.1 Solution Type I

The solution[4] was prepared by adding 170 mL isopropanol to 12 mL titanium isopropoxide. After stirring the solution for 10 min, 0.4 mL of Hcl was added, the Hcl controlling the rate of hydrolysis. The solution was stirred using the magnetic stirrer for 24hrs until the solution became slightly viscous. The viscous nature of the solution enabled the solution to stick to the substrate.

Normally, after more than 24 hrs the solution was observed to determine whether the solution is viscous visually if not, more time was allowed for the solution viscosity to increase. A highly viscous solution is not desirable as it will not have the required adhesiveness to stick to the substrate surface after calcination and it forms fragile top layers of the film.

After the solution acquired the desired viscosity (slightly jelly solution), the substrate was dipped in the solution at a controlled rate by using a dip-coater as described before. Between each dip the substrate surface was air dried and then the substrate was dipped back again in the solution and air dried after being removed again at a controlled rate. Then the film was calcined in a furnace at a temperature of 450 °C for 1 hr.

4.4.2 Solution Type II:

The solution[4] was prepared by adding 200 mL of de-ionized water to 13 mL of titanium isopropoxide under vigorous stirring. 3 mL of nitric acid added to the solution slowly for 1 minute, the solution forms a suspension after mixing for 5-8 days. The substrate was coated by dipping it in the suspension for 1 min and then it was allowed to air-dry. The substrate was further dipped three times. The substrate was later calcined in an oven at a temperature of 450 °C for an hour.

4.4.3 Solution Type III:

The sol-gel precursor was prepared by adding 165 mL of titanium isopropoxide $Ti[OCH(CH_3)_2]_4$ to 285 mL of 0.1 M nitric acid solution under vigorous stirring. The solution[4] was then heated at 80 °C for 10 hrs, for polymerization 12 g of polyethylene glycol (PEG,

molecular weight of 20,000, Merck Chemicals Ltd.) was added to the solution. The solution was deposited as a thin film of TiO_2 on a microscope slide by dipping the microscope slide 3 times in the solution using the dip coater, and then the film was calcined at 450 °C for 1hr after air drying.

4.5 Film Coating Results

The absorption spectrum of the films formed by ESA and Sol-gel Method was measured by using an absorption spectroscopy (BECKMAN DU 640 SPECTROPHOTOMETER) to analyze the absorbance peak and spectrum of individual films in UV and visible wavelength.

4.5.1 ESA

To validate the TiO_2 film deposition using the ESA method, the microscope slides were coated using TiO_2 solution, PDDA and PSS polymer solutions[1,2,5,6]. The first microscope slide was coated with 20 layers of each polymer (PDDA+PSS) film only, Second microscope slides coated along with 20 layers of each polymer (PDDA+PSS) film 15 layers of TiO_2 film, the third microscope slide was coated with 20 layers of each polymer(PDDA+PSS) film and followed by 20 layers of TiO_2 film. The absorbance spectrum of the substrate with no TiO_2 film and two microscope slides with 15 and 20 layers of TiO_2 film can be observed in Figure 4-3.

The absorbance peak was in the UV region at a wavelength of around 264 nm for all three substrates. The substrate with polymer (PDDA+PSS) film only had absorbance increase from 280 nm onwards and had lower absorbance when compared to the substrates with 15 and 20 layers of TiO_2 on top of the 20 layers of Polymer (PDDA+ PSS) film.

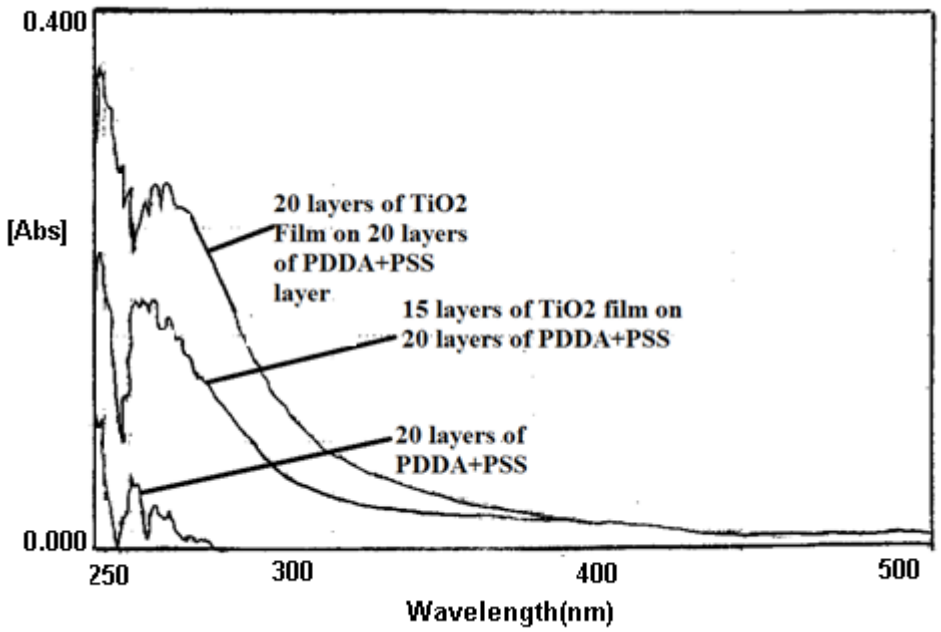

Figure 4-3. ESA film absorbance spectrum of 15 and 20 layers of TiO_2 film and polyfilm 20 layers.

The substrate with 20 layers of TiO_2 film on top of the 20 layers Polymer (PDDA+PSS) film had the highest absorbance with increase in absorbance starting from the 370 nm(3.4 *ev*) wavelength onwards, similar absorbance was also observed for the 15 layers of TiO2 film confirming the presence of TiO_2 film on the polymer film and increase in TiO2 film thickness from 15 to 20 layers of the film

We can infer from the absorbance spectrum in figure 4-3 above, among the three microscope slides that there was considerable increase in absorbance of the substrate with TiO_2+polymer film when compared to polymer only film, and also there was increase in the absorbance with the number of layers of the TiO_2 film. Even though the polymer film also has a peak in absorbance at the wavelength 264 nm, the difference in peak height of the TiO_2 film with 15 layers and 20 layers compared to the polymer only film can be clearly attributed to the TiO_2 in the film.

4.5.2 Sol-Gel Film

Type I: Type I Sol-gel film absorbance spectrum.

The absorbance peak was observed below 300 nm (Figure 4-4), which corresponds to a energy of 4.0 *ev* higher than the band gap energy of 3.4*ev* for the solid TiO_2 of 365 nm.

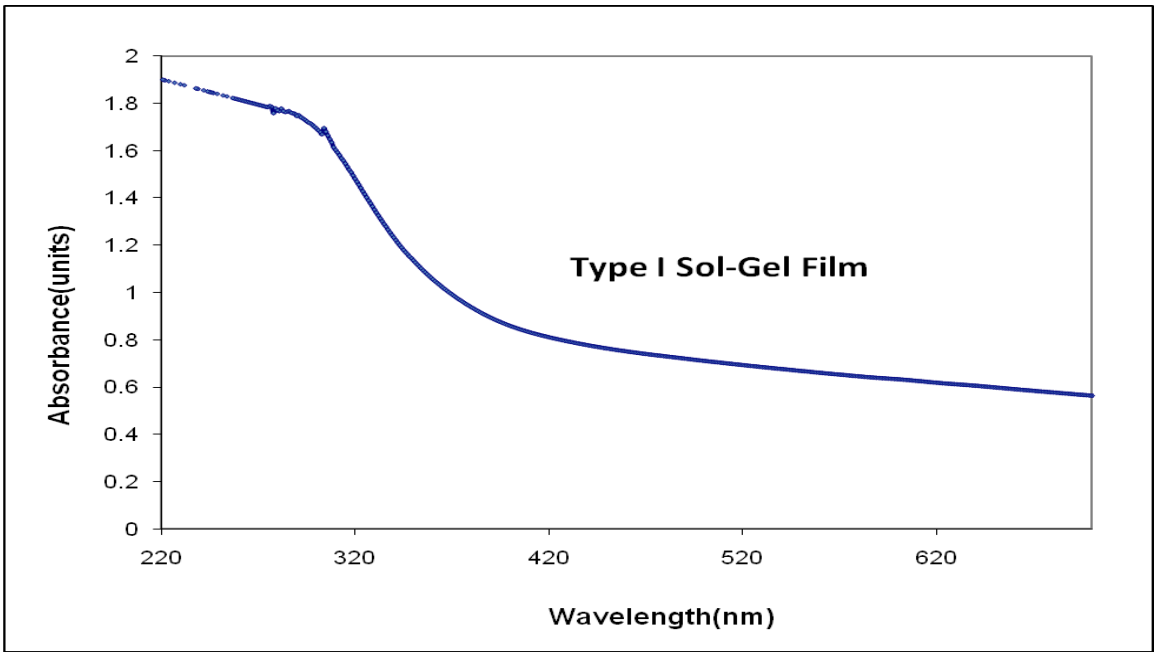

Figure 4-4. Sol-gel film absorbance spectrum from 200 nm to 500 nm with a peak absorbance at 285 nm.

The film absorbance was measured in the absorbance spectrophotometer by inserting the TiO_2 film coated quartz micro scope glass slide in the sample port. The blank quartz slide was used as blank sample to subtract the absorbance of the quartz material. The film had absorbance from 350 nm (3.5 ev) onwards, with high absorbance from 300 nm (4.0ev).

Photon of energy higher than 3.5 *ev* is required for the absorbance of TiO_2 particles and photon of higher than 4.0 *ev* is preferable due to higher absorbance for photocatalytic activity.

Type II: Type II Sol-gel film absorbance spectrum.

The absorbance was maximum at 280 nm (Figure 4-5) which corresponds to an energy level of 4.2 *ev* higher than the band gap energy of solid TiO_2 film (3.2*ev*).

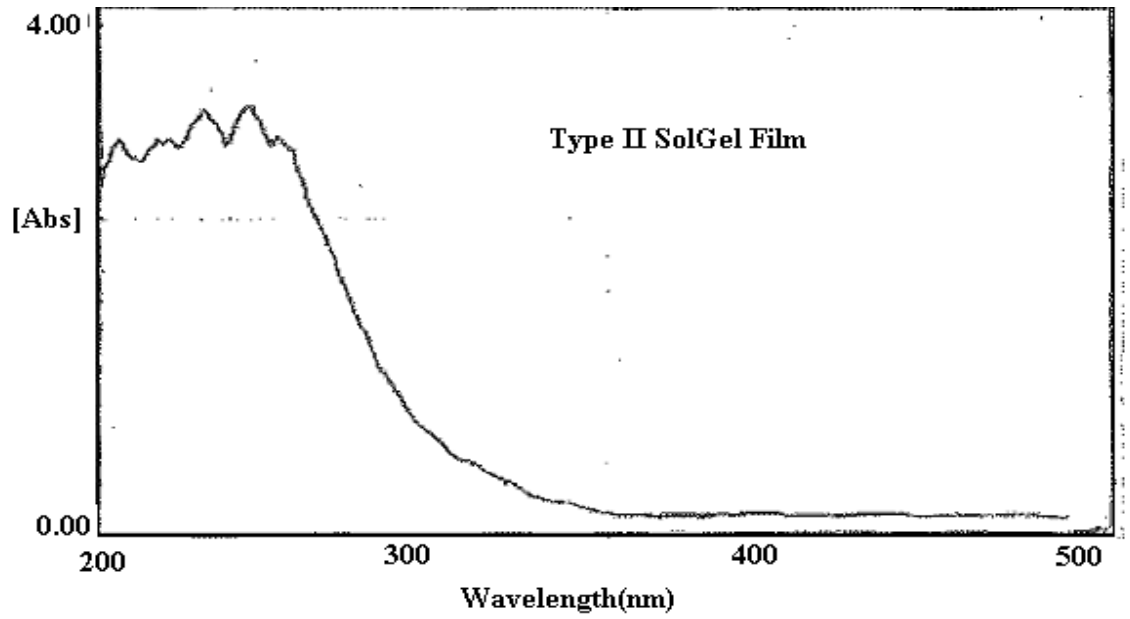

Figure 4-5. Type II Sol-gel film absorbance spectrum from 200 nm to 500 nm with a peak absorbance at 265 nm.

The film absorbance was measured in the absorbance spectrophotometer by inserting the TiO_2 film coated quartz micro scope glass slide in the sample port. The blank quartz slide was used as blank sample to subtract the absorbance of the quartz material. The film had absorbance from 300 nm (4.0 *ev*) onwards, with high absorbance from 280 nm (4.2 *ev*).

Photon of energy higher than 4.0 *ev* is required for the absorbance of TiO_2 particles and photon of higher than 4.2 *ev* is preferable due to higher absorbance for photocatalytic activity.

4.5.3 Iron doping of the TiO_2 Film

The TiO_2 sol-gel solution was mixed with the iron nitrate solution[7,8,9] at different compositions, to observe the effect on the TiO_2 film spectrum due to the different levels of Fe doping of the TiO_2 film.

The difference in the absorption spectrum can be seen from Figure 4-6 (the solution with 10% iron nitrate in solution), Figure 4-7 (the solution with 30% iron nitrate in solution) and Figure 4-8 (the solution with 50% iron nitrate in solution). The difference in the spectrum of 3 figures corresponds to the amount of iron nitrate solution in the TiO_2 solution during the preparation. With addition of iron nitrate the absorbance has increased in the UV-visible spectrum, which will help in usage of broad wavelength of UV-Visible light for the photocatalytic activity of Fe doped TiO_2.

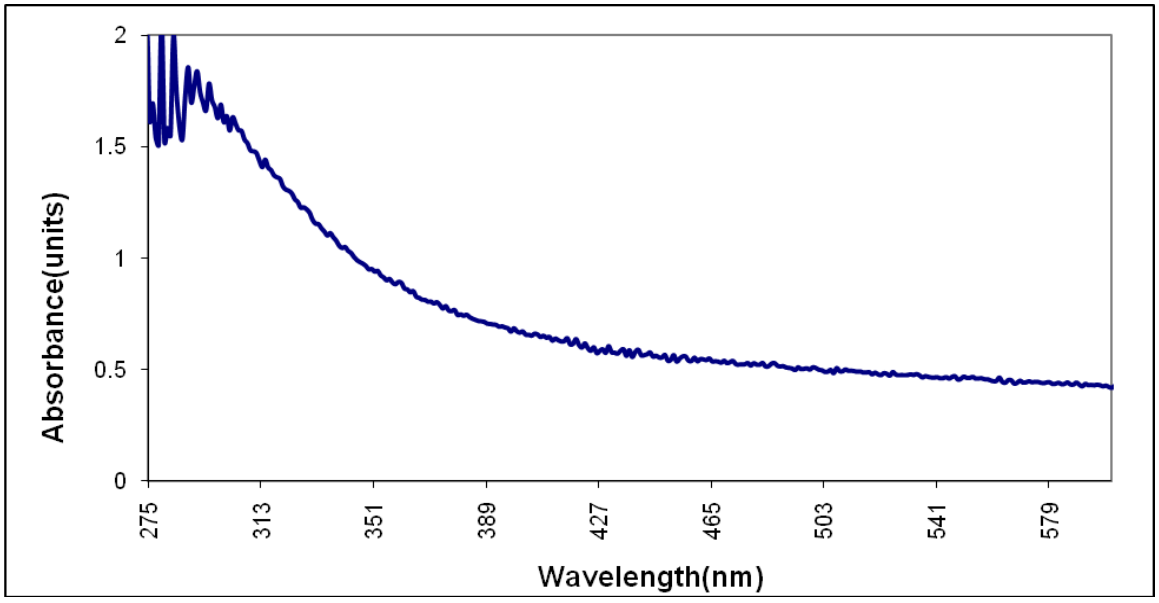

Figure 4-6.: Absorbance spectrum of iron nitrate-TiO_2 solution with 10% iron nitrate.

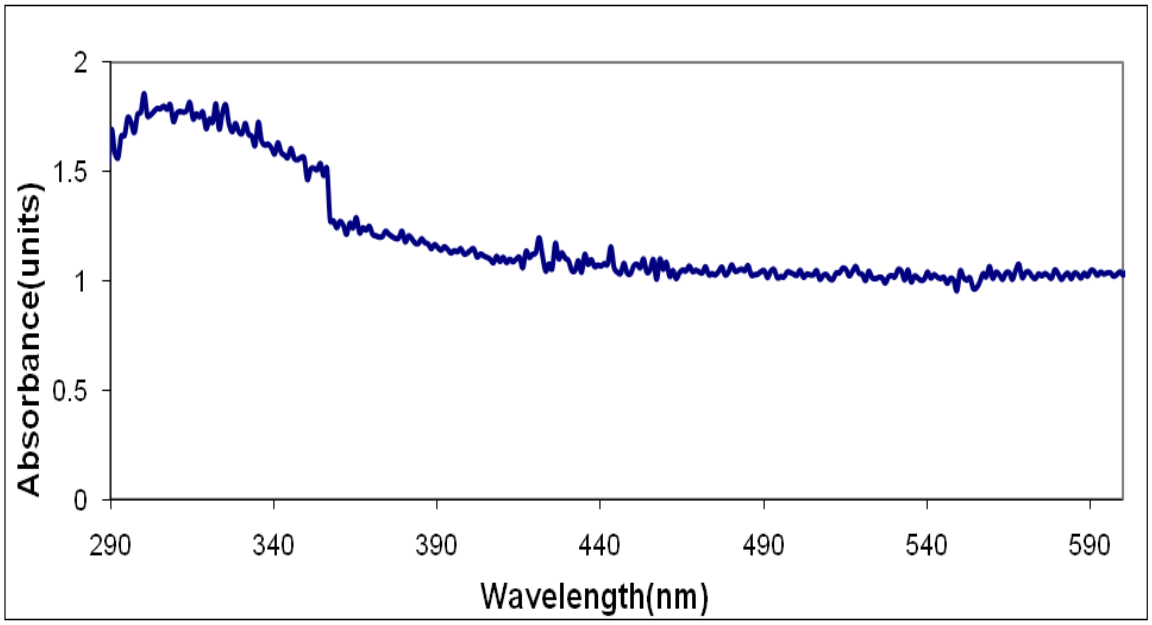

Figure 4-7. Absorption spectrum of iron nitrate-TiO_2 solution with 30% iron nitrate.

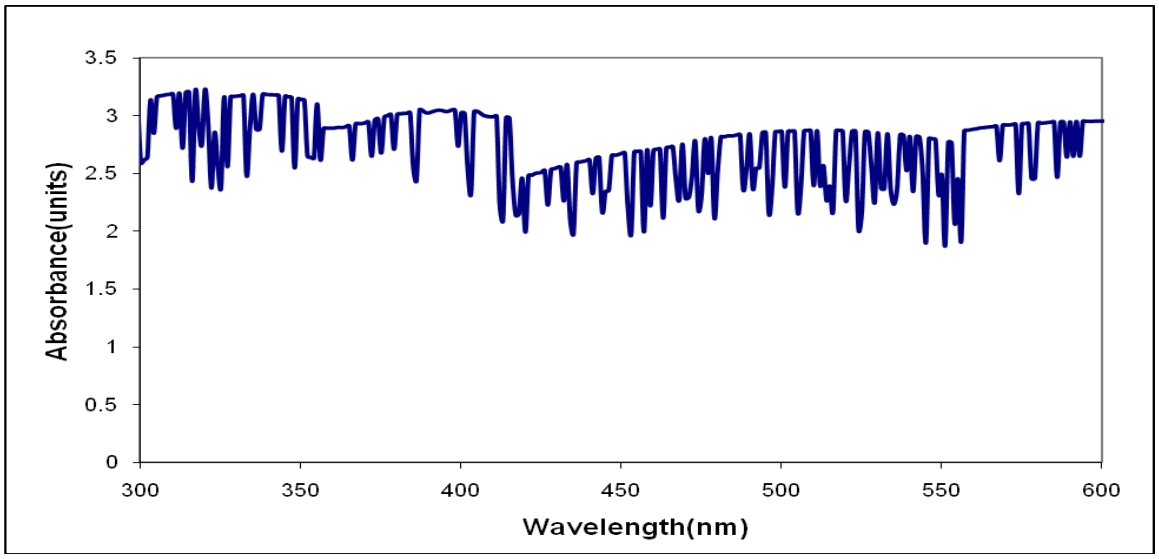

Figure 4-8. Absorption spectrum of iron nitrate-TiO_2 solution with 50% iron nitrate.

In Figure 4-9, there is a clear difference between the spectra of the different concentrations of iron nitrate solution, which had an absorbance from 410 nm onwards, where as the TiO_2 solution has an absorbance in the region from 350 nm onwards. The absorbance spectrum of the mixture of the iron nitrate and TiO_2 solution has the absorbance spectrum peak at 290 nm and absorbance

towards the end of the visible light spectrum of 900nm, so there was increase in the absorbance range of the solution mixture extended towards the visible light) which will help in the photocatalytic activity using the light energy of visible to UV wavelength.

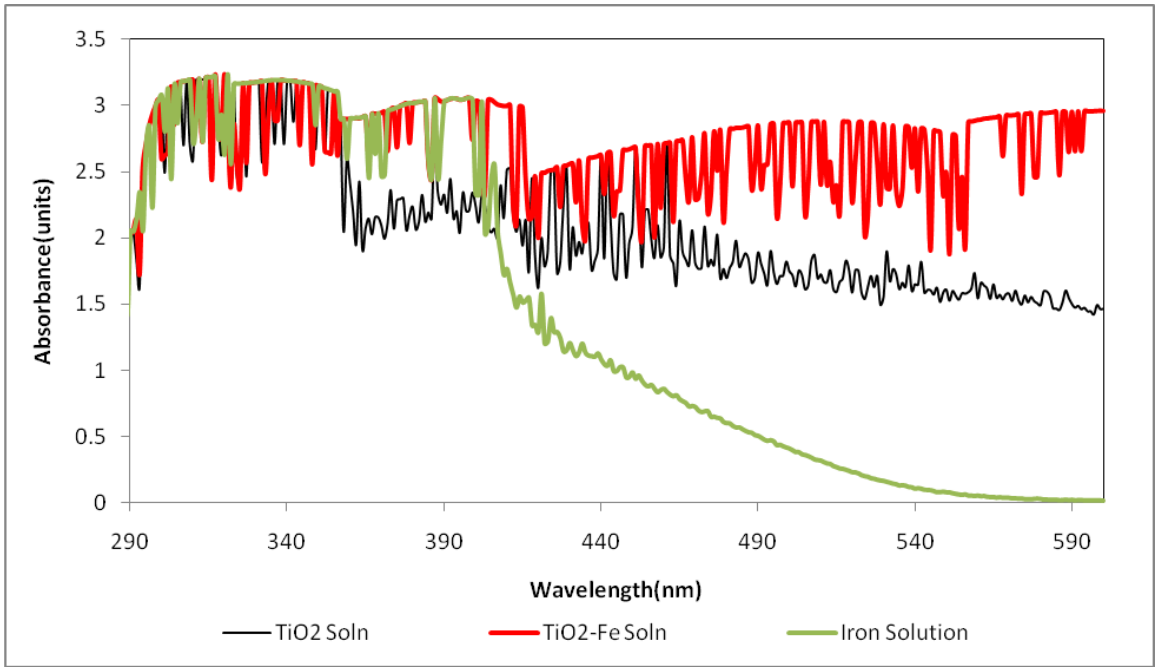

Figure 4-9. Absorption spectrum of iron nitrate, iron nitrate doped TiO_2 and TiO_2 solution.

The difference in the absorbance spectrum of the TiO_2 film coated with Fe doped and without Fe, using the sol-gel method is shown in Figure 4-10. There is clear difference in the spectrum behavior of Fe doped TiO_2 film which has absorbance from UV light region to the visible light region compared to TiO_2 film, which has absorption in the UV region. The increased wavelength of the TiO_2 absorbance spectrum allows the photocatalytic activity in the UV and extended towards visible light region.

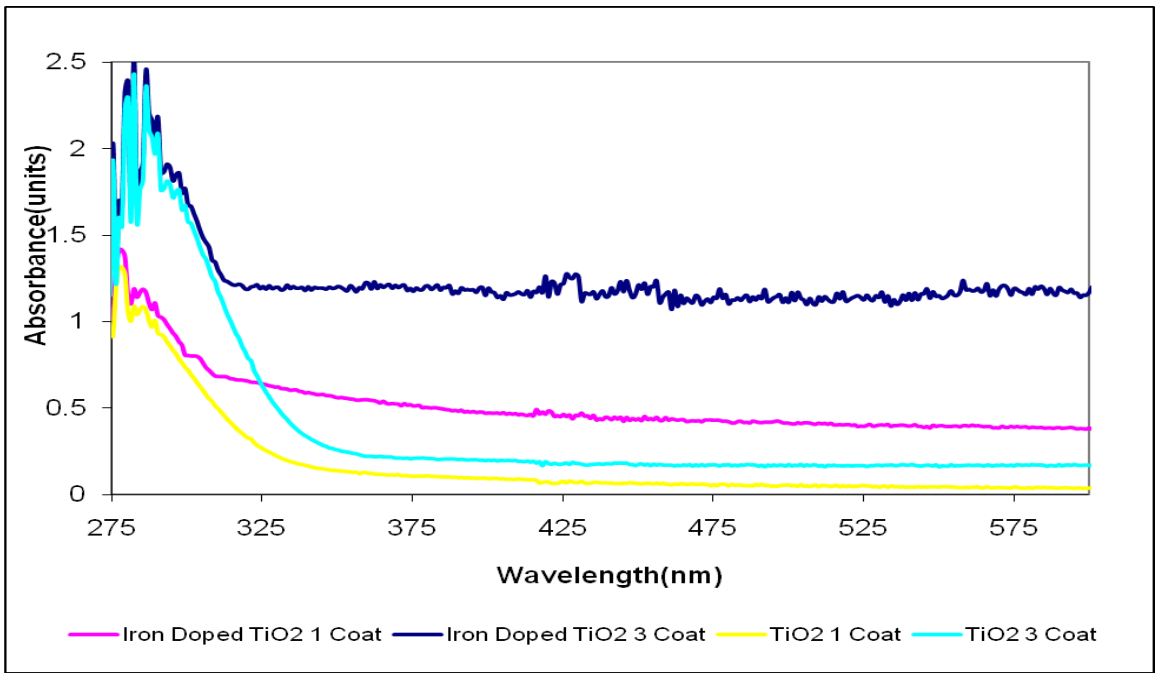

Figure 4-10. The iron doped TiO_2 film absorption spectrum compared to TiO_2 film spectrum.

A considerable increase in the absorption spectrum range can be noticed in the Figure 4-11 for the Fe-doped film. The figure shows the spectra of 1 and 3 layers iron doped TiO_2 film which has considerably greater absorption spectrum range when compared with the TiO_2 film in the UV- visible light spectrum, the broad absorption spectrum of the Fe doped TiO_2 film allows the usage of photon of UV-visible light wavelength for the photocatalytic activity on the TiO2 film and increased absorption of UV light energy.

4.6 Conclusion/Summary

The TiO_2 film was successfully coated on the substrates using the sol-gel and ESA method. The film thickness was successfully controlled by ESA method where the number of dips was directly proportional to the absorbance of the film, showing the uniformity of film coating after each layer deposition.

From the absorption spectrum of the Fe doped TiO_2 film and TiO_2 film, it was observed that Fe doping has significantly increased the absorption spectrum range of the film. It was also noticed that the change in absorption of TiO_2-Fe doped film was due to Fe dopant bonding in the TiO_2 film not due to the iron nitrate compound.

The sol-gel and ESA TiO_2 film with Fe dopant leads to a significant shift in the absorption towards the visible spectrum from UV spectrum. The Fe doped TiO_2 film using sol-gel and ESA film was preferable when compared to the TiO_2 film in testing the reactor performance due to its wider absorption spectrum in UV and visible region.

4.7 References

1. Masuda, Y., T. Sugiyama, W. S. Seo, and K. Koumoto (2003), Deposition Mechanism of anatase TiO_2 on self –assembled Monolayers from an aqueous solution". Chem Mater,2003,15,2469-2476., *Chem Mater, 15*, 2469-2476.

2. Masuda, Y., D. Wang, T. Yonezawa, and K. Koumoto (2002), Site-Selective Deposition of TiO_2 Thin Films Using Self-Assembled Monolayers and Their Dielectric properties., *Key engineering Materials, 228-229*, 125-130.

3. Jefrey, C. B. and W. S. George (1990), *Sol-Gel Science: The Physics and Chemistry of Sol-Gel Processing*, 1st ed., 912 pp., Academic Press.

4. Sol-gel Forum (2011), WWW.Sol-gelforum.com. , *2008*.

5. Spillman Jr, W. B., T. Zeng, and R. O. Claus (2002), Modeling the Electro-static self-assembly process using stochastic cellular automata., *Smart mater Structure, II*, 623-630.

6. Liu, Y., A. Rosidian, K. Lenahan, W. You-Xiong, Z. Tingying, and R. O. Claus (1999), Characterization of electrostatically self-assembled nanocomposite thin films., *Smart mater Structure, 8*, 100-105.

7. Akihiko, H. (2001), Highly Photocatalytic activity of F-Doped TiO_2 Film on Glass., *Journal of Sol-Gel Science and technology*, *22*, 47-52.

8. Navio, J. A., J. J. Testa, P. Djedjeian, J. R. Padron, D. Rodriguez, and M. I. Litter (1999), Iron doped titania powders prepared by a sol-gel method. Part II: Photocatalytic properties., *Applied Catalysis A: general*, *178*, 191-203.

9. Shah, S. I., W. Li, C. -. Huang, O. Jung, and C. Ni (2002), Study of Nd^{3+}, Pd^{2+}, Pt^{4+}, and Fe^{3+} , dopant effect on photoreactivity of TiO_2 nanoparticles ., *PNAS, 99*, 6482-6486.

5 REACTOR DESIGN, TESTING/EXPERIMENTS AND RESULTS

5. 1 Introduction:

Based on the observation of absorption spectrum results of TiO_2 films coated using different methods as discussed in Chapter 4,experiments were performed with TiO_2 film coated by different methods using a microscope slide reactor, a single tube reactor and a multiple tube reactor (seven tube reactor).

Experiments were performed using the microscope slide reactor to analyze the performance of TiO_2 photocatalyst with UV light sources of 254 nm and 385 nm in the degradation of Congo red and Methyl Orange compared to degradation by direct UV photolysis. The results demonstrate the influence of wavelength on the photocatalysis process and TiO_2 photocatalysis performance compared to UV photolysis.

Single tube reactor experiments were performed using quartz tubes coated with TiO_2 and TiO_2-Fe doped films using the sol-gel and ESA methods. Based on the experimental results from the single tube reactor using TiO_2 andTiO_2-Fe doped films, the film with higher performance in the degradation of Congo red, potassium iodide and nitro phenol was selected for experiments using multiple tube reactor.

The multiple tube reactor performance was analyzed in the degradation of Congo red, KI (potassium iodide) and nitro phenol. Factorial DOE (design of experiments) was used to analyze the individual reactor parameter affects on the reactor performance.

5.2 Micro Film Reactor

The reactor, as shown in the Figure 5-1, consisted of a stainless steel rectangular vessel with cylindrical hollow surface in the centre, and one of the side faces has been cut. At the open face of the reactor, the microscope quartz slide was inserted and sealed using a rubber gasket and steel clamp, which was tightened to the surface using thumb screws. Precautions were taken while tightening the steel clamp to prevent breaking the microscope quartz slide. The internal surface of the microscope quartz slide was coated with TiO_2 film. The solution to be degraded in the experiment was filled in the reactor, with a magnetic stirrer being kept at the bottom of the reactor.

After each run, the TiO_2 film coated microscope quartz slides were replaced.

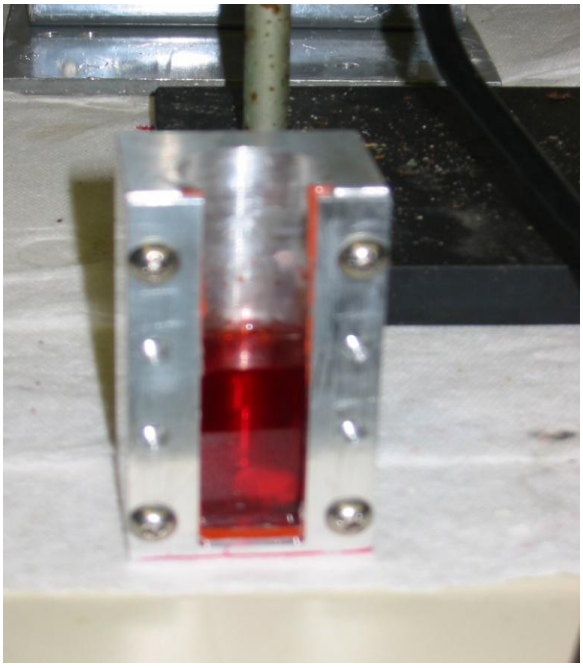

Figure 5-1. Microscope slide Reactor with microscope quartz slide and stirrer.

5.2.1 Experimental setup:

The experimental setup as shown in Figure 5-2 consisted of the microscope quartz slide reactor with a stirrer kept on the top of the magnetic stirrer. The light source and the microscope quartz slide need to be aligned for the transmission of the light from the light source to pass through to the TiO_2 film coated microscope quartz slide. The wave-lengths of the light sources used in the experiment were 254 nm and 385 nm. The light source was fixed using a stand and the alignment

of the reactor was achieved by moving the magnetic stirrer which was placed on an adjustable stand.

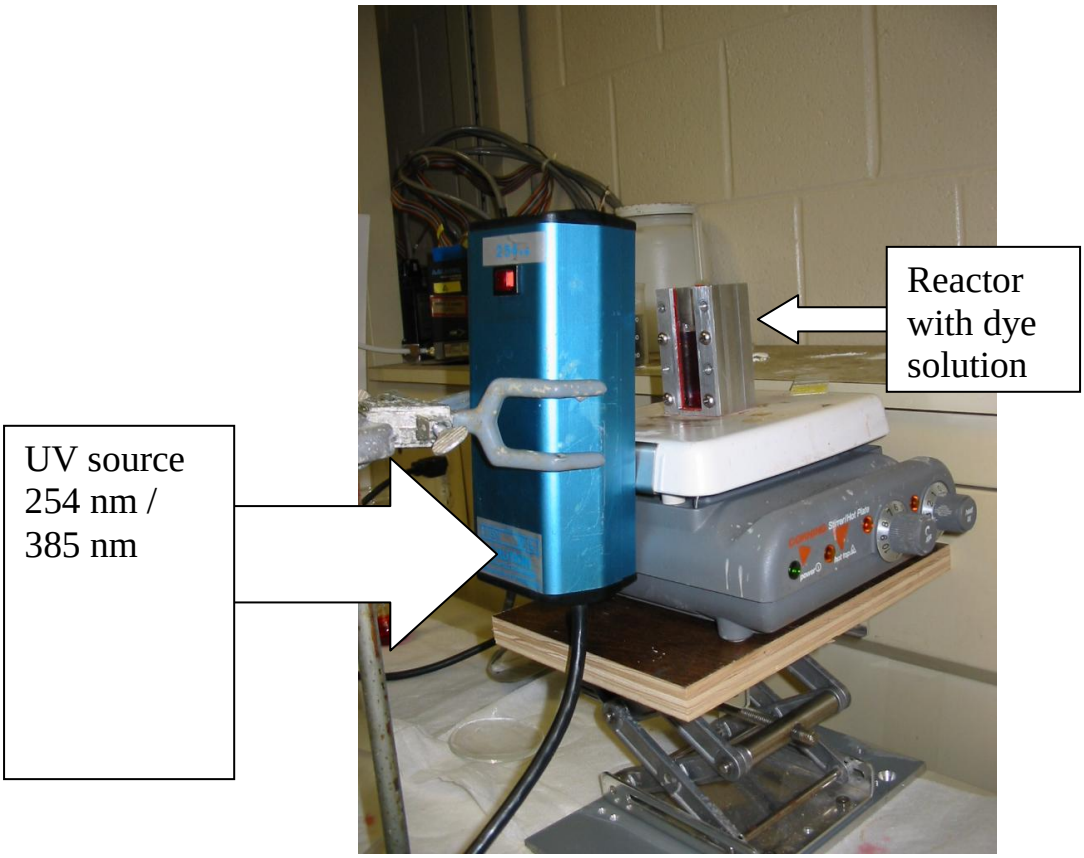

Figure 5-2. Micro film reactor set-up with UV lamp source aligned to the reactor on the stirrer table.

UV protective glasses must be worn while working near the reactor. The solution must be stirred continuously using the magnetic stirrer for uniform concentration of the solution. Prior to exposing the reactor to the UV lamp, it was warmed up for 30 min to achieve stable intensity.

5.2.2 Experimental Procedure

The TiO_2 film was coated on the quartz slide using the sol-gel method as mentioned in chapter 4, section 4.3.1, Solution Type I. One side of the quartz slide was covered with tape and then the slide was dipped in the TiO_2 solution using the dip-coater. In between each dip the glass slide was air dried, and after which the tape was removed from the slide before calcining it in the furnace for 1 hr at 450 ºC.

The 100 mg/L solution of congo red/methyl orange sample was filled in the microscope slide reactor with the stirrer rotating inside. The light was exposed on to the reactor after the 254/385 nm lamp was warmed up for 30 minutes. Every 10 min, 0.5 mL of sample was taken from the reactor and it was diluted to 5 mL using the 5 mL volumetric flask, and its concentration was measured using the absorption spectrophotometer.

5.2.3 Methyl Orange Degradation

One of the chemical compounds used to test the TiO_2 film photocatalytic performance was methyl orange. Methyl orange was selected based on the feasibility of measuring the concentration of the methyl orange.

A calibration curve for methyl orange was prepared by measuring absorption as a function of concentration at 498 nm, by using the spectrophotometer in UV-visible region spectrum at a wavelength of 498 nm.

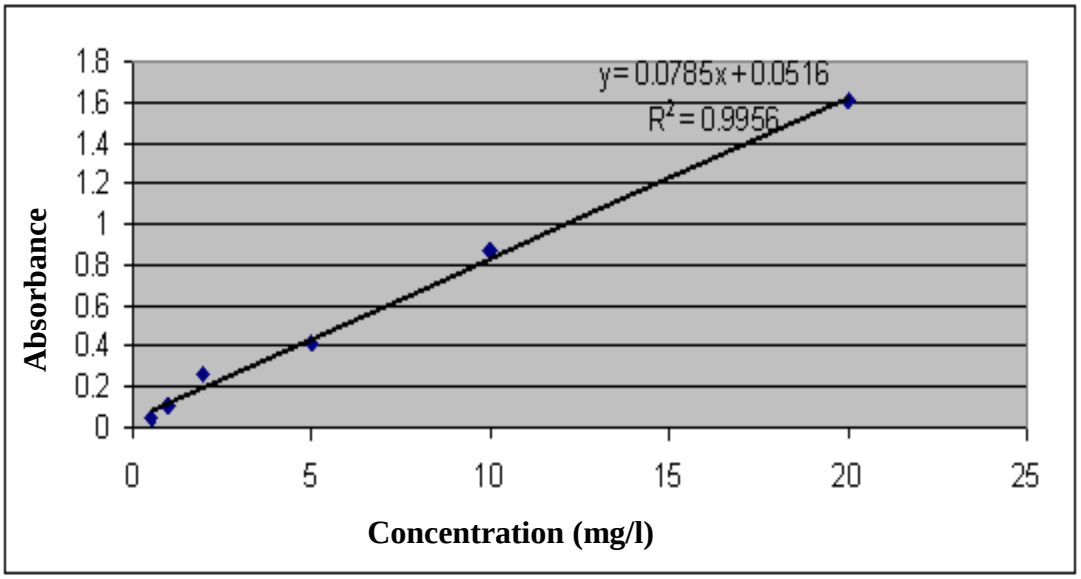

Figure 5-3. Calibration Curve of Methyl Orange

The TiO_2 film coated microscope quartz slide was tested with 254nm and 385 nm to observe the photocatalyst performance in the degradation of methyl orange at different wavelengths. To validate the photocatalyst degradation of methyl orange blank microscope quartz slide was used for direct UV photolysis using 254nm wavelength lamp in degradation of methyl orange.

The experimental results as plotted on the Figure 5-4 show the concentration drops from 100 mg/L to 42 mg/L under 254 nm lamp sources.

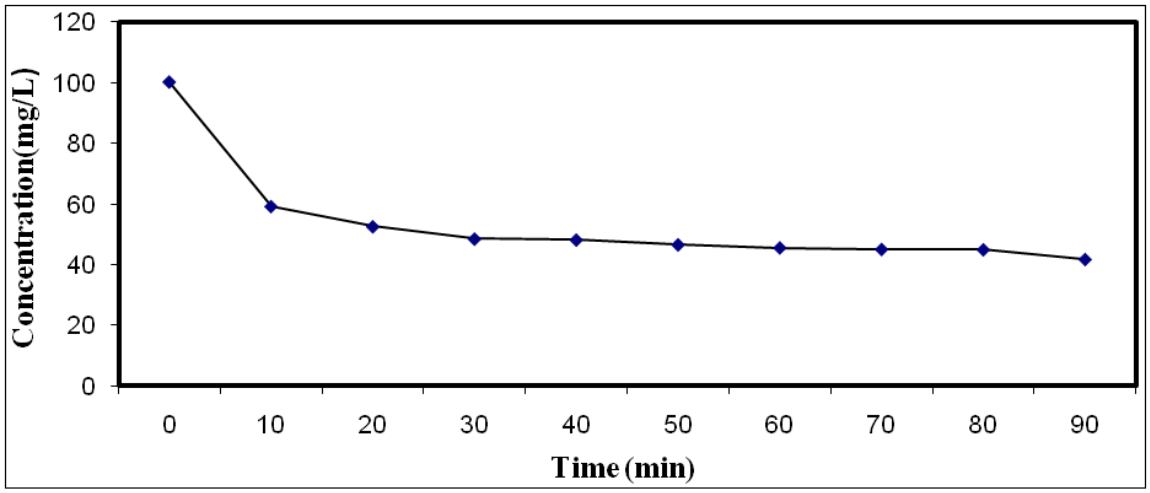

Figure 5-4. Methyl orange degradation using TiO_2 photocatalyst under 254 nm UV light irradiation.

The experimental results as shown in Figure 5-5, the drop in methyl orange concentration from 100 mg/L to 85 mg/L under 385 nm lamp source.

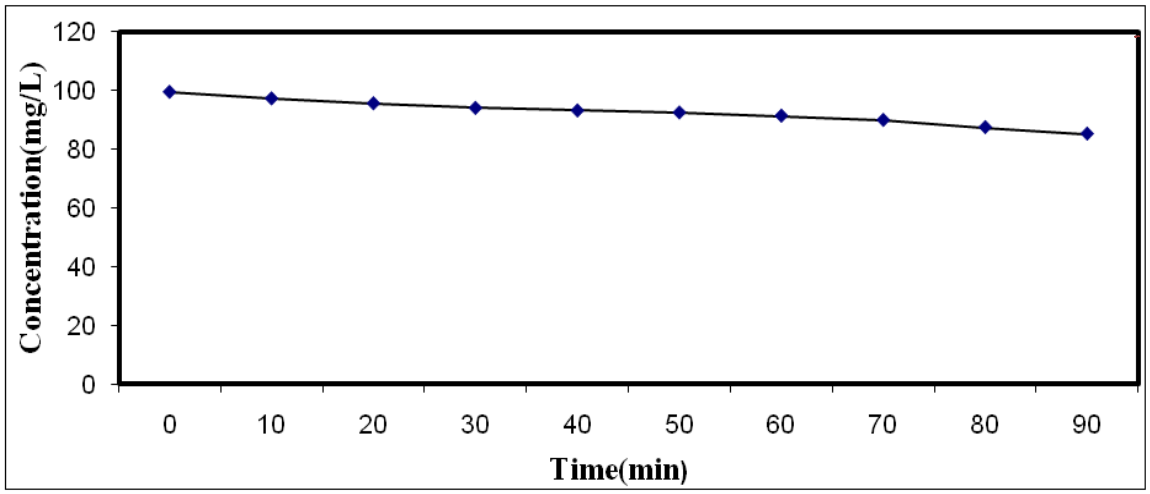

Figure 5-5. Methyl orange degradation using TiO_2 photocatalyst under 385 nm UV light irradiation.

The experiment result as shown in Figure 5-6, the concentration of methyl orange dropped from 100 mg/L to 92 mg/L with 254 nm lamp source using blank microscope slide. There was a substantial difference in the reactor performance in treating the methyl orange with TiO_2 film

compared to blank microscope slide, it can be concluded that TiO_2 had a significant role in the degradation of the methyl orange. There was considerable increase in the TiO_2 photocatalyst performance in degradation of methyl orange using 254 nm compared to 385 nm, as TiO_2 absorbance is higher for shorter wavelengths.

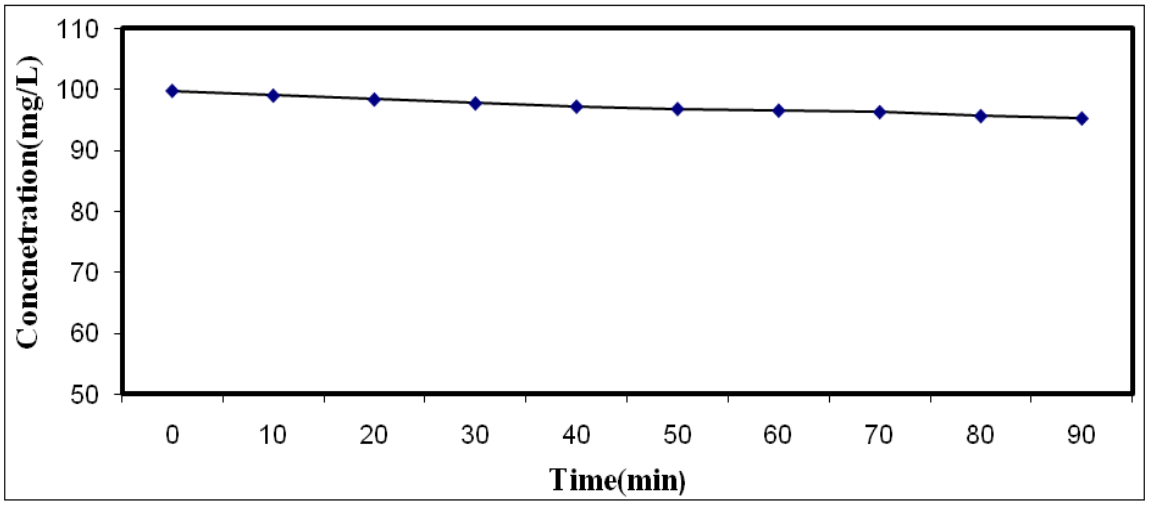

Figure 5-6. Methyl Orange degradation using blank microscope slide under 254 nm UV light irradiation.

The factors which could affect the observed reaction rate are the concentration of the methyl orange, the change in the microscope slide surface (blank vs TiO_2 film surface), and change in the light intensity of the UV lamp.

If we assume the change in the light intensity of the UV lamps in both experiments was negligible and with a significant amount of light will be absorbed by the TiO_2 film, the main factors affecting the reaction rate are concentration of the methyl orange and microscope slide surface being coated with TiO_2 film.

5.2.4 Congo Red Degradation

The TiO_2 film coated microscope quartz slide was tested with 254nm and 385 nm to observe the photocatalyst performance in the degradation of Congo red at different wavelengths. To validate the photocatalyst degradation of congo red, a blank microscope quartz slide was used for direct UV photolysis using 254nm wavelength lampas a control.

Congo red solution of 100 mg/L was prepared in a 100 mL volumetric flask and the solution was calibrated at different concentrations (figure 5-7) on the spectrophotometer in UV-visible region spectrum at a wavelength of 498 nm.

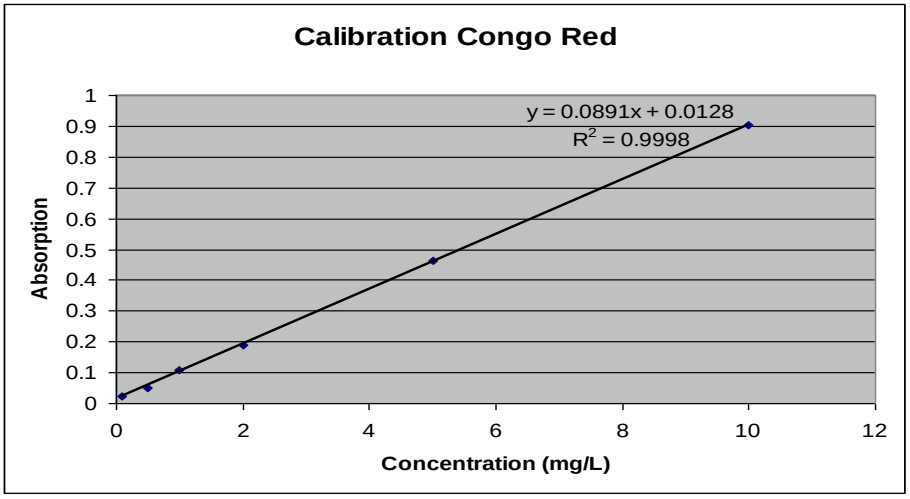

Figure 5-7. Calibration Curve of Congo red.

The experimental results in Figure 5-8 shows the drop in concentration of Congo red from 100 mg/L to 38 mg/L under 254 nm lamp source.

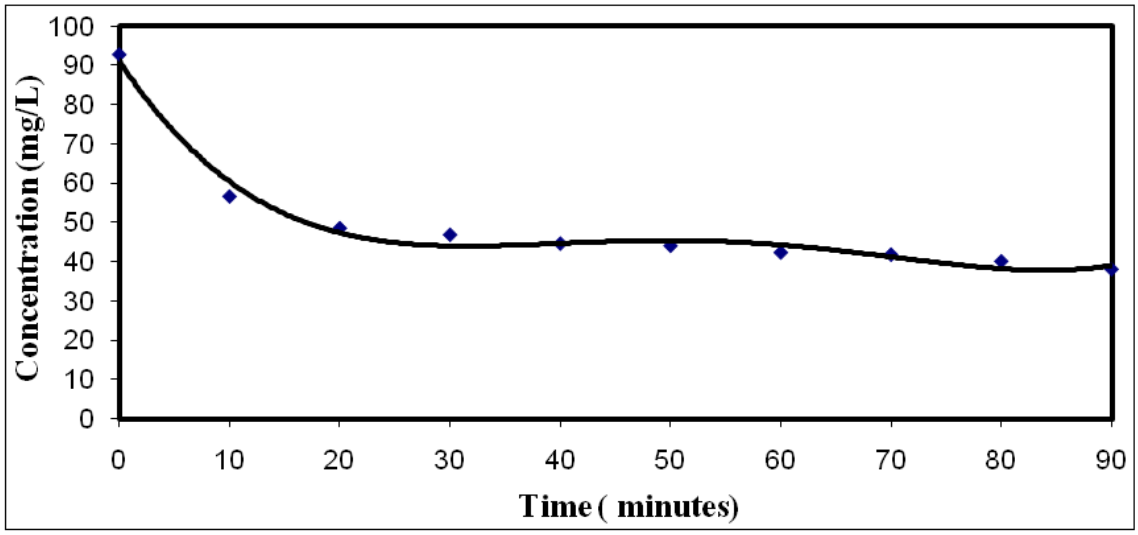

Figure 5-8. Congo red degradation using TiO_2 photocatalyst under 254 nm UV light irradiation.

The experimental results in Figure 5-9 shows the drop in concentration of Congo red from 100 mg/L to 65 mg/L under 385 nm lamp source.

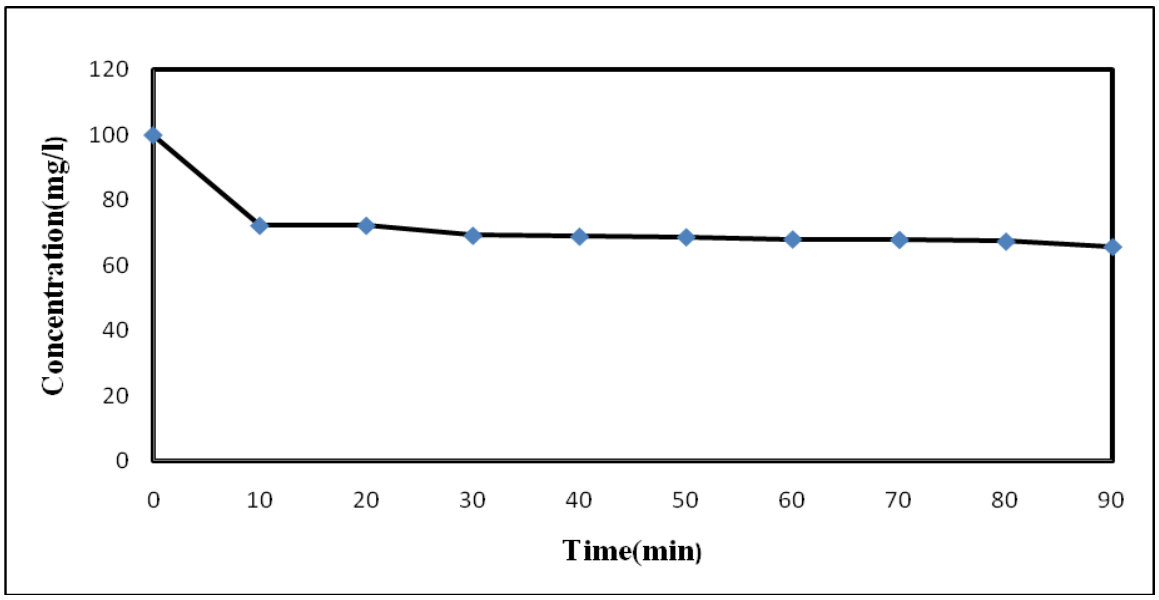

Figure 5-9. Congo red degradation using TiO_2 photocatalyst under 385 nm UV light irradiation.

The experimental results in Figure 5-10 shows the drop in concentration of Congo red from 100 mg/L to 86 mg/L under 254 nm lamp source for the blank control.

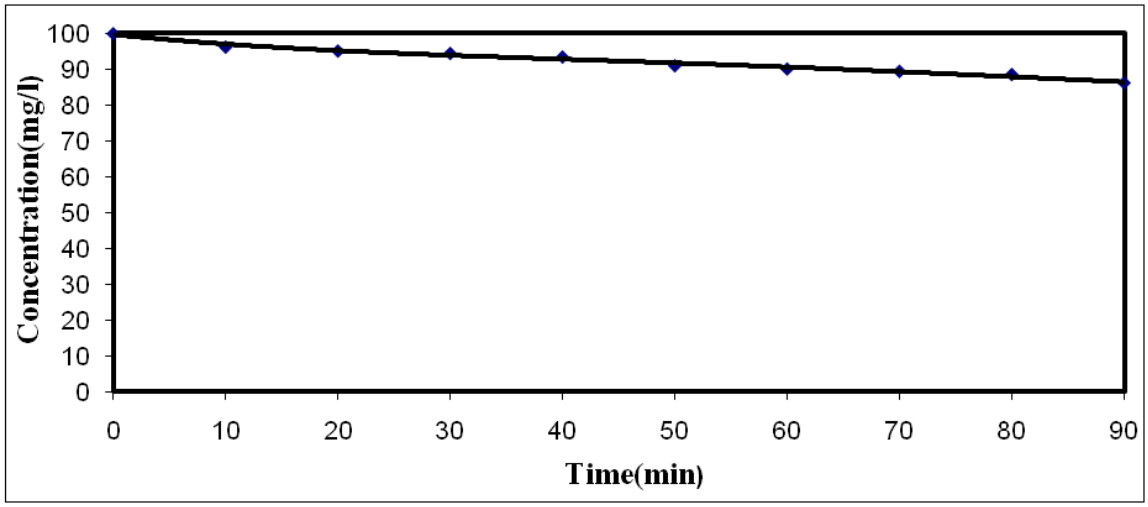

Figure 5-10. Congo red degradation using blank micro slide under 254 nm UV light irradiation.

Similar to the results in methyl orange degradation, there was a substantial difference in the reactor performance in treating the congo red with TiO_2 film compared to blank microscope slide, it can be concluded that TiO_2 had a significant role in the degradation of the congo red. There was considerable increase in the TiO_2 photocatalyst performance in degradation of congo red using 254 nm compared to 385 nm, as TiO_2 particles absorbance is higher for shorter wavelengths.

Again the possible factors affecting the difference in observed reaction rate with TiO_2 film coated and blank microscopic slides, are concentration of congo red, the change in the microscope slide surface, the mixing inside the reactor and change in the light intensity of the UV lamp.

As any possible change in the light intensity of the UV lamp can be assumed to be very minimal as both the contaminants showed similar behavior with change in UV light and photocatalyst surface, and the mixing inside the reactor should be constant as it was operated with same stirrer and rpm, the primary factors affecting the reaction rate are concentration of the Congo red and the TiO_2 film surface on microscope slide.

From the experiments in degradation of Congo red and Methyl Orange, it can be concluded the reactor was successfully able to degrade the contaminant, and there was considerable increase in reaction rate using the microscope quartz slide with TiO_2 film coated when compared to blank microscope slide.

Both the contaminants methyl orange and congo red degradation was higher by TiO_2 photocatalysis with 254 nm UV light source when compared to 385 nm UV light source.

5.3 SINGLE TUBE REACTOR

The performance of the TiO_2 photocatalyst surface coated on quartz tubes by different coating methods were analyzed using single tube reactor (Figure 5-11). The single tube reactor consists of a quartz tube in the middle of the rectangular vessel, with a magnetic stirrer at the bottom to mix the solution for uniform concentration in the vessel.

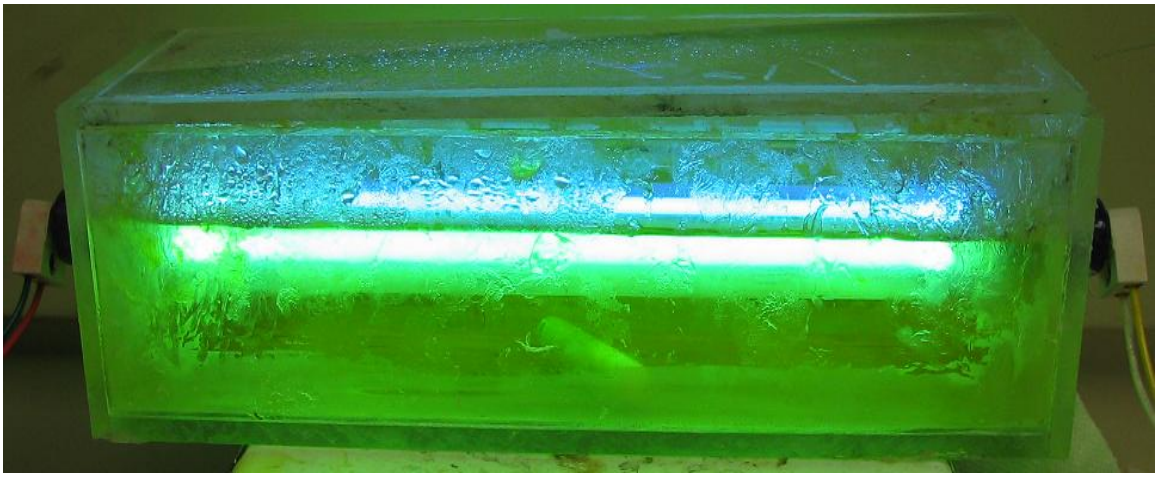

Figure 5-11. The single tube reactor with UV lamp and KI solution.

Experiments were performed in the single tube reactor using solutions of Congo red, KI (potassium iodide) and nitro phenol as the contaminants to be treated.

5.3.1 Congo red Degradation

The single tube reactor was tested in the degradation of Congo Red by photocatalysis process with TiO_2 film coated by various methods on the quartz tube.

5.3.1.1 Experimental Procedure

In this experiment a quartz tube coated with TiO_2 film using sol-gel and ESA method, was fixed in the single tube reactor using silica caulk and allowed to air dry for 24 hrs until it was totally dried. When the silica caulk was dried and the reactor was ready for the experiment, Congo red solution of 100 mg/L concentration was prepared in an l000 mL volumetric flask after stirring the solution to mix the Congo red in water. The solution was then transferred to the single tube reactor to fill it slightly above the quartz tube a magnetic stirrer was placed inside it and the reactor was placed on a magnetic stirrer.

The UV lamp was inserted through the quartz tube and wired to ballast, which was connected to the power source. After the lamp was switched on, the magnetic stirrer was rotated and samples of the solution were taken each 1 hr to measure the concentration.

The experiment was performed by coating sand blasted tubes with TiO_2 and TiO_2-Fe doped film by sol-gel and ESA methods as explained in Chapter 4, section 4.3 and 4.4.

The results as plotted in Figure 5-10, shows there was considerable difference in performance of reactor in degradation of Congo red using TiO_2 film when compared to blank film quartz tube. The results also showed TiO_2-Fe doped film has slightly better performance when compared to just TiO_2 film.

Table 5.1: Congo red degradation in single tube reactor by different methods.

Method	Order of Reaction	Rate Constant (1/sec)	Initial Concentration (mg/L)	Final concentration After 6hrs (mg/L)
Sol-gel TiO_2	First Order	0.0814	96	60
Sol-gel TiO_2-Fe	First Order	0.0852	89	51
ESA TiO_2	First Order	0.0772	99	66
ESA TiO_2-Fe	First Order	0.0821	89	54
Blank	First Order	0.0472	95	71

The sol-gel film had slightly better performance when compared to ESA method the sol-gel TiO_2-Fe doped has the better performance among all the methods in degradation of Congo red.

Figure 5-13 shows that a plot of Ln (C) vs time (hr) was linear, suggesting a first order reaction in the degradation of Congo red in single tube reactor for all experiments. The rate constant also confirmed the better performance of TiO_2 –Fe doped and TiO_2 film when compared to blank tube. The Sol-gel TiO_2-Fe doped has better performance among all the TiO_2 film methods in Congo red degradation.

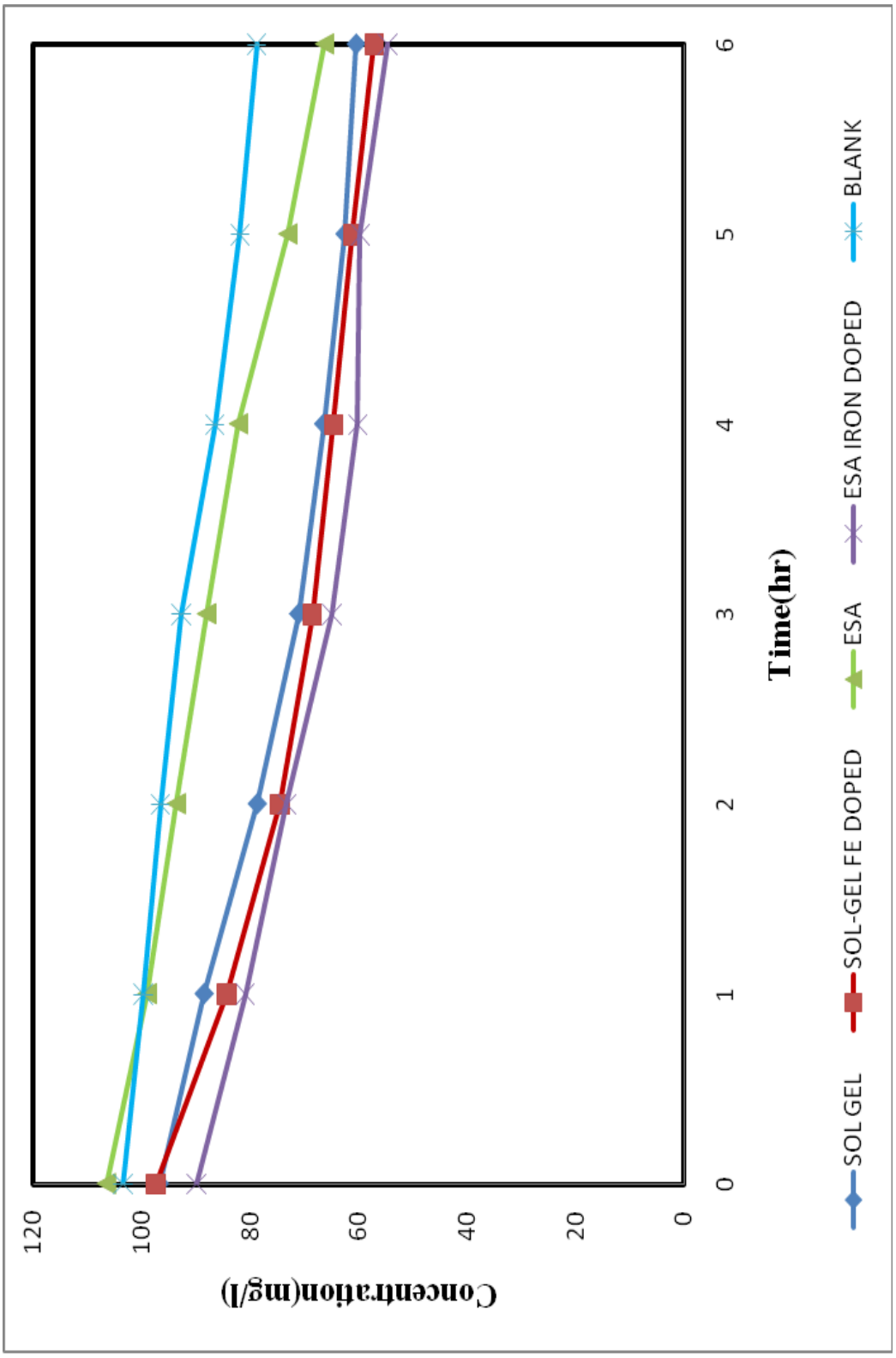

Figure 5-12. Concentration vs time of Congo red degradation using different film coated quartz tubes and blank quartz tube.

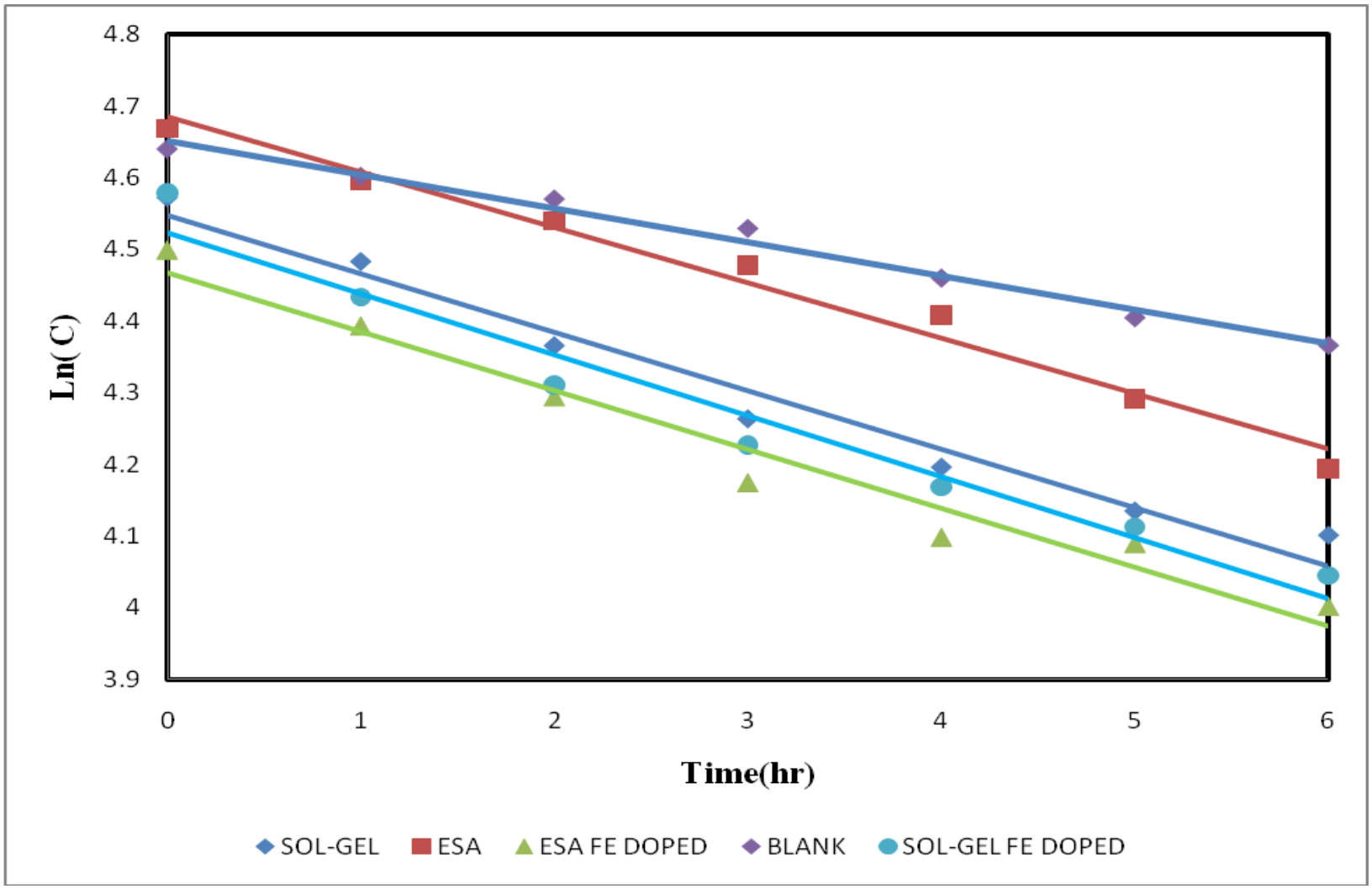

Figure 5-13. Ln(C) vs time of Congo red degradation using different film coated quartz tubes and blank quartz tube.

5.3.2 Potassium Iodide (KI)

The single tube reactor was tested using iodine (I_2) liberation from KI reaction with various film coating on the quartz tube.

The typical absorption spectrum of I_2 is shown in Figure 5-14. The calibration curve was prepared plotted before performing the experiments to measure the concentrations.

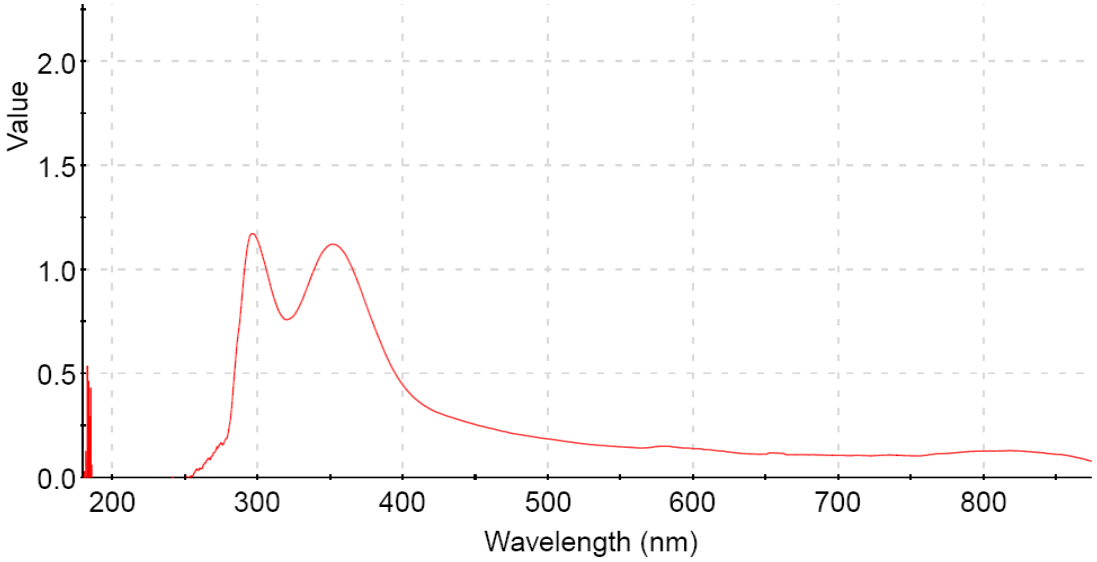

Figure 5-14. Absorbance spectrum of the I_2 in the UV-Visible spectrum from 200 -800 nm.

The KI solution was transparent in color *i.e.* with no color, with the generation of iodine during the photocatalytic process the solution turns yellow indicating the presence of iodine in the solution as shown in Figure 5-15. The iodine concentration in the solution with respect to time was used to evaluate the reactor performance and the rate constant of the reaction in the reactor.

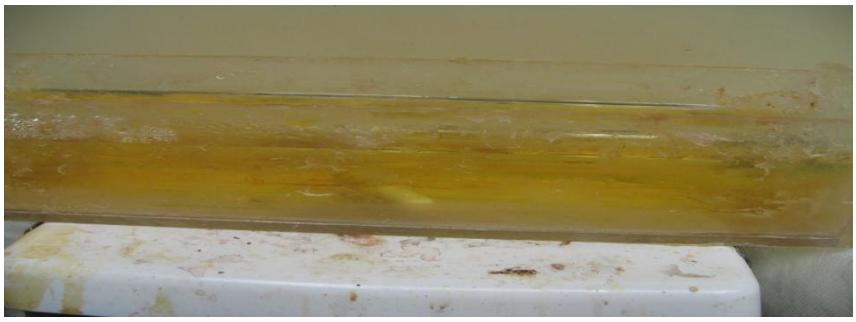

Figure 5-15. The I_2 liberated in single tube reactor by KI degradation.

The generation of iodine in the solution was confirmed by adding starch solution. The blue color generated by the addition of the starch further confirms the presence of iodine in the reactor, *i.e.* the generation of iodine during the reaction process in the single tube reactor.

Figure 5-16 shows the reactor with the starch indicator added to the solution with iodine in the top picture and picture below was the one with the light shown in it.

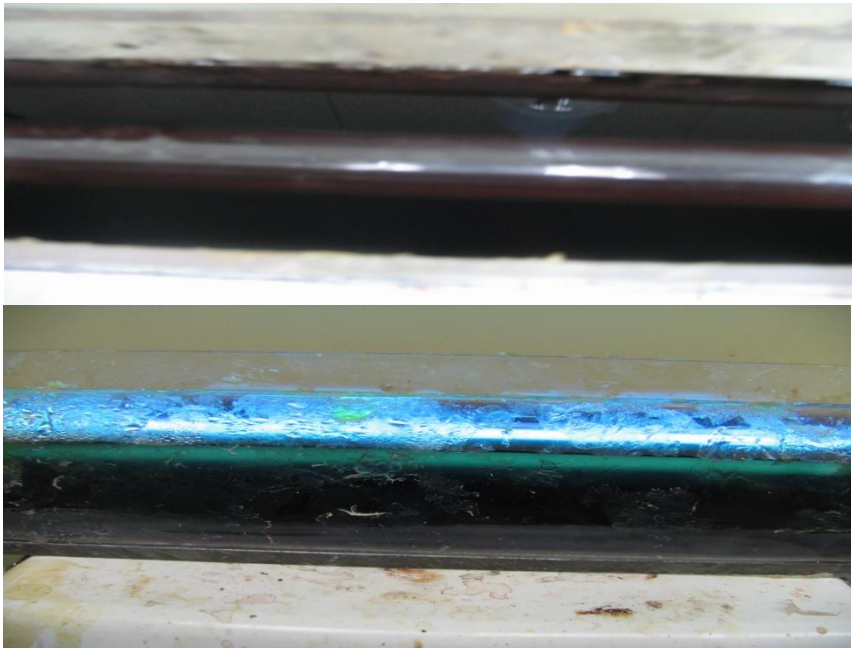

Figure 5-16. The I_2 solution with starch indicator turning the solution blue.

5.3.2.1 Experiment Procedure

In this experiment a quartz tube coated with TiO_2 film was fixed in the single tube reactor using silica gel and it was allowed to air dried for 24 hrs or more until it was totally dried. When the silica gel was dried and the reactor was ready for the experiment a KI (Potassium Iodide) solution of concentration 0.1 N by adding 34 mg/L in a l000 mL conical flask after shaking the solution to mix the KI in water. The solution was then transferred to the single tube reactor covering the quartz tube.

The UV lamp was inserted through the quartz tube and wired to ballast which was connected to the power source. After the lamp was connected to power source and switched on the magnetic stirrer was rotated and samples of reactor solution were taken each 1 hr to measure the concentration of the I_2 liberated in the solution.

Before starting the experiment the I_2 solution absorbance at different concentration was measured using the absorption spectrophotometer to make a calibration curve plot figure 5-17 of concentration to the absorbance of the I_2 at 293 nm.

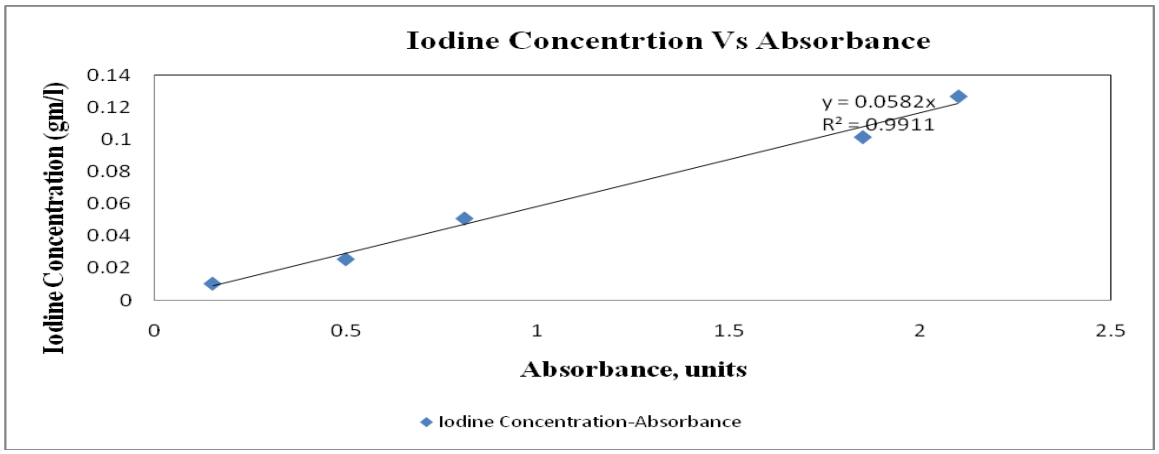

Figure 5-17. Calibration Curve of I_2 Concentration Vs Absorbance

The concentration vs time in Figure 5-18, shows the degradation of KI in single tube reactor using TiO_2, TiO_2-Fe doped film by sol-gel and ESA method and blank quartz tube. It shows the sol-gel-iron doped quartz tube performance was better when compared to the ESA and ESA-Fe doped TiO_2 film performance. The blank quartz tube performance was far below to the TiO_2 and TiO_2-Fe doped film performance.

Table 5.2: KI degradation in single tube reactor by different methods

Method	Order of Reaction	Initial Concentration (mg/L)	Final concentration After 6hrs (mg/L)
Sol-gel TiO_2	Pseudo First Order	34	33.15
Sol-gel TiO_2-Fe Doped	Pseudo First Order	34	33.1
ESA TiO_2	Pseudo First Order	34	33.4
ESA TiO_2-Fe	Pseudo First Order	34	33.3
Blank	Pseudo First Order	34	33.65

The Ln (C) vs time graph shown in Figure 5-19 demonstrates that the KI degradation was different in first 2 hr and the final 2-6 hrs. All the individual lines for each film show similar behavior from 0 – 6 hrs, during the first 2 hrs the reaction rate was higher when compared to the 2-6 hrs showing it was dependent on the concentration of KI. The experimental results showed it was first order reaction from 2-6 hrs.

Based on the experimental results of KI degradation using TiO_2 and TiO_2–Fe doped photocatalyst coated by sol-gel and ESA method were significantly different compared to blank quartz tube(without TiO_2 film) degradation by UV treatment.

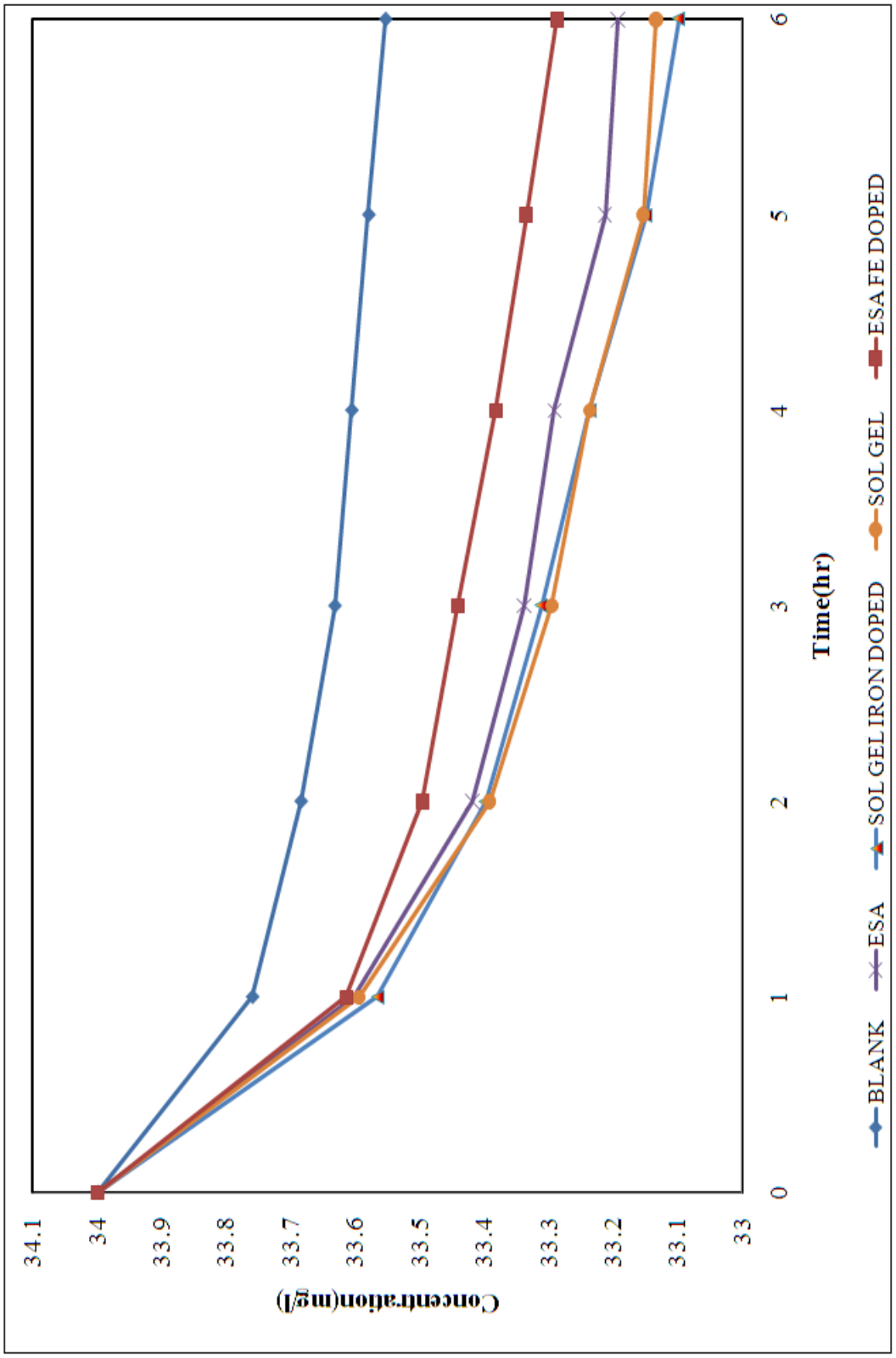

Figure 5-18. Concentration vs time of KI degradation using different film coated quartz tubes and blank quartz tube.

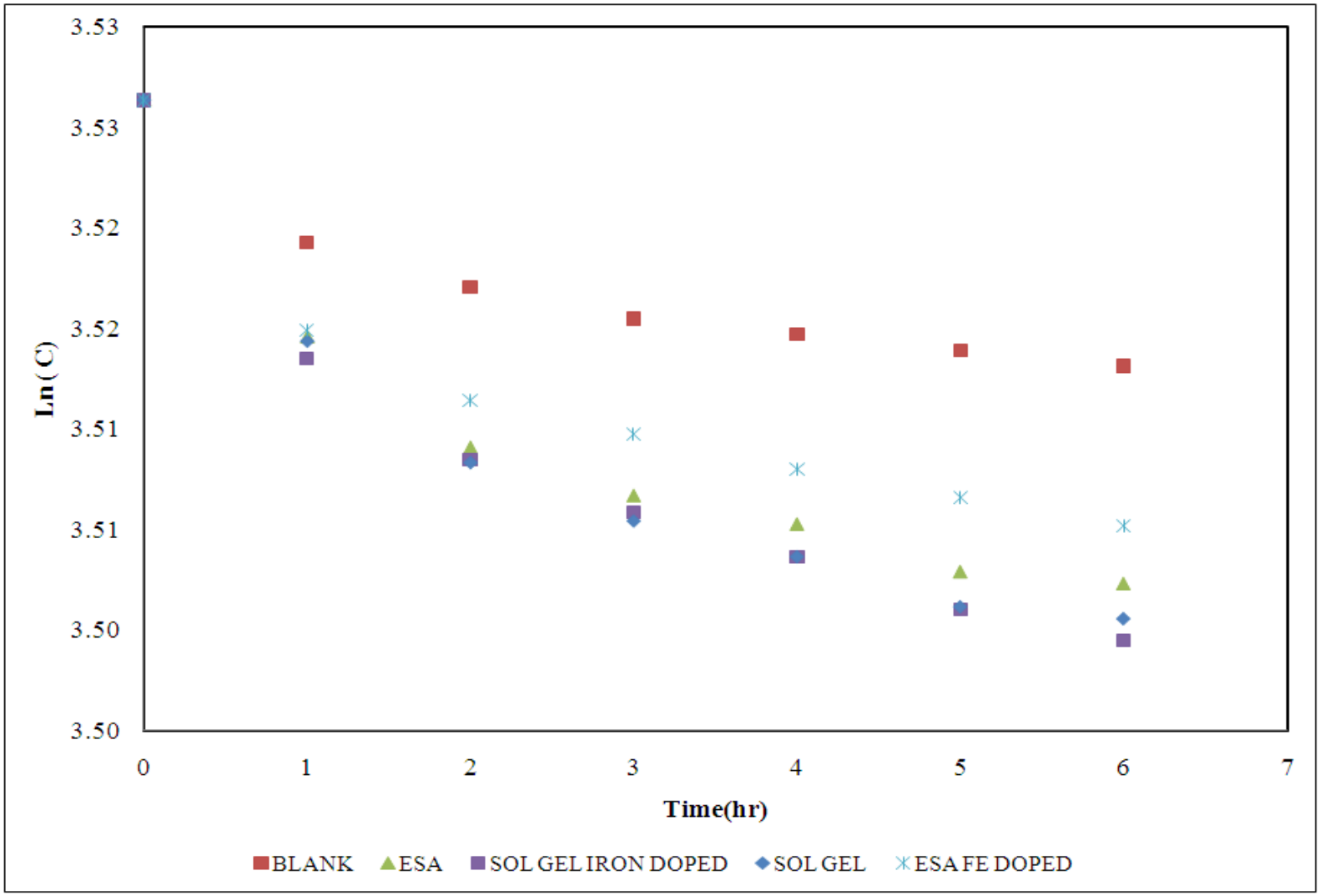

Figure 5-19. Ln (C) vs time of KI degradation using different film coated quartz tubes and blank quartz tube.

It verifies the degradation of contaminant in water by TiO_2 photocatalysis process and also to show the increase in performance when compared to direct UV treatment. The observed difference in reaction rate 0-2 hrs to 2-6 hrs might be due to the deposition of I_2 layer on the film where the film once stabilized started reacting with KI or decrease in TiO_2 film.

5.3.3 Nitro phenol Degradation

Single tube reactor was also used in testing the degradation of the nitro phenol. Experiments were performed using quartz tubes coated with sol-gel TiO_2 film, sol-gel TiO_2-Fe doped, ESA TiO_2 and ESA TiO_2-Fe doped film.

Based on safety toxicity limit of exposure for nitro phenol, the initial concentration of the nitro phenol solution used for the experiment was 20 mg/L.

Typical absorbance spectrum of nitro phenol using spectrophotometer is shown in the below figure (Figure 5-20).

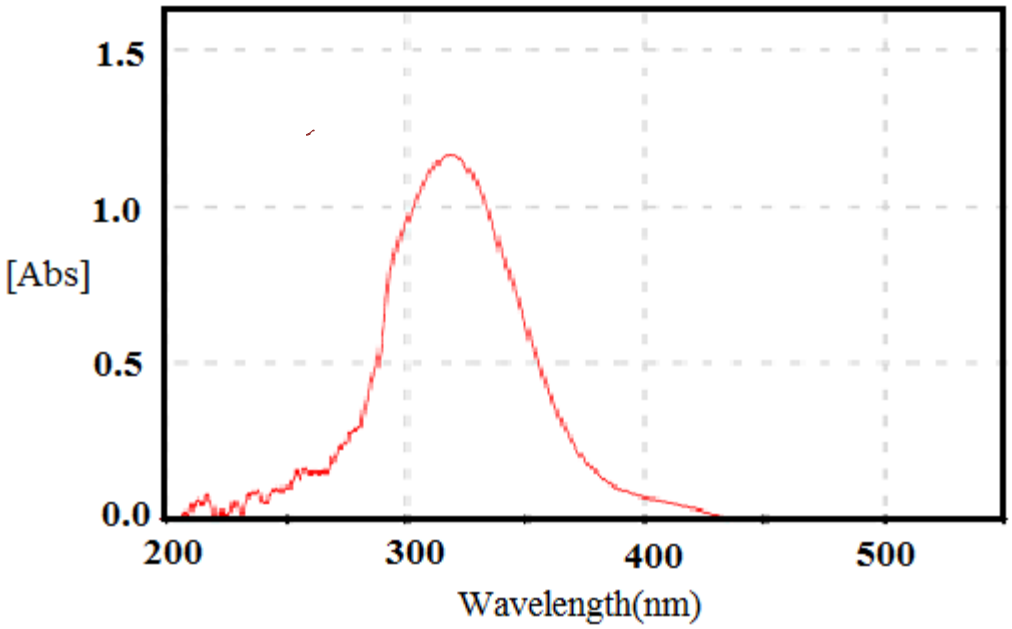

Figure 5-20. Absorbance spectrum of the nitrophenol in the UV –Visible spectrum of 200-850 nm.

5.3.3.1 Experiment Procedure

The experiment was performed using TiO_2 and TiO_2-Fe doped film coated on quartz tube using sol-gel and ESA methods. A 20 mg/l nitro phenol solution concentration was used as the initial concentration, and the sample concentration was measured every hour using the spectrophotometer.

The concentration vs. time in Figure 5-21, shows the degradation of nitro phenol in the single tube reactor with blank quartz tube and quartz tubes with TiO_2, TiO_2-Fe doped film by sol-gel and ESA method, and blank quartz tube. The blank quartz tube performance is far below when compared to the TiO_2 and TiO_2-Fe doped film performance.

Figure 5-22 Ln(C) Vs time shows the degradation of nitro phenol was a first order reaction, as shown in above Table 5-3 the rate constant of blank quart tube was approximately 3 times less when compared to of sol-gel TiO_2-Fe doped film.

Table 5.3: Nitro phenol degradation in single tube reactor by different methods

Method	Order of Reaction	Rate Constant (1/sec)	Initial Concentration (mg/L)	Final concentration After 6hrs (mg/L)
Sol-gel TiO_2	First Order	0.169	20.0	7.8
Sol-gel TiO_2-Fe	First Order	0.198	20.2	7.4
ESA TiO_2	First Order	0.172	20.5	8.2
ESA TiO_2-Fe	First Order	0.187	20.0	7.3
Blank	First Order	0.063	20.0	14.5

The single tube reactor experiments studying the degradation of Congo red, KI (potassium iodide) and Nitro phenol confirmed the better performance by TiO_2 photocatalysis when compared to UV photolysis in direct treatment of contaminant by UV light.

The results of the single tube reactor helped in the selection of the TiO_2 film and the coating method for the seven tube reactor experiments, based on the single tube reactor results the Sol-gel TiO_2-Fe doped film method had better performance among all the film coating methods.

The results also confirmed the enhanced photocatalytic activity with Fe doped TiO_2 film when compared to TiO_2 film in sol-gel and ESA methods.

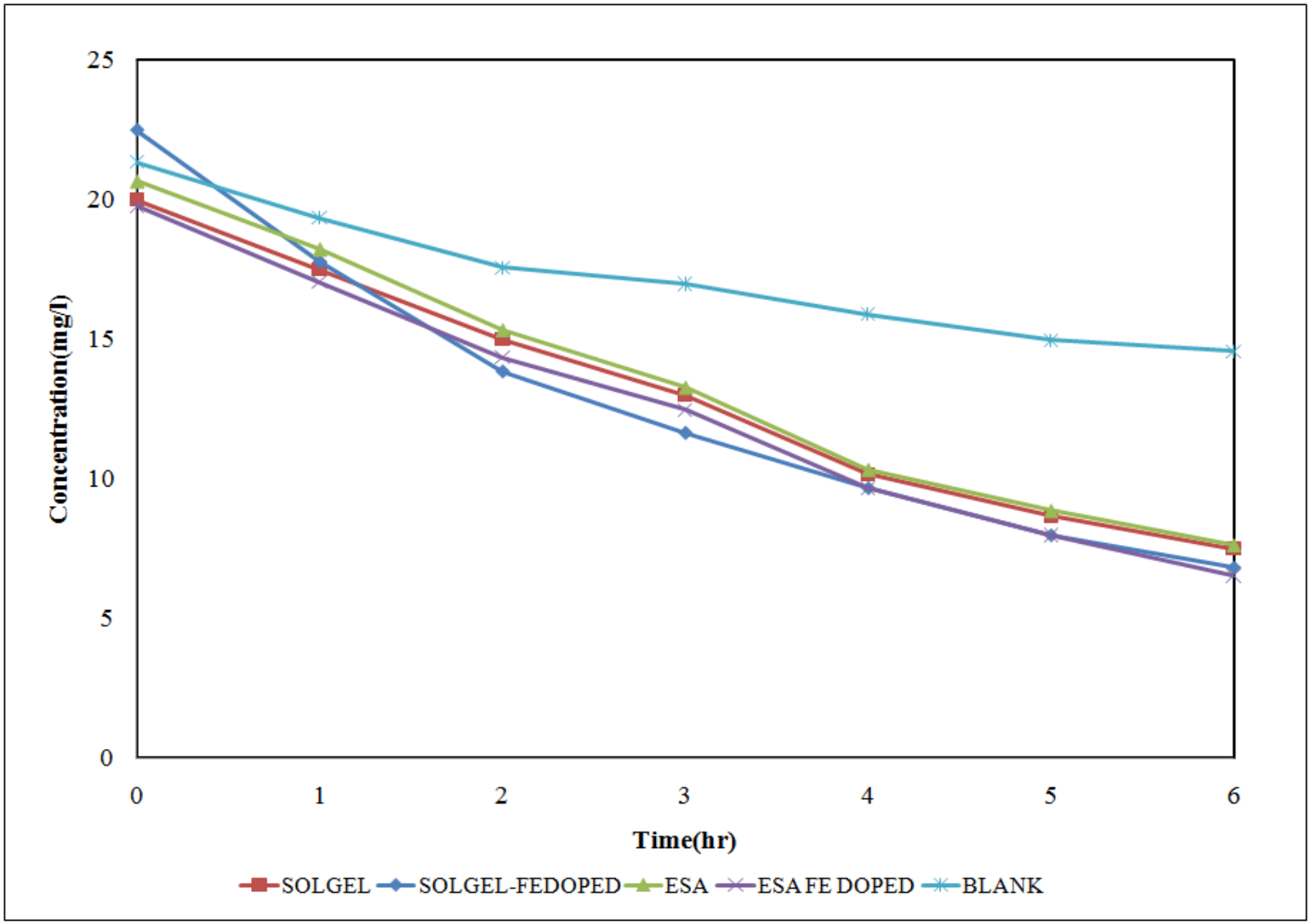

Figure 5-21. Concentration vs time of nitrophenol degradation using different film coated quartz tubes and blank quartz tube.

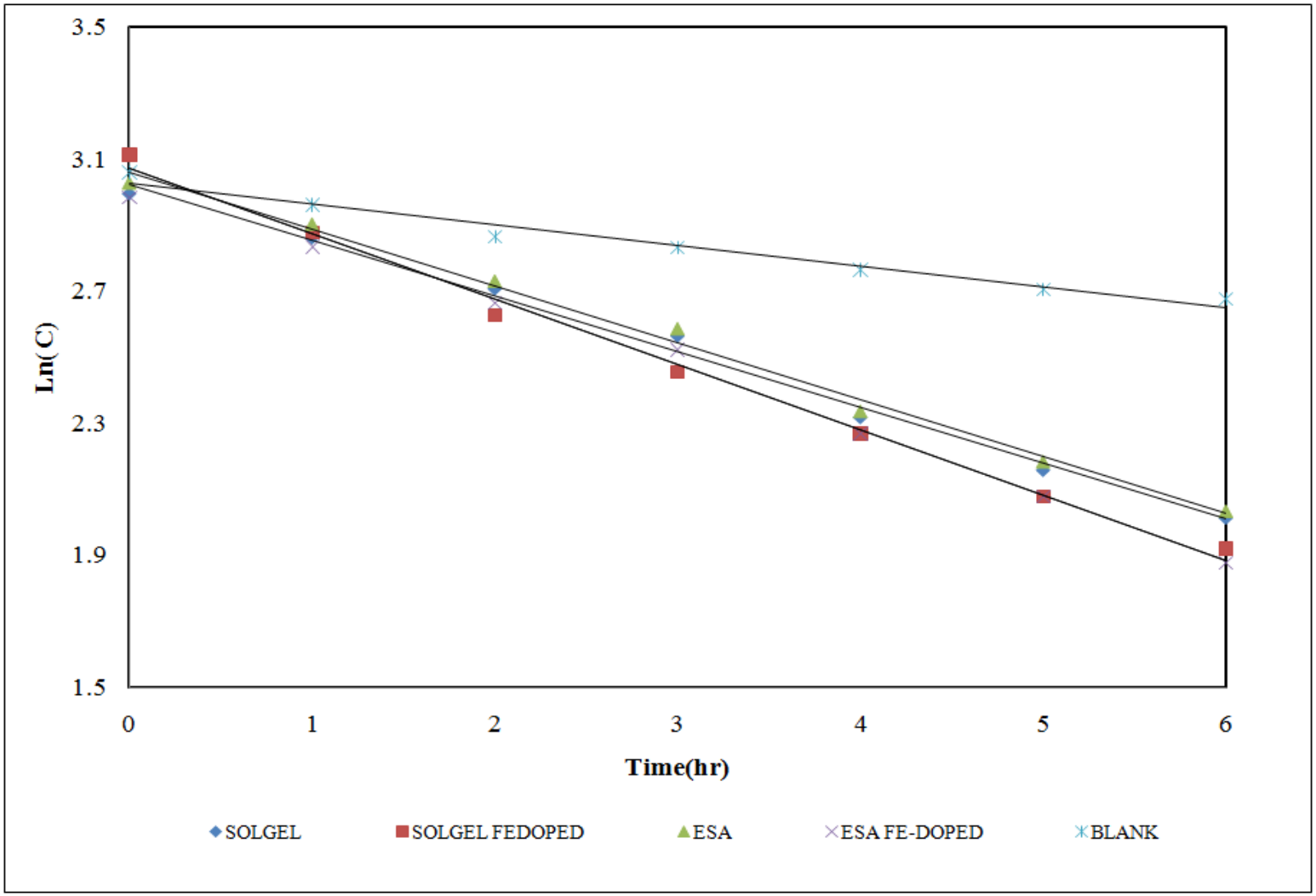

Figure 5-22. Ln(C) vs time of nitrophenol degradation using different film coated quartz tubes and blank quartz tube.

5.4 Seven Tube Reactor

The reactor configuration is similar to a shell and tube heat exchanger with seven tubes arranged in a tubular shell of diameter 89 mm as shown in the Figure 5-23. Seven tubes of outer diameter 23 mm were arranged in a triangular pitch of 5 mm between each other. 8 baffles were spaced at equal distance with alternate openings in the opposite direction across the reactor length. The reactor length was 30 cm and the lamps were inserted inside the tubes, which were connected to a power source using ballast.

In the Figure 5-24, the reactor with lamps inside quartz tubes and the alternate baffles opening are arranged in opposite direction. At the right end of the reactor a port is located for injecting samples and also for collecting samples. In Figure 5-25 the pump was connected to one end of reactor through pipe on one side and the outlet of the reactor was connected to tank for recirculating the solution through the pump.

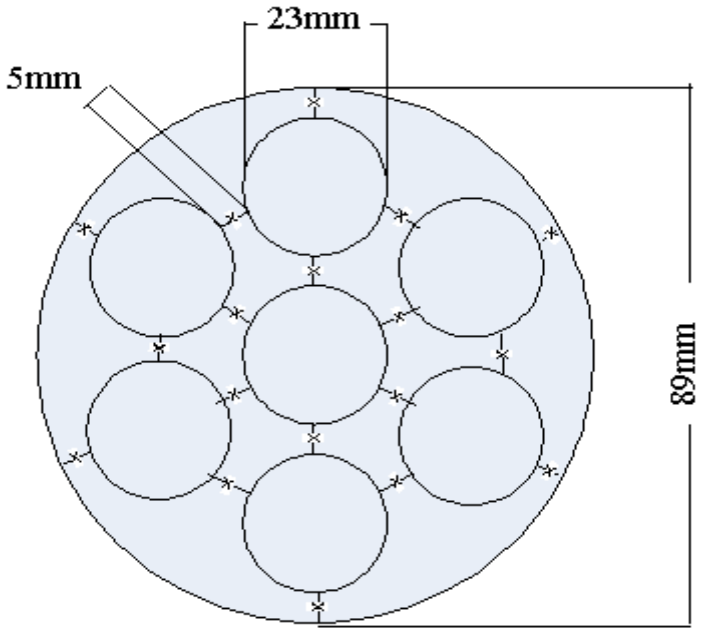

Figure 5-23. Reactor view lay out.

The control valve at the discharge side of the pump was used to control the flow rate of the feed to reactor, which was monitored using a rotameter. During startup, the valve was gradually increased from completely closed position as the liquid fills in the reactor. The effluent from the reactor was re-circulated back to a tank, which was circulated back to the pump in re-circulating process.

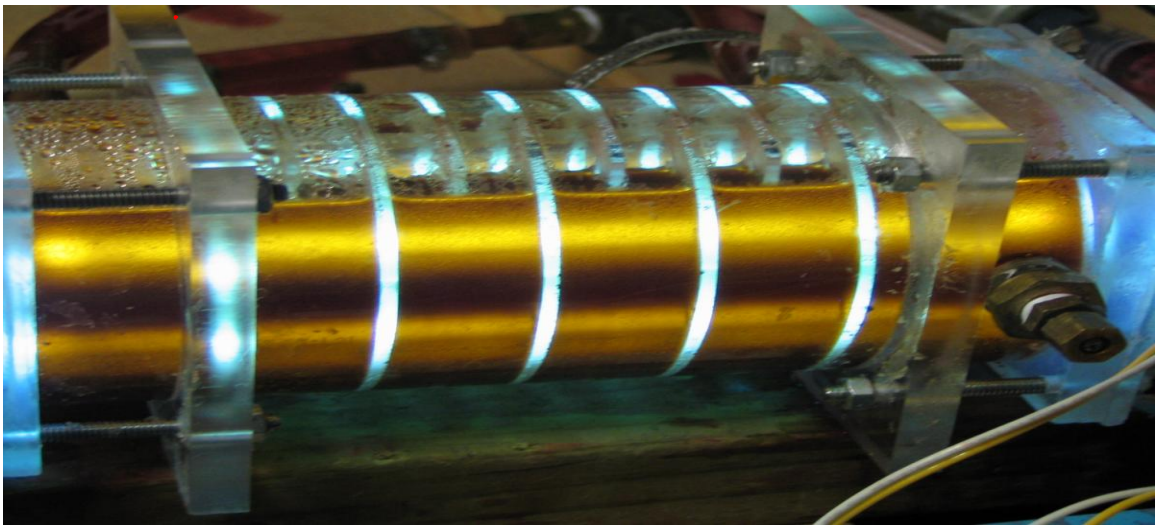

Figure 5-24. Reactor front view with lights on and congo red solution.

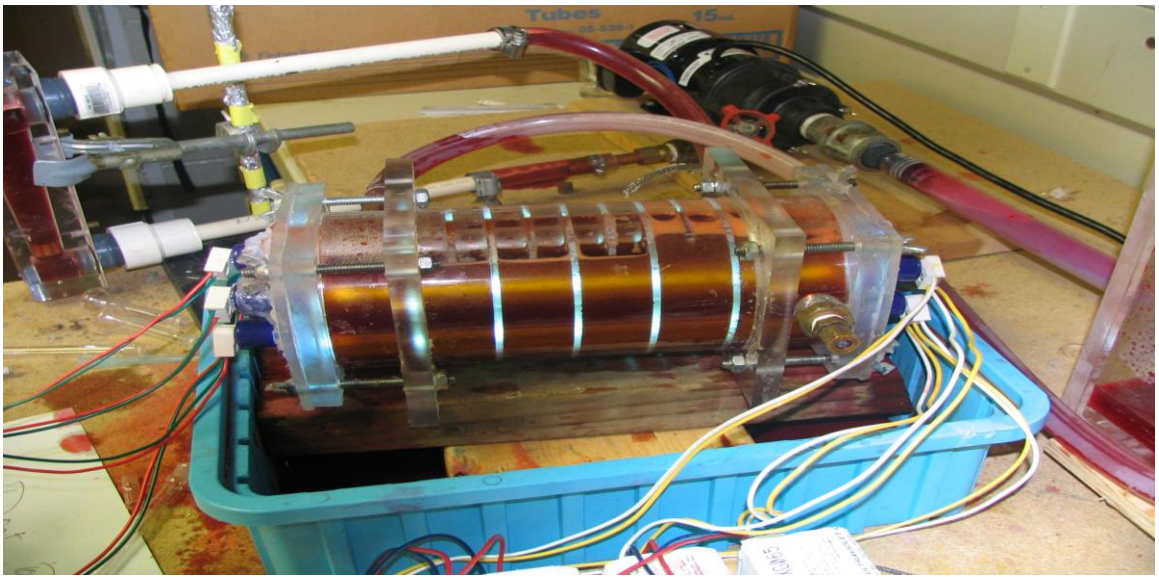

Figure 5-25. Experimental configuration of the reactor.

5.4.1 Congo red degradation

The 7 tube reactor performance in the degradation of the Congo red was performed using the quartz tubes coated with TiO_2- Fe doped film by Sol-gel method. The film was selected based on the performance of single tube reactor using TiO_2-Fe doped film coated by sol-gel method when compared to TiO_2 film coated by sol-gel and ESA method.

A few sets of experiments were performed using the same quartz tubes, which were coated with the TiO_2-Fe doped film by sol-gel method in degradation of Congo red, and the film behavior was observed with the number of experiments.

Table 5-4. Tabulated results of congo red degradation and reactor conditions.

Experiment	Initial Concentration (mg/L)	Flow rate (gpm)	Baffles	Lamps	Final Concentration (mg/L)	Rate constant K , 1/sec	R^2
I	73.5	2gpm	8	7	36.7	0.079	0.991
II	64.6	2gpm	8	7	35.4	0.067	0.978
III	62.8	2gpm	8	7	36.5	0.056	0.986
IV	68.6	2gpm	8	7	43.2	0.052	0.998
V	73.2	1gpm	8	7	46.7	0.054	0.985
VI	71.2	2gpm	8	7	48.5	0.043	0.996

The durability/life of the TiO_2 film on the quartz surface in the reactor was evaluated by repeating the experiment with same tubes. The tubes were cleaned before starting each experiment by using deionized water rinse through the reactor at 2 gpm for 30 min.

The results of the experiment are plotted in a Figure 5-26 concentration vs. time from 0-9 hr. The plot of ln(C) vs time in Figure 5-27 is linear and shows the reaction being a first order.

The experiment results showed decline in reactor performance from experiment I to experiment VI, the decline can be attributed to decline in the photocatalytic activity of the TiO_2 surface. The results in experiment V showed the reaction rate was faster when compared to experiment IV and VI can be attributed to change in flow rate from 2 gpm (experiment IV and VI) to 1 gpm (experiment V).

The rate constant in table 5-1 also shows decline in reactor performance from experiment I to VI, change in reactor performance with flow rate in experiment V.

The decline in reactor performance can be attributed to either the loss of TiO_2 film on the quartz surface or adsorption of Congo red onto the TiO_2 surface and thereby reducing the active TiO_2 surface area available.

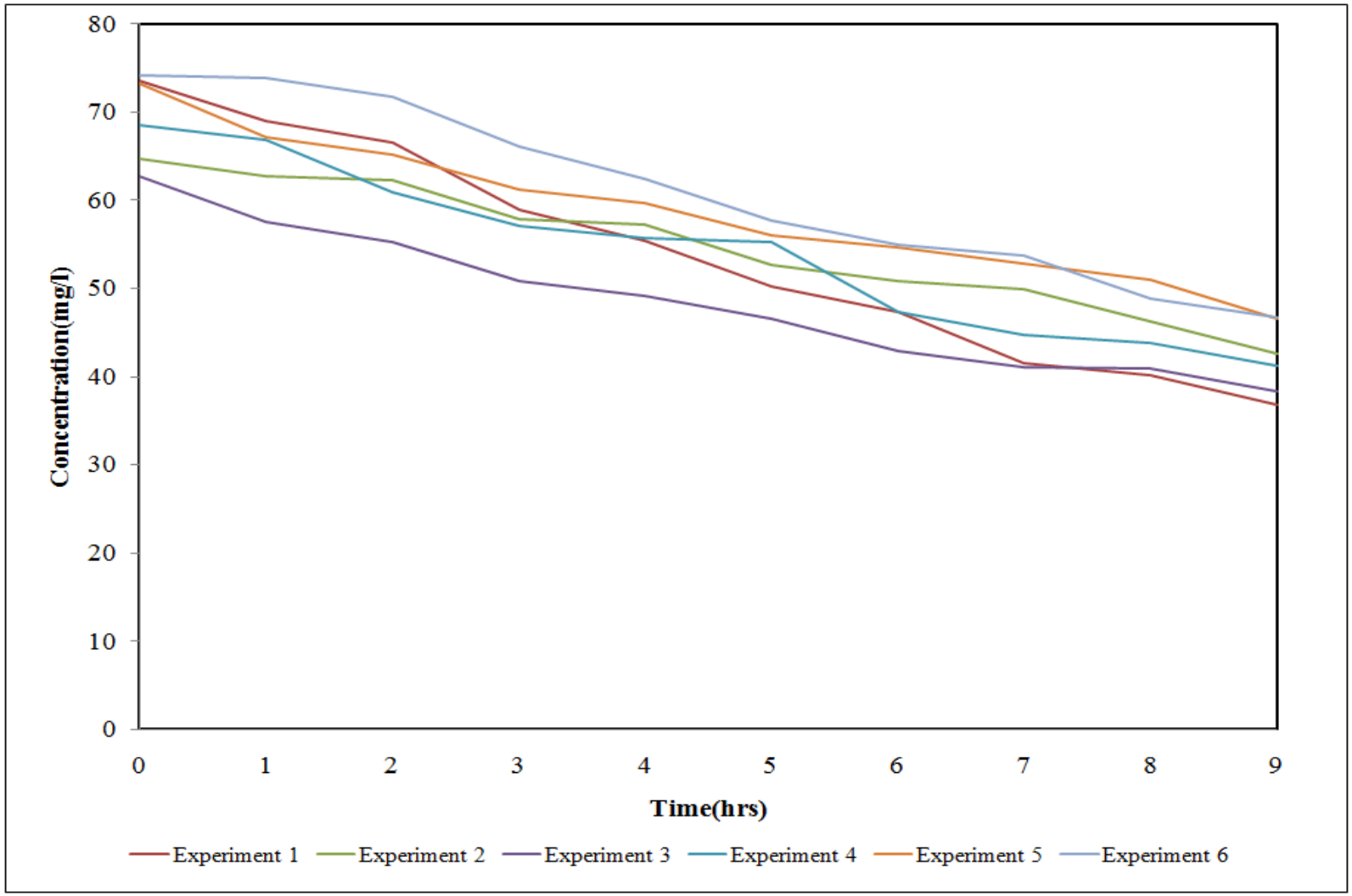

Figure 5-26. Concentration vs time of congo red degradation in 7 tube reactor.

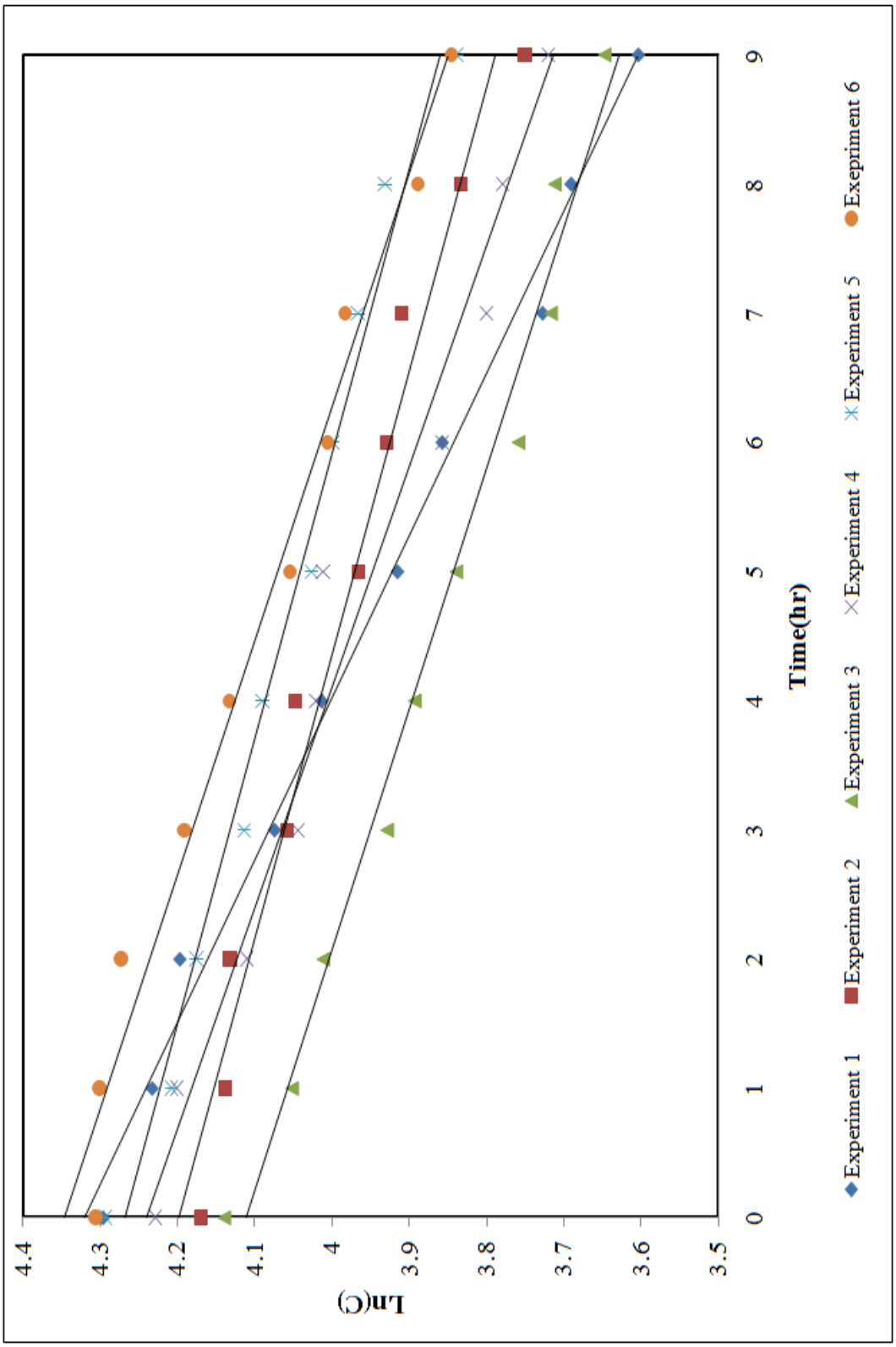

Figure 5-27. Ln(C) Vs Time of Congo red Degradation in 7 tube reactor.

5.4.2 Nitrophenol Degradation

The experiments were conducted using TiO_2 and TiO_2-Fe doped film coated using sol-gel and ESA method, in testing the 7 tube reactor. The table below presents the experimental condition.

Table 5-5. Tabulated results and experimental conditions of nitro phenol degradation and reactor conditions.

Experiment	Initial Concentration (mg/L)	Flow rate	Baffles	Lamps	Final Concentration (mg/L)	Rate constant K, 1/sec	R^2
Sol-gel	20.84	2 gpm	8	7	7.50	1.75	0.996
Sol-gel-Fe	22.79	2 gpm	8	7	6.42	0.19	0.996
ESA	20.67	2 gpm	8	7	7.05	0.18	0.994
ESA-Fe	20.57	2 gpm	8	7	6.54	0.196	0.992
Blank	21.35	2 gpm	8	7	14.10	0.07	0.983

The 7 tube reactor performance in the degradation of nitrophenol using different films was analyzed for reactor performance in the degradation of the nitrophenol using different film coating mechanisms. The results of the nitrophenol degradation using quartz tube coated with TiO_2/TiO_2-Fe doped films by sol-gel and ESA method are plotted in Figure 5-28. The Ln(C) vs time plot in Figure 5-29 shows that the reaction was first order.

The seven tube reactor showed similar results as the single tube reactor, the Sol-gel TiO_2-Fe doped showed better performance among all the methods. There was distinguishable difference in performance of seven tube reactor in degradation of contaminant using quartz tube coated with TiO_2 and TiO_2-Fe doped film when compared to blank quartz tubes.

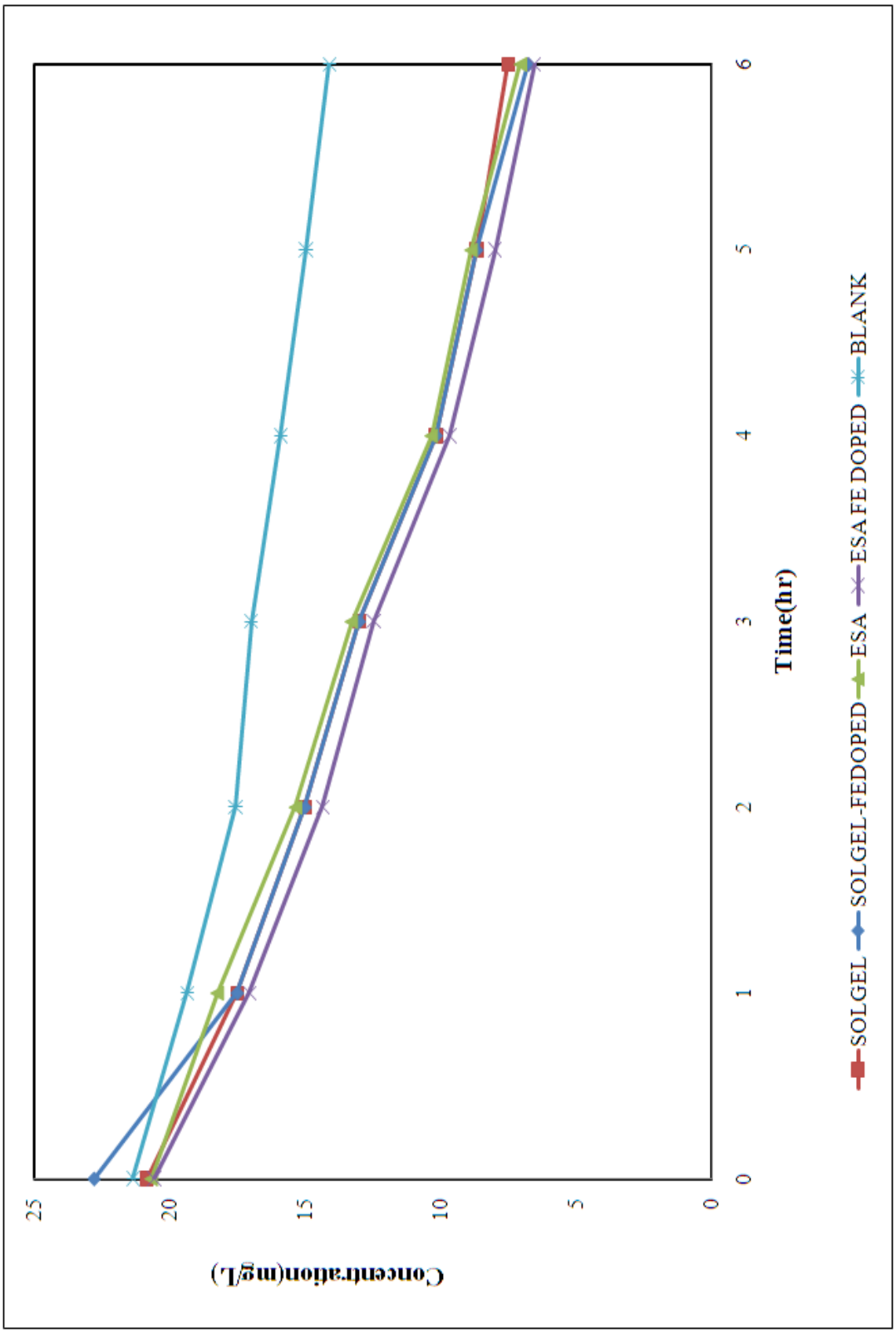

Figure 5-28. Concentration vs time of nitrophenol degradation using sol-gel and ESA TiO_2 / TiO_2-Fe doped film coated quartz tubes.

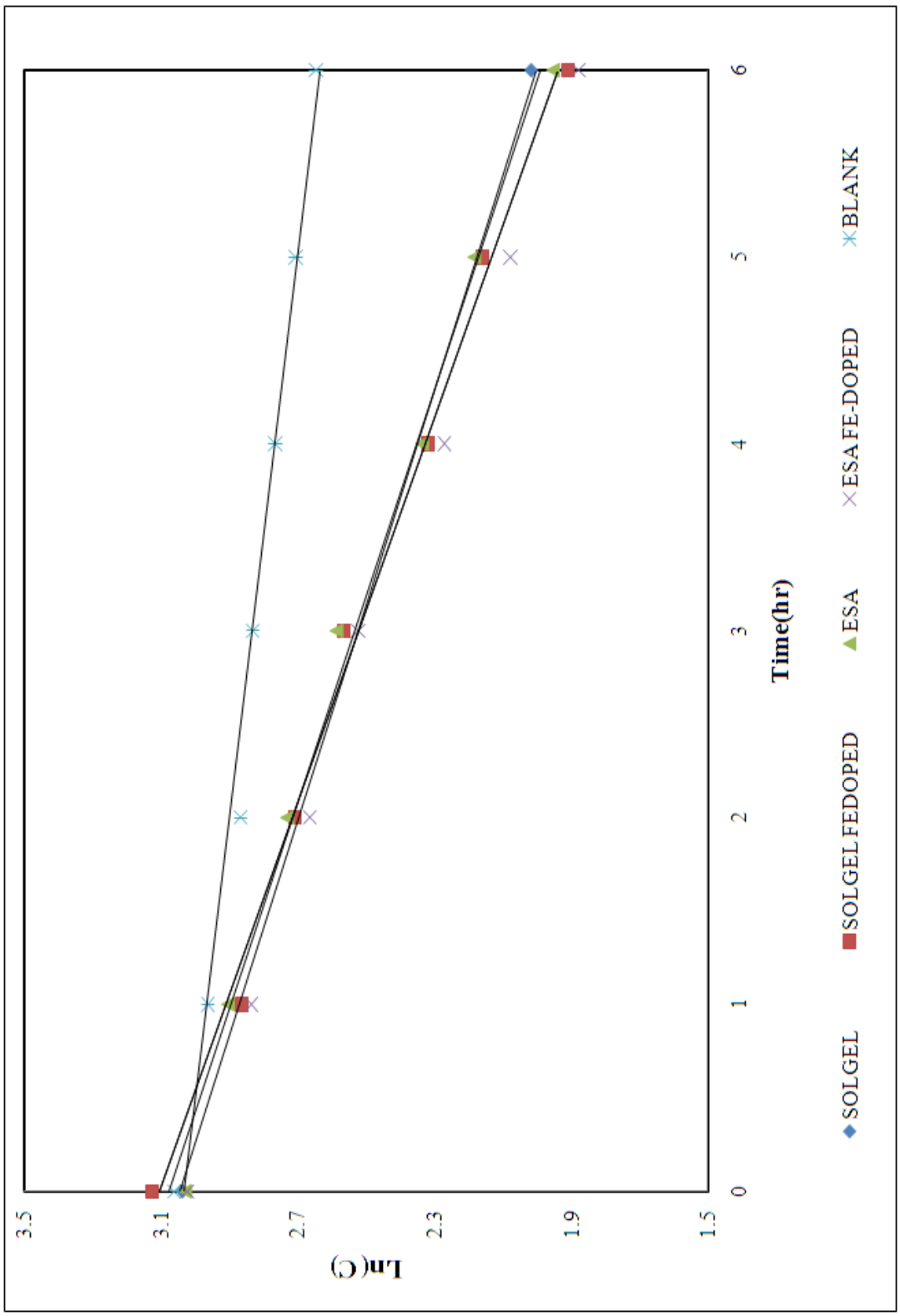

Figure 5-29. Ln(C) vs time of nitrophenol degradation using TiO_2 /TiO_2-Fe doped film coated quartz tubes in 7 tube reactor.

5.4.3 Factorial Design of Experiment results using 7 tube reactor

The 7 tube reactor performance as a function of variation in reactor variables and their mutual dependency was analyzed by design of experiments. Experiments were conducted in different combinations, by changing the reactor parameters the number of lamps to 4 and 7, the number of baffles to 6 and 8, and flow rates at 1 and 2 gpm.

The results are explained and the experimental combinations are tabulated below:

Table 5-6. Experimental combinations conducted for the DOE (design of experiments).

Experiment	**I**	**II**	**III**	**IV**	**V**	**VI**	**VII**	**VIII**
Flow rate	2	2	2	2	1	1	1	1
Baffles	6	6	8	8	8	8	6	6
Lamps	4	7	7	4	4	7	7	4

5.4.3.1 Experiment I

The experiment was conducted by modifying the reactor to 6 baffles with equal spacing between them after sealing the reactor using the silica gel. 4 lamps were used on the four corners in a rectangular fashion in the outer quartz tubes. The flow rate was maintained at 2gpm during the experiment with 4 liters of 0.1N KI solution.

The concentration of the iodine formation increased from 0 gm/L to 0.16 gm/l, the results are plotted in Figure 5-30. The reaction rate showed similar behavior as in single tube reactor, it was first order reaction from 2-6 hrs as shown in Figure 5-31.

5.4.3.2 Experiment II

The experiment was conducted by modifying the reactor to 6 baffles with equal spacing between them after sealing the reactor using the silica gel. The flow rate was maintained at 2gpm during the experiment with 4 liters of 0.1N KI solution.

The concentration of the iodine formation increased from 0 gm/L to 0.19 gm/L, the results are plotted in Figure 5-30.

5.4.3.3 Experiment III

The experiment was conducted by modifying the reactor to 8 baffles with equal spacing between them after sealing the reactor using the silica gel. The flow rate was maintained at 2gpm during the experiment with 4 liters of 0.1N KI solution.

The concentration of the Iodine formation increased from 0 gm/l to 0.205 gm/l, the results are plotted in figure 5-30.

5.4.3.4 Experiment IV

The experiment was conducted by modifying the reactor to 6 baffles with equal spacing between them after sealing the reactor using the silica gel , 4 lamps were used on the four corners in a rectangular fashion on the outer tubes of the quartz . The flow rate was maintained at 2gpm during the experiment with 4 liters of 0.1N KI solution.

The concentration of the Iodine formation increased from 0 gm/l to 0.178gm/l, the experimental results are plotted in figure 5-30.

5.4.3.5 Experiment V

The experiment was conducted by modifying the reactor to 8 baffles with equal spacing between them after sealing the reactor using the silica gel , 4 lamps were used on the four corners in a rectangular fashion on the outer tubes of the quartz . The flow rate was maintained at 1gpm during the experiment with 4 liters of 0.1 N KI solution.

The concentration of the Iodine formation increased from 0 gm/l to 0.185 gm/l, the results are plotted in figure 5-30.

5.4.3.6 Experiment VI

The experiment was conducted by modifying the reactor to 8 baffles with equal spacing between them after sealing the reactor using the silica gel, 7 lamps were used. The flow rate was maintained at 1gpm during the experiment with 4 liters of 0.1N KI solution.

The concentration of the Iodine formation increased from 0 gm/l to 0.23gm/l, the experimental results are plotted in figure 5-30.

5.4.3.7 Experiment VII

The experiment was conducted by modifying the reactor to 6 baffles with equal spacing between them after sealing the reactor using the silica gel, 7 lamps were used. The flow rate was maintained at 1gpm during the experiment with 4 liters of 0.1N KI solution.

The concentration of the Iodine formation increased from 0 gm/l to 0.22 gm/l, the results are plotted in figure 5-30.

5.4.3.8 Experiment VIII

The experiment was conducted by modifying the reactor to 6 baffles with equal spacing between them after sealing the reactor using the silica gel, 4 lamps were used on the four corners in a rectangular arrangement on the outer tubes of the quartz . The flow rate was maintained at 1gpm during the experiment with 4 liters of 0.1N KI solution.

The concentration of the iodine increased from 0 gm/l to 0.175gm/l, the experimental results are plotted in figure 5-30.

The I_2 concentration vs time plot shown in Figure 5-30, shows the configuration with 8 baffles, 7 lamps and operated at a flow rate of 1 gpm was better in performance when comapred to the experimental results with other combinations. All the above experiments were performed using sol-gel TiO_2-Fe doped film quartz tubes.

It can be observed from the reactor test results, the reaction rate varies with time. Which is similar to reaction rate behavior observed in the single tube reactor degradation of the KI. In single tube reactor the reaction rate was constant after the first 2 hrs, a similar behaviour can be observed in the Ln(C) vs time plot in figure 5-31 of the 7 tube reactor, the reaction rate changed in first 2 hours and was reaching a steady reaction rate after the first few hours of starting the reactor.

The most likely reason for the observed pattern may be the absorption of I_2 on to the quartz tube surface or the dissolution of the TiO_2 from the quartz surface into water.

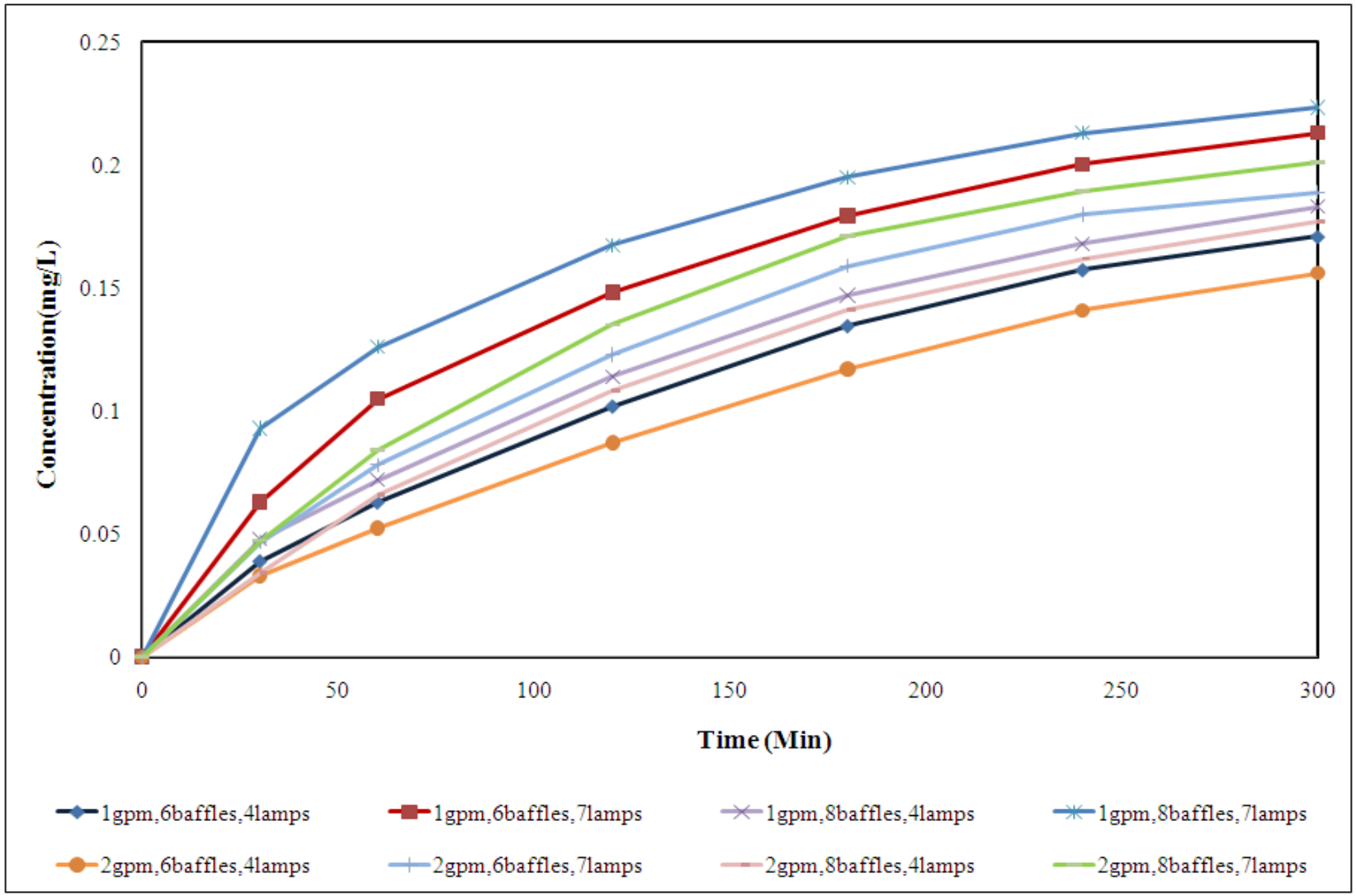

Figure 5-30: Concentration vs time of I_2 liberation using 6 and 8 baffles ,4and 7 lamps ,1and 2gpm using sol-gel TiO_2–Fe doped TiO_2 film coated quartz tubes.

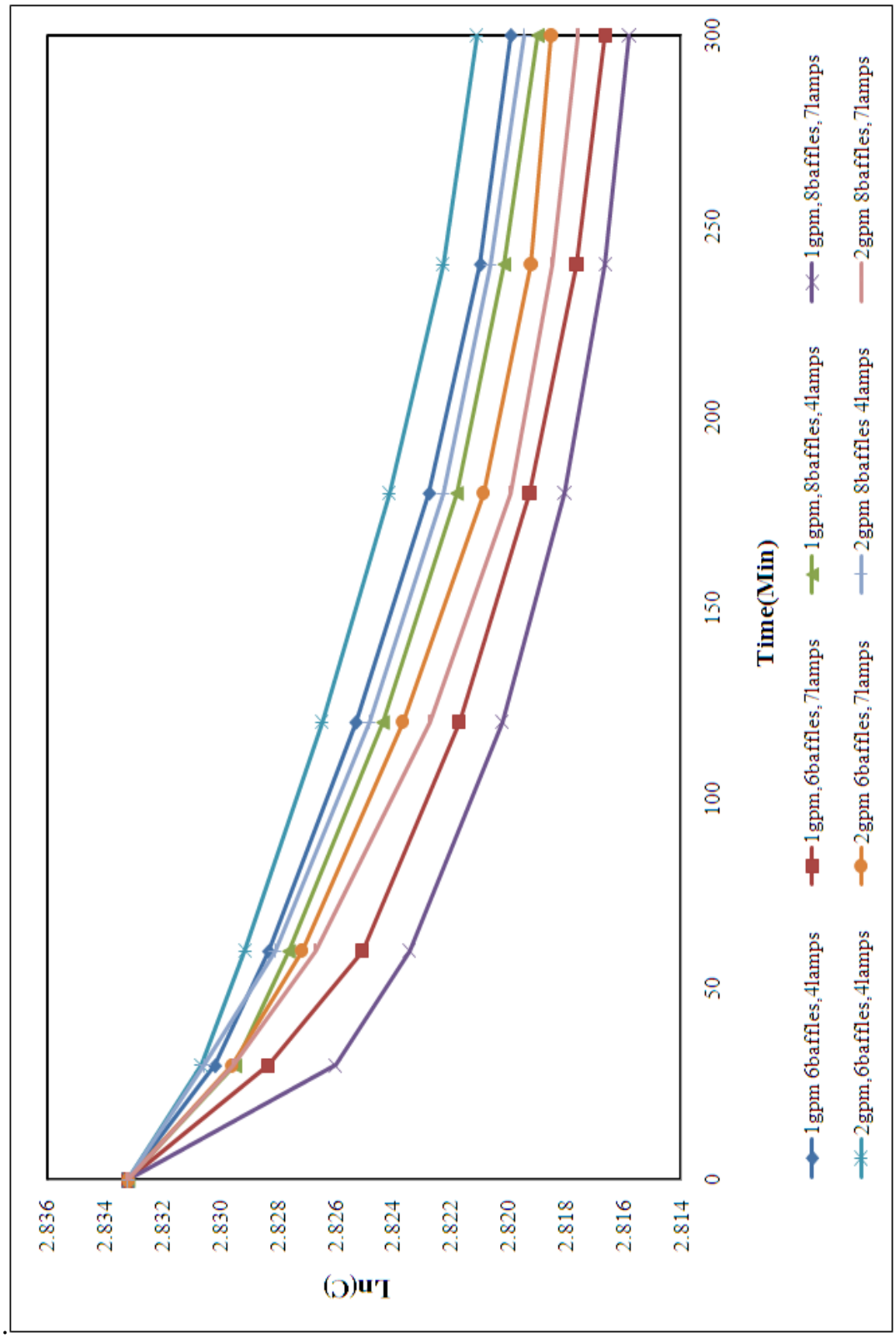

Figure 5-31: Ln(C) vs time of KI degradation in factorial experiments using sol-gel –Fe doped TiO_2 film coated quartz tubes.

5.4.3.9 Factorial experimental statistical analysis:

Statistical ANOVA analysis of the factorial experiment is analyzed using MINITAB software (Minitab Inc., State College, Pennsylvania).

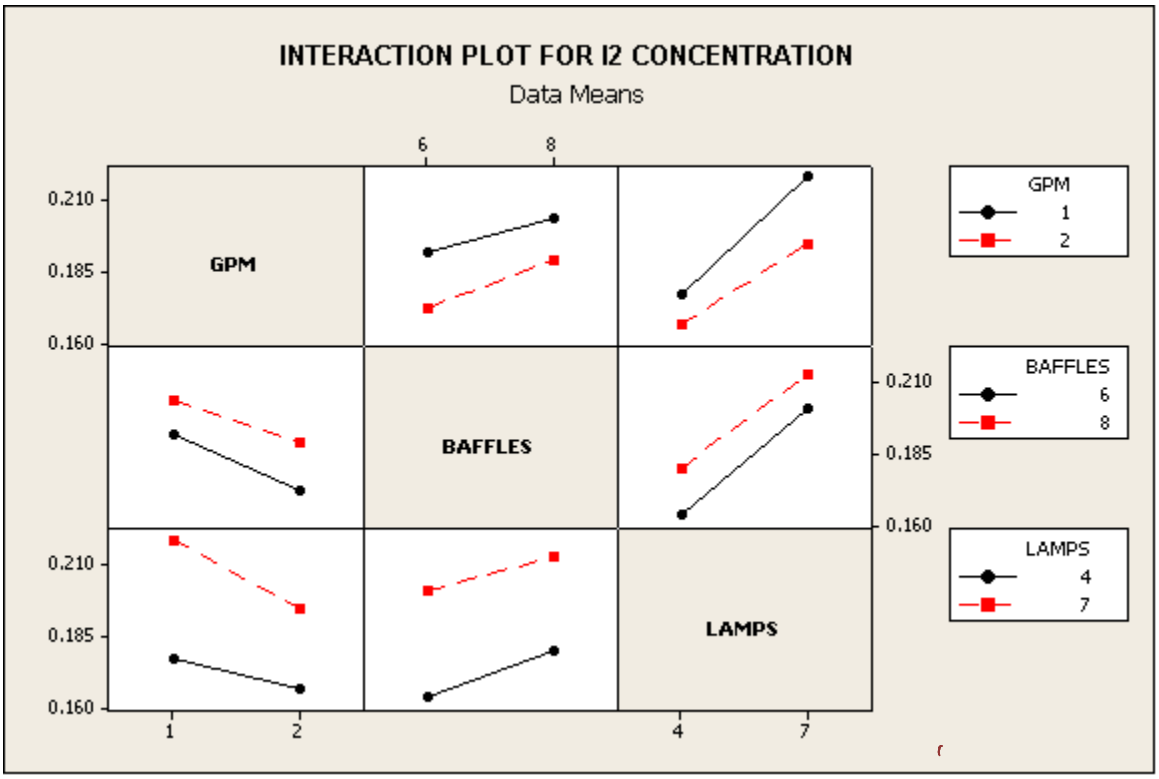

Figure 5-32. Interaction plot of recirculation rate, baffles, lamps and I_2 Concentration.

Factorial Fit: I2 CONCENTRATION versus GPM, BAFFLES, LAMPS
Estimated Effects and Coefficients for I_2 CONCENTRATION

Term	Effect	Coef
Constant		0.138
GPM	-0.125	-0.062
BAFFLES	0.006	0.003
LAMPS	0.02	0.009
GPM*BAFFLES	0.02	0.01
GPM*LAMPS	0.011	0.005
BAFFLES*LAMPS	0.003	0.001
GPM*BAFFLES*LAMPS	-0.003	-0.001

Analysis of Variance for I_2 CONCENTRATION

Source	DF	Seq SS	Adj SS	Adj MS	F	P
Main Effects	3	0.0035	0.00015	0.00005	*	*
2-Way Interactions	3	0.0001	0.00005	0.00002	*	*
3-Way Interactions	1	0.0000	0.00001	0.00001	*	*
Residual Error	0	*	*	*		
Total	7	0.0036				

Estimated Coefficients for I_2 CONCENTRATION using data

Term	Coef
Constant	0.138
GPM	-0.062
BAFFLES	0.003
LAMPS	0.009
GPM*BAFFLES	0.01
GPM*LAMPS	0.005
BAFFLES*LAMPS	0.001
GPM*BAFFLES*LAMPS	-0.0014

* NOTE * some factors have more than 2 levels, no alias table was printed.

The plot shown in Figure 5-29 presents the interaction of each variable *i.e.,* recirculation flow rate (gpm), baffles and lamps on the reactor performance. The recirculation flow rate has a negative effect on I_2 concentration with increase in flow rate there was decrease in amount of I_2 liberated. Number of Baffles also had positive effect on the I_2 concentration with increase in number of baffles from 6 to 8 there was increase in I_2 liberated and the number of lamps has positive effect on the I_2 liberated with increase in the number of lamps there was increase in the amount of the I_2 liberated, the results showed increased flow rate has resulted in decrease of the contact time of contaminant to the photocatalyst surface, and increase in number of baffles showed it provided more mixing inside the reactor and allowed the contact of contaminant to the photocatalyst surface, and the increase in number of lamps resulted in increasing the photocatalyst activity .

The mutual interaction between the variables flow rate –baffles, baffles-lamps, flow rate-lamps has positive effect on the I_2 liberation and the mutual interaction between three variables together flow rate-baffles-lamps has negative effect on the I_2 liberation. For any future design modification or reconfiguration of reactor, there is need to perform factorial design of experiment at flow rates of below 1gpm and increasing the baffles to more than 8 baffles, and changing the layout of the quartz tubes.

To study the flow field inside the reactor, mixing and any dead zones inside the reactor Computational fluid dynamic model of the single tube reactor and seven tube reactor was performed, which will be discussed in the following sections.

5.5 Computational Fluid Dynamics Model (CFD)

5.5.1 2D Model of Single Tube Reactor

2D model of the single tube reactor was built in the COMSOL using Moving Mesh and Incompressible Navier Stoke models. Side view of the single tube reactor was modeled to test mass transfer limitation associated with mixing, with the inner circle representing the quartz tube and a stirrer vertically beneath the quartz tubes to reflect the stirrer inside the reactor

The model result shown in Figure 5-33, was generated with a stirrer speed of 120 rpm. The moving mesh and incompressible Navier-Stokes equations were used together, the moving mesh took into account the stirrer rotation and navier stoke model computed the flow field across the reactor taking in to account of the moving mesh model. A detailed report of the model is attached in Appendix I.

The velocity profile shows the maximum velocity around the stirrer and minimum at the surface of the quartz tubes or walls of the reactor, the velocity increases as the distance from the stirrer increases and decreases as it approaches the wall surface or quartz tube surface, the velocity in the reactor ranged from zero to 0.05 m/s.

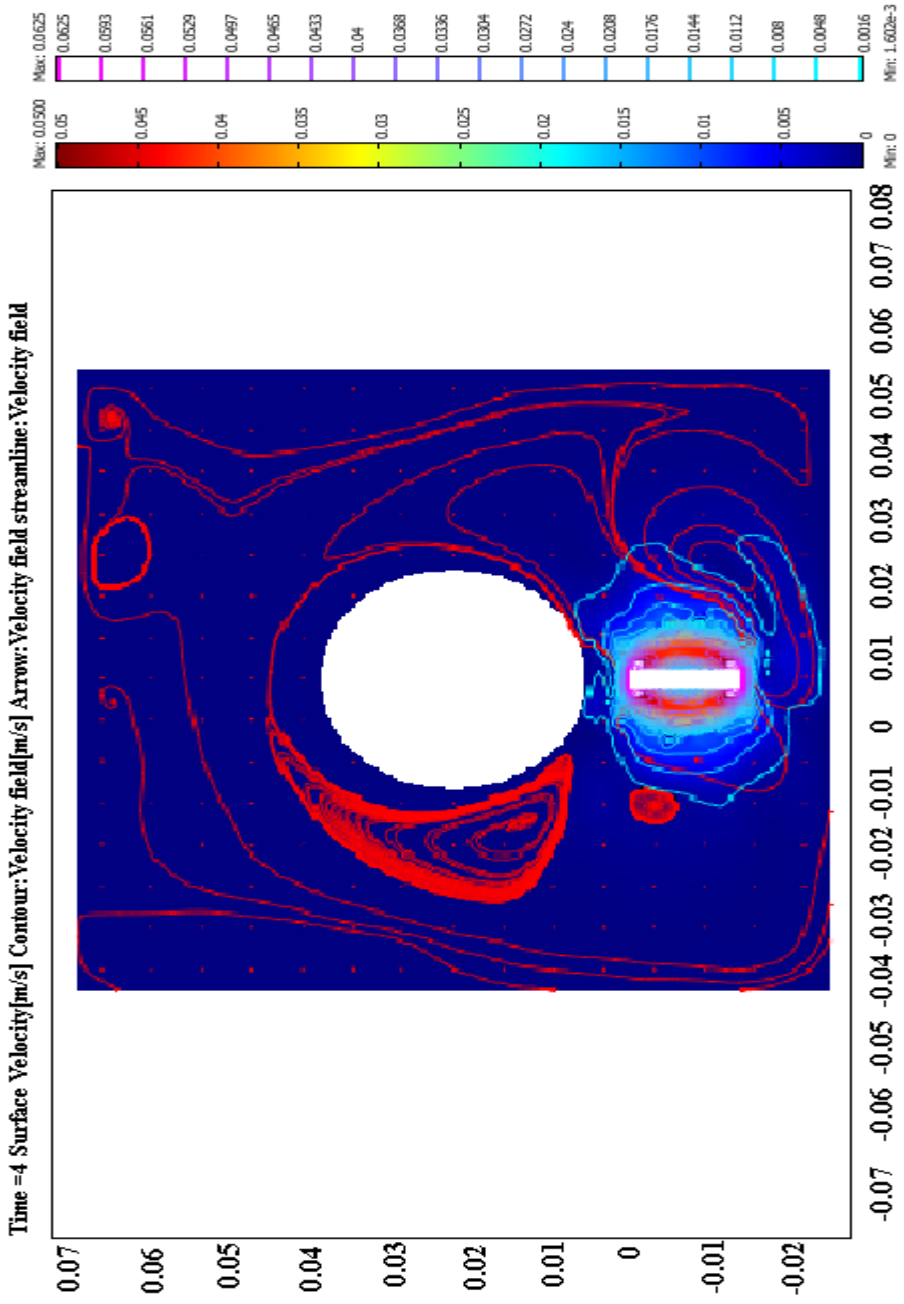

Figure 5-33: Flow field of the reactor showing velocity field generated using COMSOL model.

5.5.2 3D Model of 7 Tube Reactor

A 3D model of the reactor was designed using predefined models in COMSOL software. The dimensions of the reactor in the model were made to represent the actual reactor dimensions.

Meshing was fine mesh predefined in the COMSOL across the reactor and coarse mesh at the edges and the boundaries at the baffles. Boundary conditions were assigned, and influent conditions were specified in "Incompressible Navier-Stokes (Chemical Engineering Module)" among the predefined models in the COMSOL 3.4.0.248 version.

The flow field generated using the COMSOL model showed the flow being laminar, the Reynolds number ranged from 0-3000. The Reynolds number was minimum at the surfaces of the reactor and edges, and was up to 3000 between the baffles, the maximum Reynolds number was noticed in the region between the baffles, and passage across the baffles opening has Reynolds number in the range of 200-2500 as shown in the Figure 5-34 below. The detailed report of the COMSOL is attached in the Appendix I.

The results of model showed the reactor provided the required mixing inside the reactor and thereby the potential limiting factor will be reaction at photocatalyst surface not the diffusion of particles from bulk to photocatalyst surface and model can be used to simulate the flow field with change in reactor layout and process parameter.

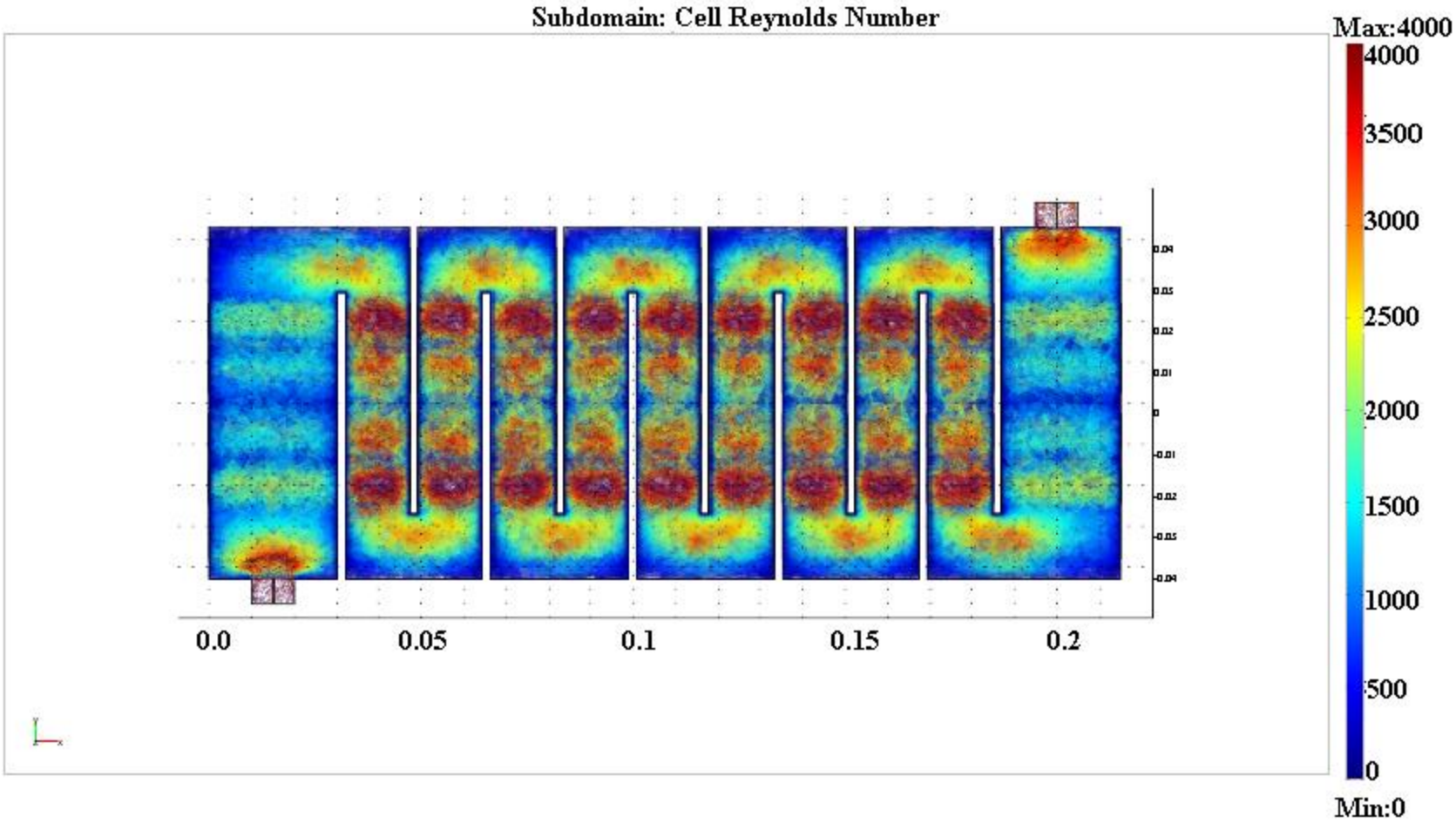

Figure 5-34: Flow field of the reactor showing Reynolds number generated using COMSOL model.

5.6 Appendix

5.6.1 2D Model Report:

2d model of the single tube reactor was built in the COMSOL using Moving Mesh and Navier Stroke models, the side view of the single tube reactor was modeled with the inner circle showing the quartz tube and stirrer even though doesn't reflect the actual location in the reactor was used to reflect the mixing in the single tube reactor.

The report generated in COMSOL is shown below

COMSOL Model Report

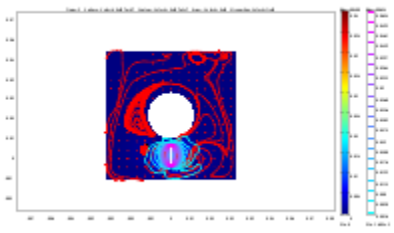

Table of Contents

5.6.1.1 Model Properties

Property	Value
Model name	
Author	
Company	
Department	
Reference	
URL	
Saved date	Jun 27, 2007 10:30:40 PM
Creation date	May 6, 2007 12:03:58 AM
COMSOL version	COMSOL 3.4.0.248

Application modes and modules used in this model:

- Geom1 (2D)
    - Incompressible Navier-Stokes (Chemical Engineering Module)
    - Moving Mesh (ALE)

5.6.1.2 Constants

Name	Expression	Value	Description
dens	1e3		
visc	11e-2		
rpm	120		
co	100		
kads	1e-6		
kdes	1e-9		
theta0	1000		
Ds	1e-11		
D	1e-9		
v_max	1e-3		
delta	1e-4		

5.6.1.3 Geometry

Number of geometries: 1

Geom1

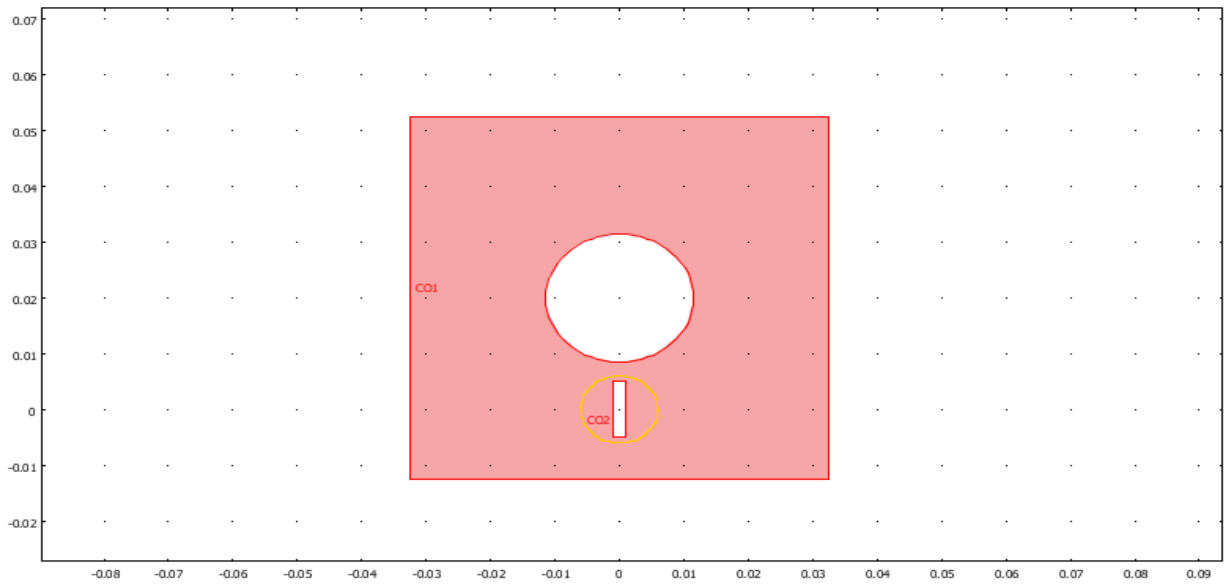

Point mode

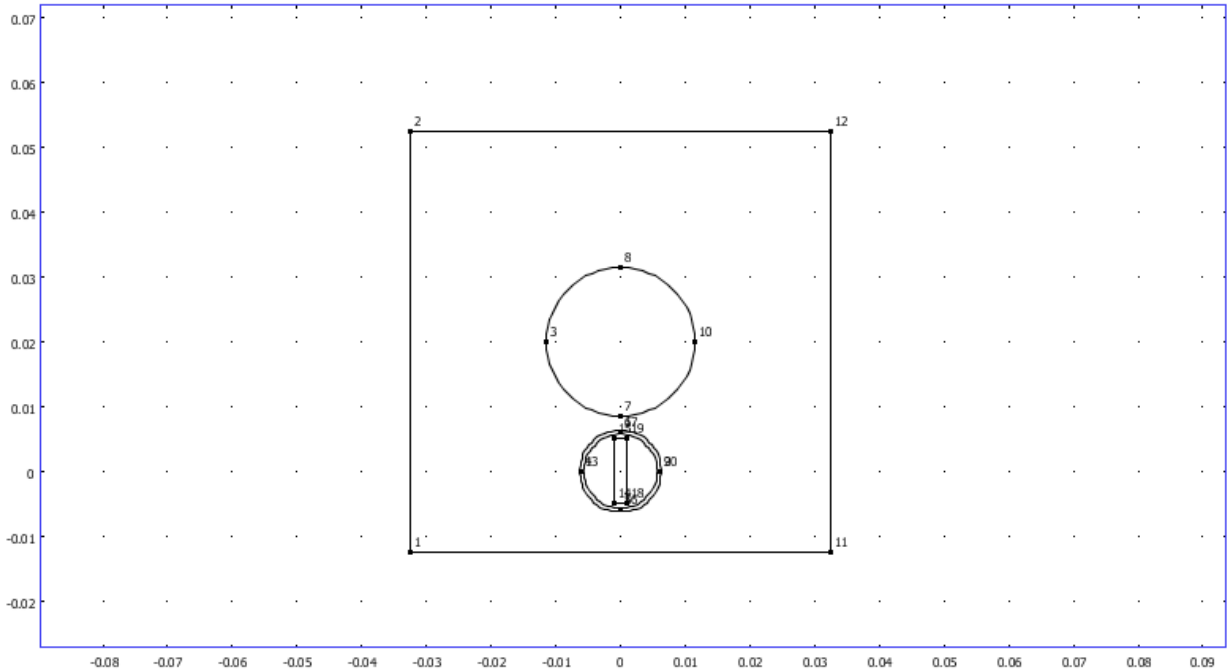

Boundary mode

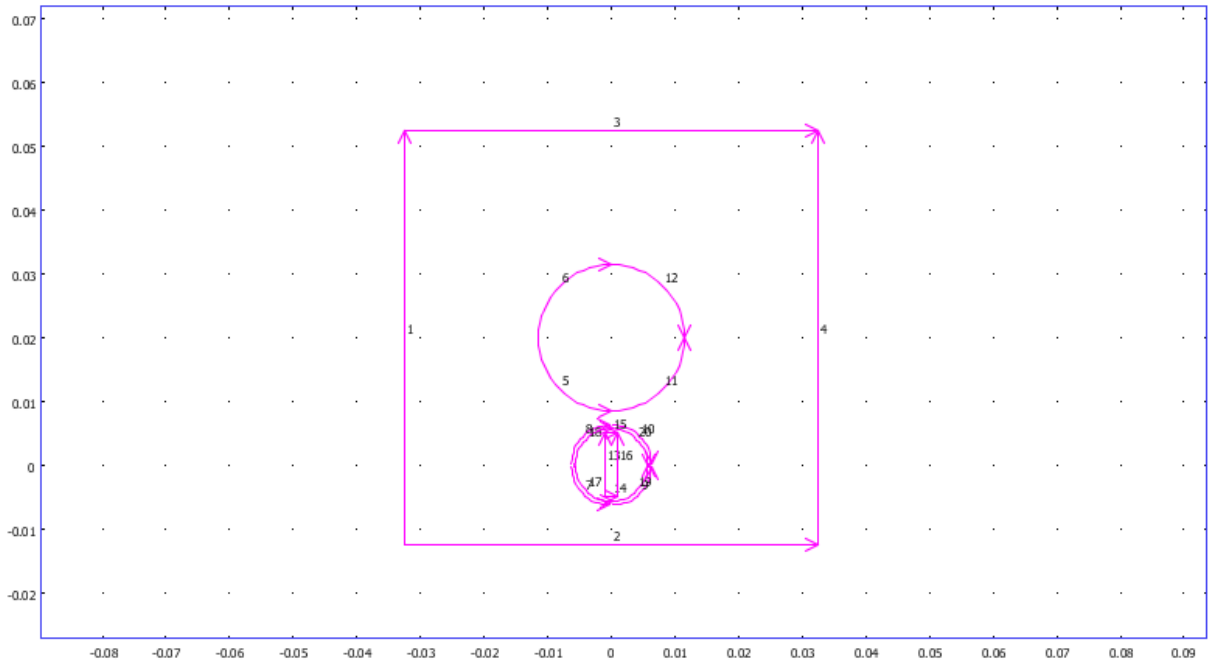

Subdomain mode

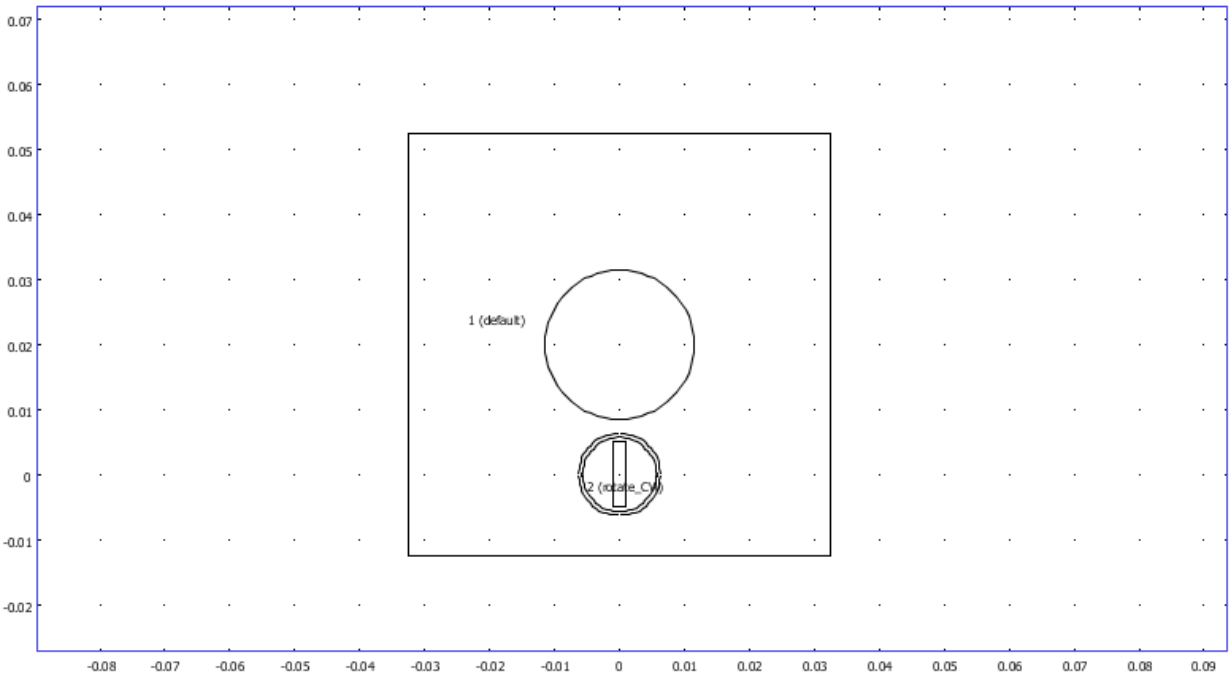

5.6.1.4 Geom1

Space dimensions: 2D

Independent variables: X, Y, Z

Expressions

Boundary Expressions

Boundary		5-6, 11-12
react_surf		kads*c*(theta0-cs)-kdes*cs

Subdomain Expressions

Subdomain		1	2
v_lam	m^2	v_max*(1-(2*(x-0.5*delta)/delta)^2)	v_max*(1-(2*(x-0.5*delta)/delta)^2)

Identity Pairs

Identity Point Pairs

Identity pairs	Source points	Destination points
Pair 1	4-6, 9	13, 16-17, 20

Identity Boundary Pairs

Identity pairs	Source boundaries	Destination boundaries
Pair 1	7-10	17-20

Mesh

Mesh Statistics

Number of degrees of freedom	1809
Number of mesh points	221
Number of elements	351

Triangular	351
Quadrilateral	0
Number of boundary elements	93
Number of vertex elements	20
Minimum element quality	0.675
Element area ratio	0.006

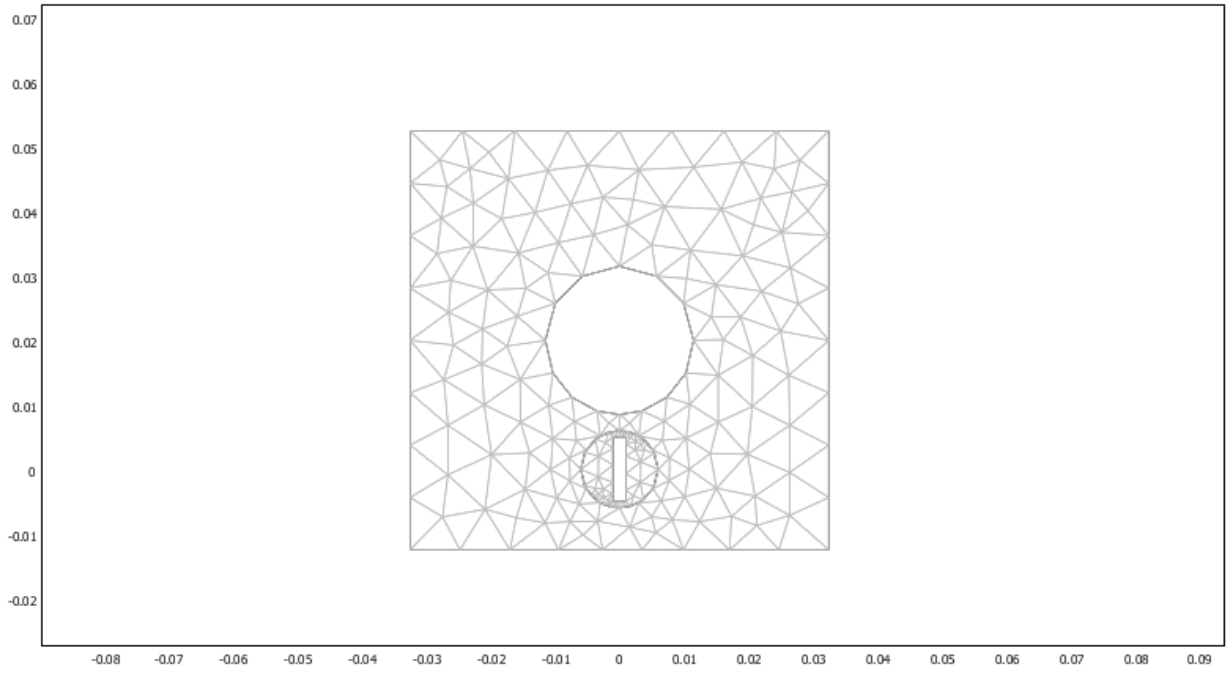

Application Mode: Incompressible Navier-Stokes (chns)

Application mode type: Incompressible Navier-Stokes (Chemical Engineering Module)

Application mode name: chns

Application Mode Properties

Property	**Value**
Default element type	Lagrange - P_2 P_1
Analysis type	Transient
Corner smoothing	Off
Weakly compressible flow	Off

Turbulence model	None
Realizability	Off
Non-Newtonian flow	Off
Brinkman on by default	Off
Two-phase flow	Single-phase flow
Frame	Frame (ale)
Weak constraints	Off
Constraint type	Ideal

Variables

Dependent variables: u, v, p, logk, logd, logw, phi, nxw, nyw

Shape functions: shlag(2,'u'), shlag(2,'v'), shlag(1,'p')

Interior boundaries active

Boundary Settings

Boundary		1-2, 4-12, 17-20	3	13-16
Type		Wall	Symmetry boundary	Inlet
Name				**no_slip_CW**
velType		U0in	U0in	**u0**
x-velocity (u0)	m/s	0	0	**-pi*rpm*sin(pi*rpm*t/30)*x/30+pi*rpm*cos(pi*rpm*t/30)*y/30**
y-velocity (v0)	m/s	0	0	**-pi*rpm*cos(pi*rpm*t/30)*x/30-pi*rpm*sin(pi*rpm*t/30)*y/30**
Turbulent kinetic energy (k0)	m^2/s^2	**0**	**0**	**0**
Turbulent dissipation rate (d0)	m^2/s^3	**0**	**0**	**0**
Specific	1/s	**0**	**0**	**0**

turbulent dissipation rate (omega0)				
Turbulent length scale (LT)	m	**0.07**	**0.07**	**0.07**
Turbulent intensity (IT)	1	**0.054**	**0.054**	**0.054**
Wall offset (dw)	m	**h**	**h**	**H**

Pair		Pair 1
Type		Interior boundary
Turbulent kinetic energy (k0)	m^2/s^2	**0**
Turbulent dissipation rate (d0)	m^2/s^3	**0**
Specific turbulent dissipation rate (omega0)	1/s	**0**
Turbulent length scale (LT)	m	**0.07**
Turbulent intensity (IT)	1	**0.054**
Wall offset (dw)	m	**h**

Subdomain Settings

Subdomain		1-2
Integration order (gporder)		**4 4 2**
Constraint order (cporder)		**2 2 1**
Density (rho)	kg/m^3	**dens**
Dynamic viscosity (eta)	Pa·s	**visc**
Streamline diffusion switch (sdon)		**0**
Streamline diffusion type (sdtype)		**pgc**
idTon		**1**
delidT		**0.5**
sdTtype		**ad**

5.6.1.4 Application Mode: Moving Mesh (ALE) (ale)

Application mode type: Moving Mesh (ALE)

Application mode name: ale

Application Mode Properties

Property	**Value**
Default element type	Lagrange - Quadratic
Smoothing method	Laplace
Analysis type	Transient
Allow remeshing	Off
Defines frame	Frame (ale)
Original reference frame	Frame (ale)
Motion relative to	Frame (ref)
Weak constraints	On
Constraint type	Non-ideal

Variables

Dependent variables:

Shape functions: shlag(2,'lm5'), shlag(2,'lm6'), shlag(2,'x'), shlag(2,'y')

Interior boundaries not active

Subdomain Settings

Subdomain		1	2
Shape functions (shape)		**shlag(2,'lm5') shlag(2,'lm6') shlag(2,'x') shlag(2,'y')**	**shlag(2,'lm5') shlag(2,'lm6') shlag(2,'x') shlag(2,'y')**
Integration order (gporder)		**4 4**	**4 4**
Name		**Default**	**rotate_CW**
Type		**None**	**pres**
Displacement	M	{0;0}	**{cos(pi*rpm*t/30)*X+sin(pi*rpm*t/30)*Y-X;-**

expressions (presexpr)			**sin(pi*rpm*t/30)*X+cos(pi*rpm*t/30)*Y-Y}**

Subdomain initial value		1	2
Spatial coordinate (x)	m	xinit_ale	xinit_ale
Spatial coordinate (y)	m	yinit_ale	yinit_ale

5.6.1.5 Solver Settings

Solve using a script: off

Analysis type	Transient
Auto select solver	On
Solver	Time dependent
Solution form	Automatic
Symmetric	auto
Adaption	Off

Direct (UMFPACK)

Solver type: Linear system solver

Parameter	**Value**
Pivot threshold	0.1
Memory allocation factor	0.7

Time Stepping

Parameter	**Value**
Times	0:0.1:4
Relative tolerance	1e-2
Absolute tolerance	1e-3
Times to store in output	Specified times
Time steps taken by solver	Free
Manual tuning of step size	Off
Initial time step	0.0010

Maximum time step	1.0
Maximum BDF order	5
Singular mass matrix	Maybe
Consistent initialization of DAE systems	Backward Euler
Error estimation strategy	Exclude algebraic
Allow complex numbers	Off

Advanced

Parameter	**Value**
Constraint handling method	Elimination
Null-space function	Automatic
Assembly block size	5000
Use Hermitian transpose of constraint matrix and in symmetry detection	Off
Use complex functions with real input	Off
Stop if error due to undefined operation	On
Store solution on file	Off
Type of scaling	None
Manual scaling	
Row equilibration	On
Manual control of reassembly	Off
Load constant	On
Constraint constant	On
Mass constant	On
Damping (mass) constant	On
Jacobian constant	On
Constraint Jacobian constant	On

5.6.1.6 Post processing

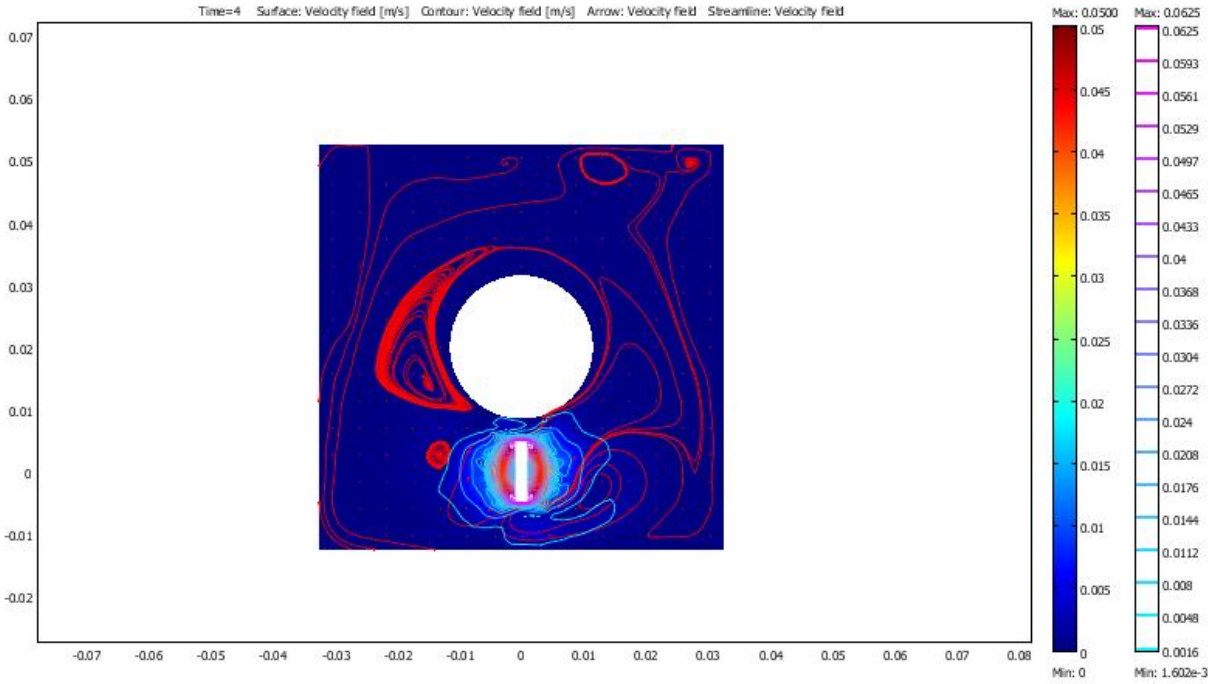

5.6.1.7 Variables

Point

Name	Description	Unit	Expression
xinit_ale	x coordinate initial value	M	X
yinit_ale	y coordinate initial value	M	Y

Boundary

Name	Description	Unit	Expression
K_x_chns	Viscous force per area, x component	Pa	eta_chns * (2 * nx_chns * ux+ny_chns * (uy+vx))
T_x_chns	Total force per area, x component	Pa	-nx_chns * p+2 * nx_chns * eta_chns * ux+ny_chns * eta_chns * (uy+vx)
K_y_chns	Viscous force per area, y component	Pa	eta_chns * (nx_chns * (vx+uy)+2 * ny_chns * vy)
T_y_chns	Total force per area, y component	Pa	-ny_chns * p+nx_chns * eta_chns * (vx+uy)+2 * ny_chns * eta_chns * vy
xinit_ale	x coordinate initial value	m	X

yinit_ale	y coordinate initial value	m	Y

Subdomain

Name	Description	Unit	Expression
U_chns	Velocity field	m/s	sqrt(u^2+v^2)
V_chns	Vorticity	1/s	vx-uy
divU_chns	Divergence of velocity field	1/s	ux+vy
cellRe_chns	Cell Reynolds number	1	rho_chns * U_chns * h_ale/eta_chns
res_u_chns	Equation residual for u	N/m^3	rho_chns * (u * ux+v * uy)+px-F_x_chns-eta_chns * (2 * uxx+uyy+vxy)
res_sc_u_chns	Shock capturing residual for u	N/m^3	rho_chns * (u * ux+v * uy)+px-F_x_chns
res_v_chns	Equation residual for v	N/m^3	rho_chns * (u * vx+v * vy)+py-F_y_chns-eta_chns * (vxx+uyx+2 * vyy)
res_sc_v_chns	Shock capturing residual for v	N/m^3	rho_chns * (u * vx+v * vy)+py-F_y_chns
beta_x_chns	Convective field, x component	kg/(m^2*s)	rho_chns * u
beta_y_chns	Convective field, y component	kg/(m^2*s)	rho_chns * v
Dm_chns	Mean diffusion coefficient	Pa*s	eta_chns
da_chns	Total time scale factor	kg/m^3	rho_chns
xinit_ale	x coordinate initial value	m	X
yinit_ale	y coordinate initial value	m	Y
dx_ale	x-displacement	m	x-X
dy_ale	y-displacement	m	y-Y

5.6.2 3D Model of Seven tube reactor

CFD model of seven tube reactor was built in 3d view using the Comsol and the using the predefined model incompressible Navier stroke model the flow field in the seven tube reactor was generated.

The Comsol report of the seven tube reactor shown below shows the flow field is not turbulence

COMSOL Model Report

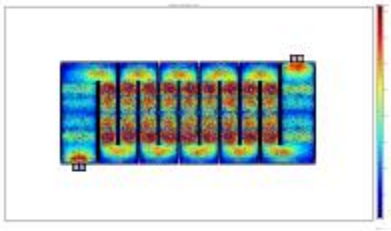

Table of Contents

5.6.2.1 Model Properties

Property	Value
Model name	
Author	
Company	
Department	
Reference	
URL	
Saved date	Jun 27, 2006 1:03:57 PM
Creation date	Mar 7, 2006 1:14:07 PM
COMSOL version	COMSOL 3.4.0.248

Application modes and modules used in this model:

- Geom1 (3D)
    - Incompressible Navier-Stokes (Chemical Engineering Module)

5.6.2.2 Constants

Name	Expression	Value	Description
T	298		

5.6.2.3. Geometry

Number of geometries: 1

Geom1

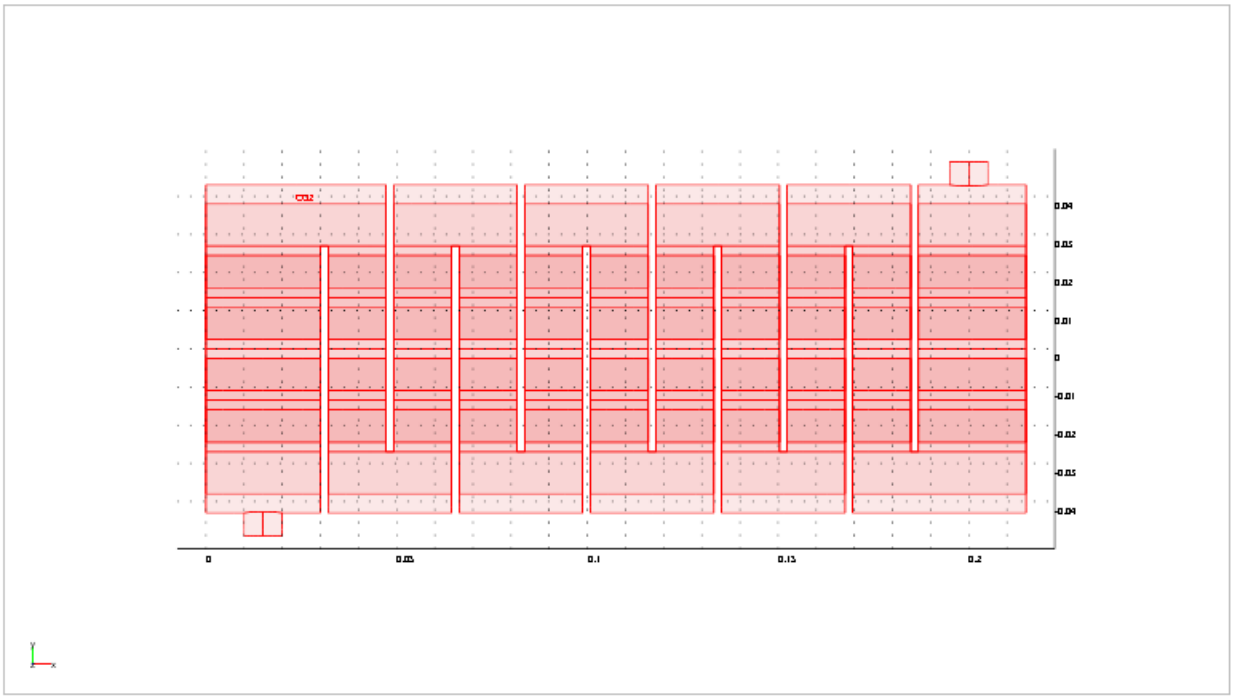

Point mode

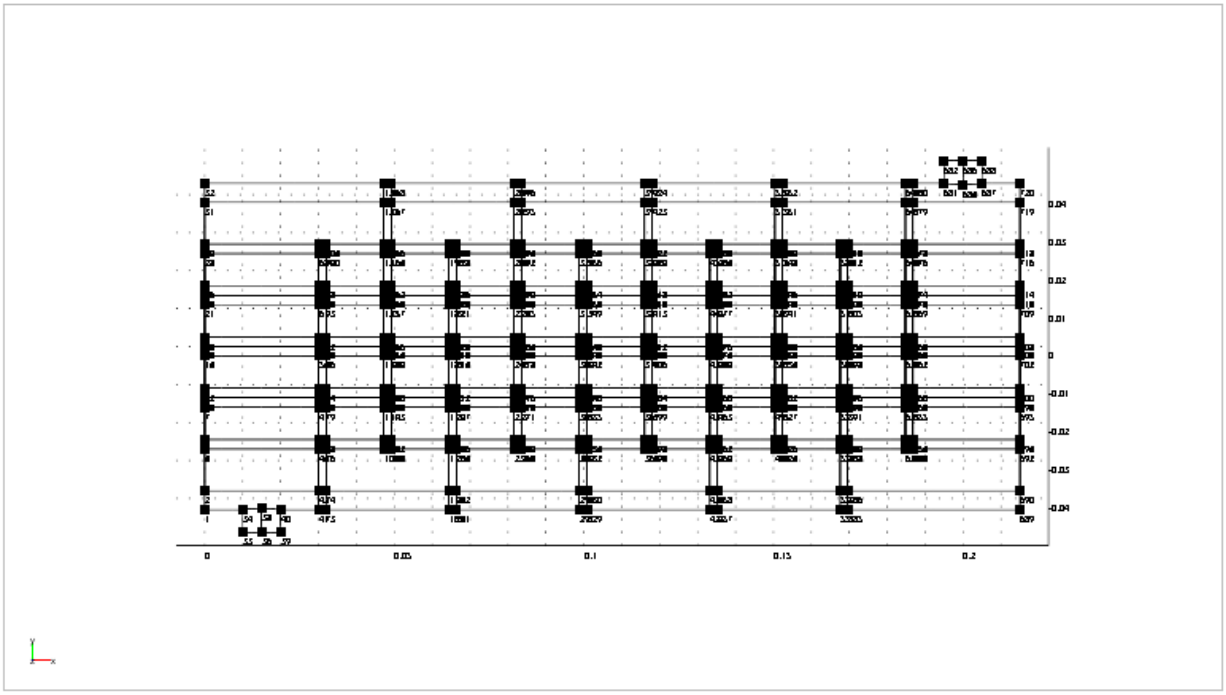

Edge mode

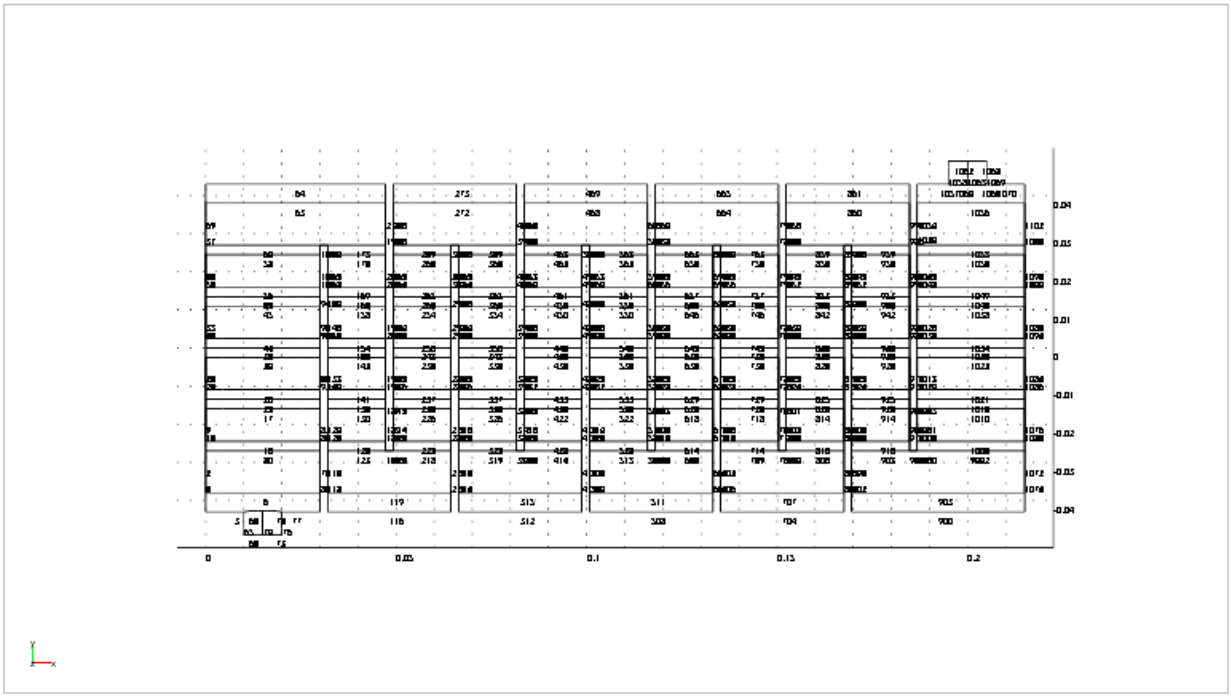

Boundary mode

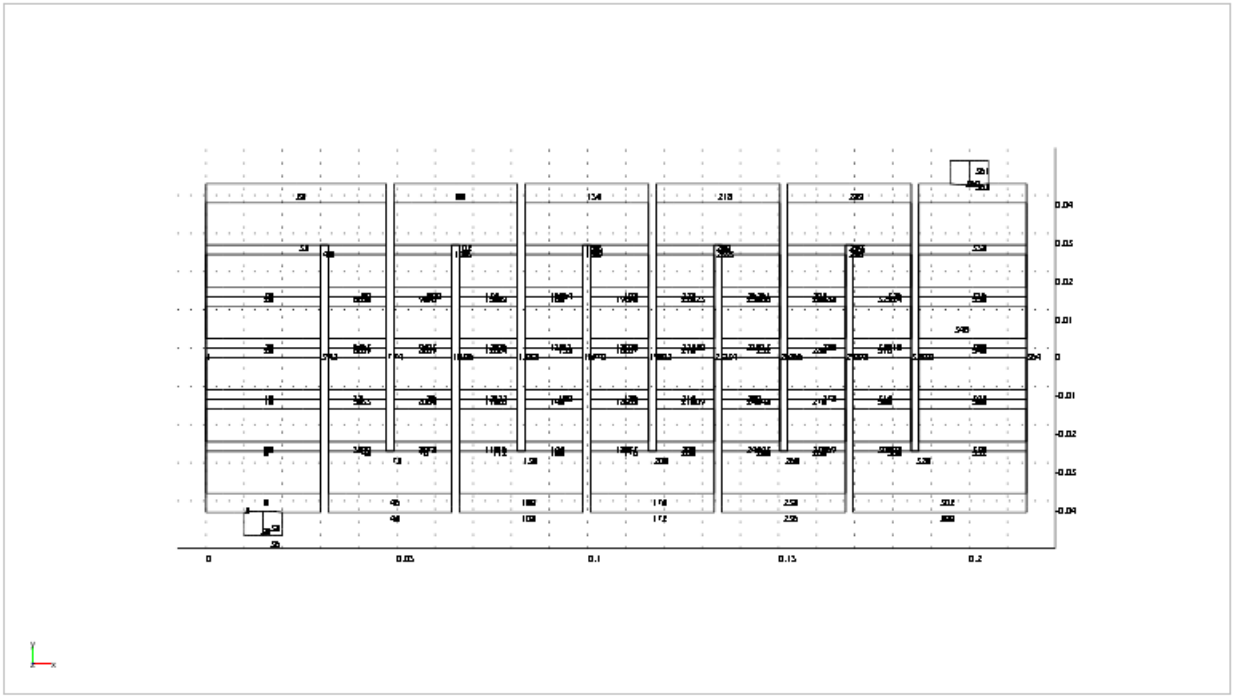

Sub domain mode

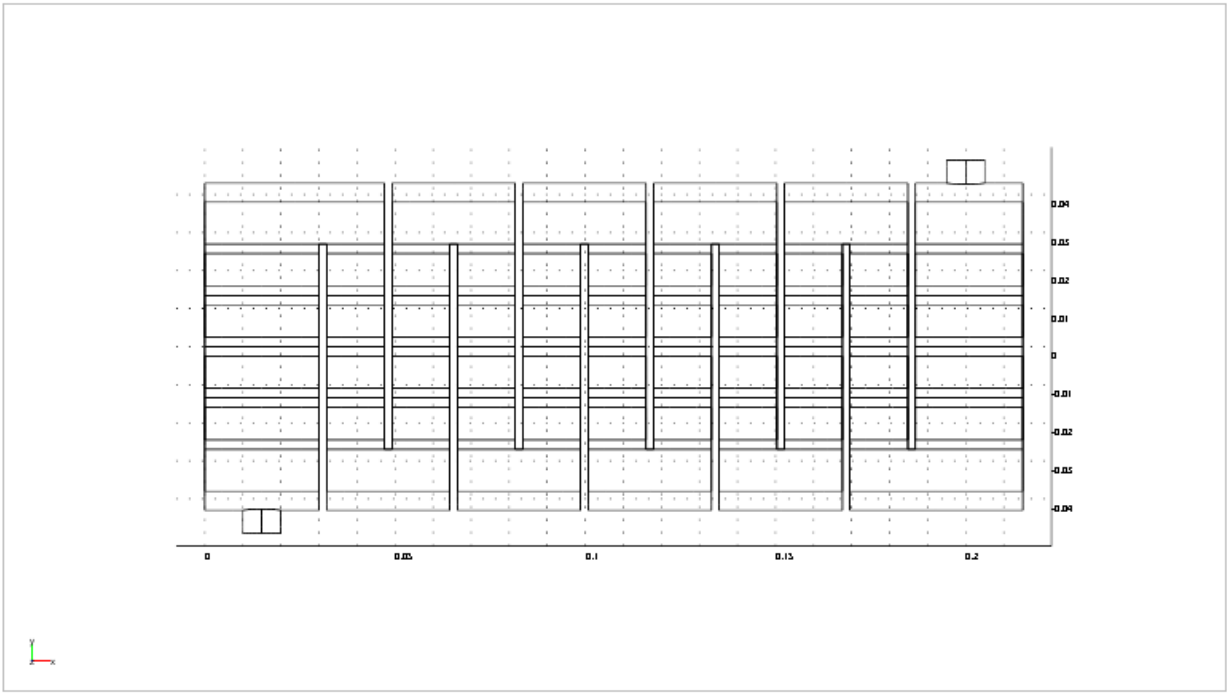

5.6.2.4 Geom1

Space dimensions: 3D

Independent variables: x, y, z

Mesh

Mesh Statistics

Number of degrees of freedom	860008
Number of mesh points	41620
Number of elements	160866
Tetrahedral	160866
Prism	0
Hexahedral	0
Number of boundary elements	57228
Triangular	57228

Quadrilateral	0
Number of edge elements	6833
Number of vertex elements	720
Minimum element quality	0.299
Element volume ratio	0.001

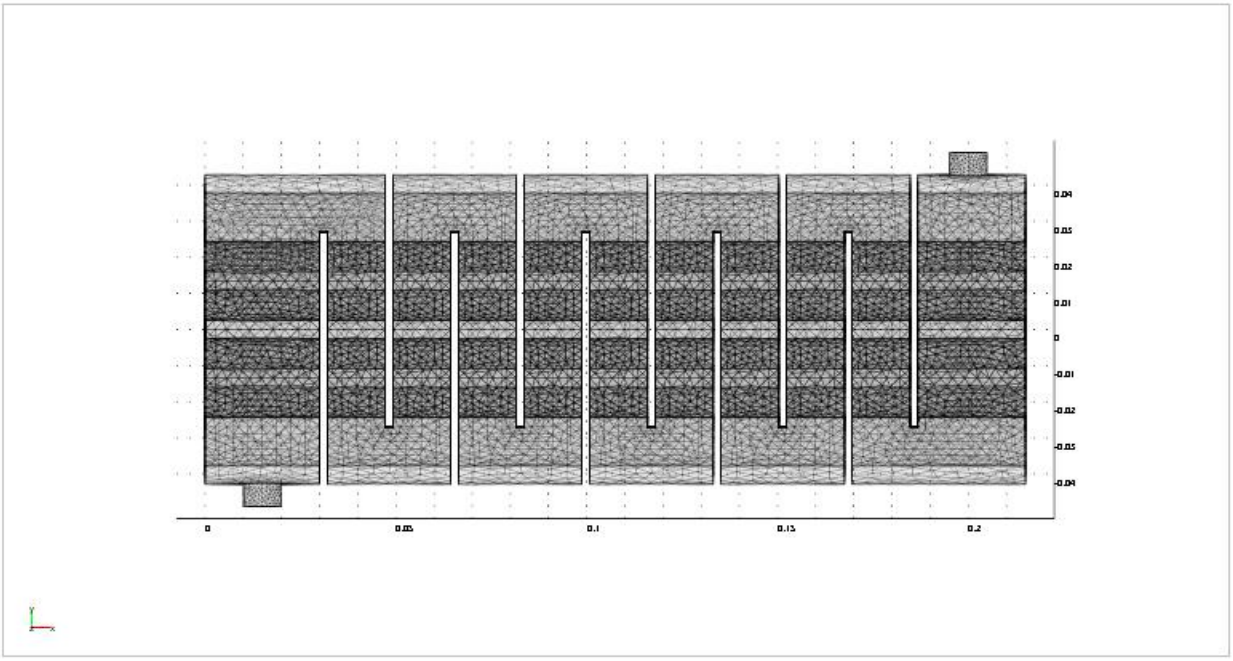

Application Mode: Incompressible Navier-Stokes (chns)

Application mode type: Incompressible Navier-Stokes (Chemical Engineering Module)

Application mode name: chns

Application Mode Properties

Property	**Value**
Default element type	Lagrange - P_2 P_1
Analysis type	Stationary
Corner smoothing	Off

Weakly compressible flow	Off
Turbulence model	None
Realizability	Off
Non-Newtonian flow	Off
Brinkman on by default	Off
Two-phase flow	Single-phase flow
Frame	Frame (xyz)
Weak constraints	Off
Constraint type	Ideal

Variables

Dependent variables: u, v, w, p, logk, logd, logw, phi, nxw, nyw, nzw

Shape functions: shlag(2,'u'), shlag(2,'v'), shlag(2,'w'), shlag(1,'p')

Interior boundaries not active

Boundary Settings

Boundary		1-35, 37-360, 362-364	36	361
Type		Wall	Inlet	Open boundary
velType		U0in	**u0**	U0in
y-velocity (v0)	m/s	0	**3**	0

Subdomain Settings

Subdomain		1
Integration order (gporder)		**4 4 4 2**
Constraint order (cporder)		**2 2 2 1**
Density (rho)	kg/m^3	**1000**
Dynamic viscosity (eta)	Pa·s	**0.001**
Isotropic diffusion switch (idon)		**1**
Streamline diffusion switch (sdon)		**0**

Streamline diffusion type (sdtype)		**pgc**

5.6.2.5 Materials/Coefficients Library

Water, liquid

Parameter	**Value**
Heat capacity at constant pressure (C)	Cp(T)
Dynamic viscosity (eta)	eta(T)
Thermal conductivity (k)	k(T)
Kinematic viscosity (nu0)	nu0(T)
Density (rho)	rho(T)

Functions

Function	**Expression**	**Derivatives**	**Complex output**
nu0(T)	(3.34e-10*T^4-4.57e-07*T^3+2.36e-4*T^2-0.054*T+4.67)/(-1.1538E-07*T^4+1.6538E-04*T^3-9.1327E-02*T^2+22.333*T-1014.6)	diff((3e-10*T^4-5e-07*T^3+0.0002*T^2-0.054*T+4.67)/(2E-05*T^3-0.0187*T^2+6.7496*T+234.1),T)	false
Cp(T)	4200	diff(4200,T)	false
rho(T)	-1.1538E-07*T^4+1.6538E-04*T^3-9.1327E-02*T^2+22.333*T-1014.6	diff(2E-05*T^3-0.0187*T^2+6.7496*T+234.1,T)	false
eta(T)	3.34e-10*T^4-4.57e-07*T^3+2.36e-4*T^2-0.054*T+4.67	diff(3e-10*T^4-5e-07*T^3+0.0002*T^2-0.054*T+4.67,T)	false
k(T)	0.0015*T+0.1689	diff(0.0015*T+0.1689,T)	false

5.6.2.6 Solver Settings

Solve using a script: off

Analysis type	Stationary
Auto select solver	On
Solver	Stationary
Solution form	Automatic
Symmetric	Off
Adaption	Off

Direct (UMFPACK)

Solver type: Linear system solver

Parameter	**Value**
Pivot threshold	0.1
Memory allocation factor	0.7

Stationary

Parameter	**Value**
Linearity	Nonlinear
Relative tolerance	1.0E-6
Maximum number of iterations	40
Manual tuning of damping parameters	Off
Highly nonlinear problem	Off
Initial damping factor	1.0
Minimum damping factor	1.0E-4
Restriction for step size update	10.0

Advanced

Parameter	Value
Constraint handling method	Elimination
Null-space function	Automatic
Assembly block size	5000
Use Hermitian transpose of constraint matrix and in symmetry detection	Off
Use complex functions with real input	Off
Stop if error due to undefined operation	On
Store solution on file	Off
Type of scaling	None
Manual scaling	
Row equilibration	On
Manual control of reassembly	Off
Load constant	On
Constraint constant	On
Mass constant	On
Damping (mass) constant	On
Jacobian constant	On
Constraint Jacobian constant	On

5.6.2.7 Postprocessing

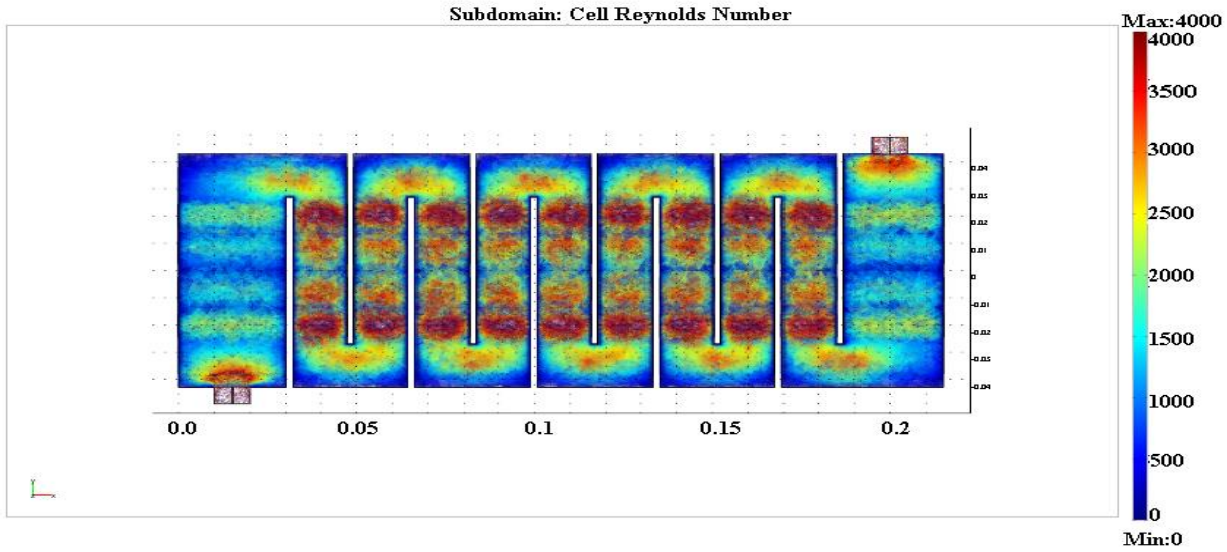

5.6.2.8 Variables

Boundary

Name	Description	Unit	Expression
K_x_chns	Viscous force per area, x component	Pa	eta_chns * (2 * nx_chns * ux+ny_chns * (uy+vx)+nz_chns * (uz+wx))
T_x_chns	Total force per area, x component	Pa	-nx_chns * p+2 * nx_chns * eta_chns * ux+ny_chns * eta_chns * (uy+vx)+nz_chns * eta_chns * (uz+wx)
K_y_chns	Viscous force per area, y component	Pa	eta_chns * (nx_chns * (vx+uy)+2 * ny_chns * vy+nz_chns * (vz+wy))
T_y_chns	Total force per area, y component	Pa	-ny_chns * p+nx_chns * eta_chns * (vx+uy)+2 * ny_chns * eta_chns * vy+nz_chns * eta_chns * (vz+wy)
K_z_chns	Viscous force per area, z component	Pa	eta_chns * (nx_chns * (wx+uz)+ny_chns * (wy+vz)+2 * nz_chns * wz)
T_z_chns	Total force per area, z component	Pa	-nz_chns * p+nx_chns * eta_chns * (wx+uz)+ny_chns * eta_chns * (wy+vz)+2 * nz_chns * eta_chns * wz

Subdomain

Name	Description	Unit	Expression
U_chns	Velocity field	m/s	sqrt(u^2+v^2+w^2)
Vx_chns	Vorticity, x component	1/s	wy-vz
Vy_chns	Vorticity, y component	1/s	uz-wx
Vz_chns	Vorticity, z component	1/s	vx-uy
V_chns	Vorticity	1/s	sqrt(Vx_chns^2+Vy_chns^2+Vz_chns^2)
divU_chns	Divergence of velocity field	1/s	ux+vy+wz
cellRe_chns	Cell Reynolds number	1	rho_chns * U_chns * h/eta_chns
res_u_chns	Equation residual for u	N/m^3	rho_chns * (u * ux+v * uy+w * uz)+px-F_x_chns-eta_chns * (2 * uxx+uyy+vxy+uzz+wxz)
res_sc_u_chns	Shock capturing residual for u	N/m^3	rho_chns * (u * ux+v * uy+w * uz)+px-F_x_chns
res_v_chns	Equation	N/m^3	rho_chns * (u * vx+v * vy+w * vz)+py-F_y_chns-

	residual for v		eta_chns * (vxx+uyx+2 * vyy+vzz+wyz)
res_sc_v_chns	Shock capturing residual for v	N/m^3	rho_chns * (u * vx+v * vy+w * vz)+py-F_y_chns
res_w_chns	Equation residual for w	N/m^3	rho_chns * (u * wx+v * wy+w * wz)+pz-F_z_chns-eta_chns * (wxx+uzx+wyy+vzy+2 * wzz)
res_sc_w_chns	Shock capturing residual for w	N/m^3	rho_chns * (u * wx+v * wy+w * wz)+pz-F_z_chns
beta_x_chns	Convective field, x component	kg/(m^2*s)	rho_chns * u
beta_y_chns	Convective field, y component	kg/(m^2*s)	rho_chns * v
beta_z_chns	Convective field, z component	kg/(m^2*s)	rho_chns * w
Dm_chns	Mean diffusion coefficient	Pa*s	eta_chns
da_chns	Total time scale factor	kg/m^3	rho_chns

6 CONCLUSIONS

6.1 Conclusion/Summary:

Microscope slide glass reactor experimental results in the degradation of congo red and methyl-orange showed the TiO_2 photocatalysis process using UV light of wave length 254 nm had better performance when compared to the wavelength of 385 nm. It was also verified from the blank microscope glass slide experimental results that most of the degradation of congo red/methyl orange was due to the TiO_2 photocatalysis process not the UV photolysis process.

Single tube reactor experimental results showed the successful degradation of the congo red, KI (potassium iodide) and nitro phenol using TiO_2 film coated by sol-gel and ESA methods. The results also showed the doping of TiO_2 has significant improvement in the photocatalyst performance in the degradation of Congo Red/KI/nitro phenol. It was observed from the experimental results the sol-gel TiO_2-Fe doped film had better photocatalytic performance when compared to sol-gel TiO_2 film and ESA TiO_2-Fe doped film had better performance when compared to the ESA TiO_2 film.

The seven tube reactor experimental results showed same behavior to the single tube reactor in the degradation of congo red, KI and nitro phenol using sol-gel and ESA method TiO_2/ TiO_2 -Fe Doped film, the Fe-Doped TiO_2 film had higher rate constant.

From the factorial experiment of the parameters in the 7 tube reactor, it showed the significance of each variable: flow rate, baffles and number of lamps in the degradation of KI. By observing the individual coefficient and effects of the individual variables on the KI degradation , the results from the factorial experiment suggests that with increase in flow rate from 1 gpm to 2

gpm the degradation decreased. It can also be observed from the concentration vs time plot in Figure 5-28 that increase in number of baffles from 6 to 8 increased the reactor performance and with increase in number of lamps 4 to 7 the reactor performance increased, the results showed increased flow rate has resulted in decrease of the contact time of contaminant to the photocatalyst surface, and increase in number of baffles showed it provided more mixing inside the reactor and allowed the contact of contaminant to the photocatalyst surface, and the increase in number of lamps resulted in increasing the photocatalyst activity .

The CFD model of the seven tube reactor shows the flow pattern of high mixing in between the baffles, which corresponding to high Reynolds number. No mixing or low Reynolds number was noticed at the inlet and outlet opening of the reactor. Further, work needs to be done using CFD model to simulate the reaction kinetics on the photocatalytic surface, which will help in design of a large scale reactor.

We can conclude that future work needs to done in the evaluation of reactor performance using film with dopant of higher potential than the Fe-doped film. The multiple tube reactor of shell and tube configuration can be considered for design of large scale reactor, as it provides the required mixing inside the reactor and also it provides an environment for contact of UV light with photocatalyst without necessity of penetrating through the water. For successful and economically feasible large scale reactor, further research needs to be done for photocatalyst with high efficiency in terms of light usage and also driving the photocatalyst activity with the visible light.

For successful commercial application of the reactor, the durability of the film plays significant. Further work needs to be done to evaluate the durability of the film and enhance the film durability without the need of reactivating the film too often.

The thickness of the film also plays significant role as with high thickness the TiO_2 particles activated after absorbing the light photon might not be in contact with water and organic contaminant, with small thickness if it's lower than wavelength of photon then no TiO_2 photon absorption will occur. Further work needs to be done to evaluate the optimum thickness for the reactor performance.

Another area for potential commercial application is current advanced oxidation process using ozone and H_2O_2 for treating organic compounds can be replaced with TiO_2 photocatalysis process in combination with H_2O_2 or ozone. We need to evaluate the gain of using photocatalysis+ O_3/H_2O_2 compared to O_3/H_2O_2 oxidation process.

Based on the constraints of most of the existing photocatalytic reactors such as the TiO_2 film deposition, UV light transmission path to the TiO_2 surface and mixing inside the reactor. The experimental results of the proposed multiple tube photocatalytic reactor showed the required mixing with no flow dead zones inside the reactor and contact of the fluid to the photocatalytic surface, UV light transmission mechanism to TiO_2 without the necessity to transmit through water and deposition of TiO_2 film on quartz surface.

From the experimental work it can concluded that the photocatalytic reactor can be used as replacement for the existing photolysis process in commercial environment, as the photocatalytic reactor provided better performance in degradation of congo red/methyl orange/KI when compared to the direct UV photolysis.